INFORMATION TO USERS

While the most advanced technology has been used to photograph and reproduce this manuscript, the quality of the reproduction is heavily dependent upon the quality of the material submitted. For example:

- Manuscript pages may have indistinct print. In such cases, the best available copy has been filmed.

- Manuscripts may not always be complete. In such cases, a note will indicate that it is not possible to obtain missing pages.

- Copyrighted material may have been removed from the manuscript. In such cases, a note will indicate the deletion.

Oversize materials (e.g., maps, drawings, and charts) are photographed by sectioning the original, beginning at the upper left-hand corner and continuing from left to right in equal sections with small overlaps. Each oversize page is also filmed as one exposure and is available, for an additional charge, as a standard 35mm slide or as a 17"x 23" black and white photographic print.

Most photographs reproduce acceptably on positive microfilm or microfiche but lack the clarity on xerographic copies made from the microfilm. For an additional charge, 35mm slides of 6"x 9" black and white photographic prints are available for any photographs or illustrations that cannot be reproduced satisfactorily by xerography.

Order Number 8726834

Global solar oscillations observed in the visible to near infrared continuum

Oglesby, Paul Harvey, Ph.D.

The University of Arizona, 1987

U·M·I
300 N. Zeeb Rd.
Ann Arbor, MI 48106

PLEASE NOTE:

In all cases this material has been filmed in the best possible way from the available copy. Problems encountered with this document have been identified here with a check mark ___✓___.

1. Glossy photographs or pages _____
2. Colored illustrations, paper or print _____
3. Photographs with dark background _____
4. Illustrations are poor copy _____
5. Pages with black marks, not original copy _____
6. Print shows through as there is text on both sides of page _____
7. Indistinct, broken or small print on several pages ___✓___
8. Print exceeds margin requirements _____
9. Tightly bound copy with print lost in spine _____
10. Computer printout pages with indistinct print _____
11. Page(s) _____ lacking when material received, and not available from school or author.
12. Page(s) _____ seem to be missing in numbering only as text follows.
13. Two pages numbered _____. Text follows.
14. Curling and wrinkled pages _____
15. Dissertation contains pages with print at a slant, filmed as received _____
16. Other _____

_____

_____

GLOBAL SOLAR OSCILLATIONS OBSERVED IN THE VISIBLE TO NEAR INFRARED CONTINUUM

by

Paul Harvey Oglesby

A Dissertation Submitted to the Faculty of the

DEPARTMENT OF PHYSICS

In Partial Fulfillment of the Requirements
For the Degree of

DOCTOR OF PHILOSOPHY

In the Graduate College

THE UNIVERSITY OF ARIZONA

1 9 8 7

THE UNIVERSITY OF ARIZONA
GRADUATE COLLEGE

As members of the Final Examination Committee, we certify that we have read the dissertation prepared by Paul Harvey Oglesby

entitled Global Solar Oscillations Observed in the Visible to Near Infrared Continuum

and recommend that it be accepted as fulfilling the dissertation requirement for the Degree of Doctor of Philosophy.

John C. Stein, Jr.	March 17, 1987
L C Am'Entyre	March 17, 1987
Robert H. Chambers	3-17-87
[signature]	3-17-87
Henry A. Weis	3-17-87

Date

Final approval and acceptance of this dissertation is contingent upon the candidate's submission of the final copy of the dissertation to the Graduate College.

I hereby certify that I have read this dissertation prepared under my direction and recommend that it be accepted as fulfilling the dissertation requirement.

Henry A. Weis	3-17-87
Dissertation Director	Date

STATEMENT BY AUTHOR

This dissertation has been submitted in partial fulfillment of requirements for an advanced degree at The University of Arizona and is deposited in the University Library to be made available to borrowers under rules of the Library.

Brief quotations from this dissertation are allowable without special permission, provided that accurate acknowledgement of source is made. Requests for permission for extended quotation from or reproduction of this manuscript in whole or in part may be granted by the head of the major department or the Dean of the Graduate College when in his or her judgement the proposed use of the material is in the interests of scholarship. In all other instances, however, permission must be obtained from the author.

SIGNED: 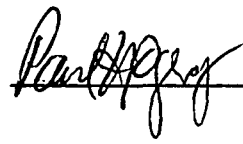

ACKNOWLEDGEMENTS

First and foremost, I would like to thank Professor Henry A. Hill for his support throughout this work. Discussions with him were very useful on a broad range of subjects ranging from instrumental design to data analysis. Professor Hill is a very dedicated scientist with a great deal of insight in approaching scientific problems. I am very grateful that I have had the opportunity to work with him.

I would also like to thank Chuck Barry and Bill Callahan for their persistence in maintaining the computer system and Craig Hagerman for helping in the installation of the instrument.

A thank you is in order for everyone at SCLERA for their support throughout the entirety of this work. Last, but certainly not least, I would like to thank those wonderful secretaries Gigi Linden, Alix Lind, and Pam Hill for spending long hard hours in the preparation of this dissertation.

This work was supported in part by the Astronomy Division of the National Science Foundation and the Air Force Office of Scientific Research.

TABLE OF CONTENTS

TABLE OF CONTENTS--continued

LIST OF ILLUSTRATIONS

LIST OF ILLUSTRATIONS--continued

LIST OF ILLUSTRATIONS--continued

LIST OF ILLUSTRATIONS--continued

LIST OF TABLES

ABSTRACT

A new technique for detecting solar oscillations in the visible to near infrared continuum has been developed and tested at the Santa Catalina Laboratory for Experimental Relativity by Astrometry (SCLERA). In 1985, measurements of the solar radiation intensity near disk center were made by Oglesby (1986, 1987). The results of these observations have been compared to the reported detections and classifications by Hill (1984, 1985) and Rabaey and Hill (1987) of the low-order, low-degree acoustic modes; the intermediate degree f-modes; and the low-order g-modes.

For the low-order, low-degree, acoustic modes and the intermediate degree f-modes, a total of 40 multiplets were used in the analysis. The coincidence rates between the peaks in the power spectrum of the 1985 observations and the classified frequency spectrum for multiplets taken in subgroups of ≈5 (same n and contiguous in ℓ) are typically 4-5 σ above the accidental coincidence rate. The maximum coincidence rates for these same subgroups of multiplets were found to occur for frequency shifts of the classified spectrum ranging from -0.27 μHz for modes that are sensitive to the internal properties near the bottom of the convection zone to 0.06 μHz for modes that are sensitive to internal properties near the top of the convection zone. Also included in this work is a comparison of diameter measurements obtained at SCLERA in 1978 (Caudell 1980) with the classified modes

mentioned above. Agreement in this case is at the 3.1 σ level for both the f-mode (n=0) multiplets with $21 \leq \ell \leq 36$ and the n=1, $6 \leq \ell \leq 12$ acoustic modes.

The confirmation of the detection and classification of the low-order g-modes of oscillation was found to be at the 3.3 σ level. Additionally, the m dependence of the 1985 power spectrum was found to behave in the manner expected for the proper classifications in m for the g-modes.

CHAPTER 1

INTRODUCTION

Perhaps the discovery of global oscillations of the Sun was one of the more important discoveries pertaining to solar physics that has ever been made. The ramifications of the discovery of solar normal mode oscillations are far-reaching. Even though man's knowledge about the Sun has increased immensely in the past 20 years, there is still much to be learned. Current models offer explanations about the solar interior and the production of energy in the core; however, the discrepancy between the observed neutrino production rate with the predicted rate is an indication that these solar models fail to accurately depict what actually takes place in the core. This does not, of course, imply that a major modification of existing theories is called for, but it does demonstrate the need for some changes in which the study of the Sun's interior through global solar oscillations will play a vital role.

1.1 The Discovery of Solar Oscillations

The first announcement of the detection of global solar oscillations came in 1974. These normal modes were detected at the Santa Catalina Laboratory for Experimental Relativity by Astormetry (SCLERA) by Hill and Stebbins (1975). The primary observing instrument at SCLERA was designed to make very accurate measurements of the Sun's oblateness in order to refine tests of general relativistic theories of gravitation. Hill and Stebbins found several fluctuations in the Sun's

apparent diameter with periods ranging from ten minutes to one hour. It was later determined that the oscillations were detected primarily through temperature changes in the solar atmosphere instead of actual surface displacements (Hill, Stebbins, and Brown 1976).

In 1960, Leighton, Noyes, and Simon (1962) discovered that patches of the solar surface were oscillating at regular intervals approximately five minutes in length. The first reactions to this discovery were skeptical. Many believed that the five-minute periodicity may be due to randomly excited oscillations of the Sun's photosphere produced by convective overshoot or simply due to terrestrial atmospheric phenomena. However, after more and more data was accumulated, it became apparent that these five-minute oscillations were in fact trapped waves in the envelope of the Sun itself.

With the discovery of global solar oscillations and of trapped waves came the birth of helioseismology. This opened up an exciting possibility for probing the interior of the Sun. Before these oscillations were discovered, observers were very limited in studying the Sun's interior, simply because it is opaque at all wavelengths of the electromagnetic spectrum, and the detection of solar neutrinos is very difficult (cf. Section 1.2).

1.2 The Neutrino Paradox

Before the discovery of global solar oscillations the only method of obtaining direct information about the solar interior was through the measurement of the solar neutrino flux. Neutrinos are produced in the main proton-proton reaction in the Sun's core. They are

produced in large quantities, but their energy is too low to be detected using available technology. However, a group of researchers from the Max-Planck Institute (MPI) and a Soviet group under the direction of G. T. Zatsepin and V. N. Gavrin have developed separate techniques to measure the neutrino produced in the p-p reaction through the capture of the solar neutrino by the reaction

$$\nu_e + {}^{71}Ga \rightarrow {}^{71}Ge + e^- \quad . \qquad 1.2.1$$

The MPI group is expected to receive enough gallium to begin the experiment in 1989 and the Soviet group is scheduled to begin measurement sometime in 1987.

On the other hand, more energetic neutrinos are produced in the reaction

$$^{7}Be + p \rightarrow {}^{8}B \rightarrow e^+ + \nu_e \quad . \qquad 1.2.2$$

The neutrino produced in the above reaction contains a sufficient amount of energy to convert a neutron in ^{37}Cl to a proton forming ^{37}Ar. Since ^{37}Ar is radioactive, it can be separated from the ^{37}Cl and detected. Using this as a means to measure the solar neutrino flux, it was found by Davis and co-workers (Rowley, Cleveland, and Davis, 1985) that the capture rate for these neutrinos was approximately one-third to one-quarter of that predicted from standard solar models. This incompatibility demonstrates the need for finding additional observational techniques to probe the solar interior such as offered by

helioseismology. Not only does helioseismology have the potential for solving many puzzles concerning the interior of the Sun, but it could very likely provide the necessary clues needed for solving the neutrino paradox.

1.3 The Primary Forces Responsible for Solar Oscillations

The Sun, like any mechanical body, can vibrate with many different frequencies. The spherical nature of the system dictates that the eigenfunctions for normal modes of oscillation are proportional to the standard spherical harmonics $Y_m^\ell(\theta,\phi)$. Spherical symmetry is assumed in the treatment of the Sun, and other effects such as rotation or magnetic fields are regarded as small perturbations. In the case of rotation, for example, there is a "Zeeman splitting" of an individual frequency into its $2\ell+1$ components. The measurement of this splitting is a powerful tool for determining the internal rotation as a function of depth (Hill, et. al., 1986).

Although the gas in a star experiences many forces, there are two primary restoring forces that are responsible for solar oscillations. These are pressure and gravity. In either case, if the gas is displaced from its original equilibrium state, these two forces may act to return the system towards its initial state leading to oscillations if the damping mechanism is sufficiently small.

In the case where pressure acts as the restoring force, the oscillation is referred to as a pressure wave where the corresponding oscillatory mode is typically referred to as a p-mode. If gravity prevails as the dominant restoring force the mode of oscillation is

referred to as a g-mode. Examples of these types of oscillations are sound waves which are a direct result of pressure acting as the restoring force, and ocean waves which are associated with gravity acting as the restoring force. When gravity acts as the primary restoring force, the modes of oscillation are sustained through buoyancy which acts outward in the compressed phase and inward in the expanded phase. Therefore, the net restoring force is zero for radial oscillations so that the g-modes are nonradial oscillations ($\ell \neq 0$).

There are two characteristic frequencies which determine the local vibrational properties of any medium. These are the Lamb frequency and the Brunt-Väisälä frequency. These are related to the two primary restoring forces, pressure and gravity, that are responsible for the existence of oscillatory modes in the Sun. The Lamb frequency is given by

$$L_\ell^2 = \frac{\ell(\ell+1)c^2}{r^2} \qquad 1.3.1$$

and the Brunt-Väisälä frequency is

$$N^2 = g\left(\frac{d\ln p_0}{\Gamma_1 dr} - \frac{d\ln \rho_0}{dr}\right) , \qquad 1.3.2$$

where

$$c^2 = \Gamma_1 \frac{p_0}{\rho_0} , \qquad 1.3.3$$

$$\Gamma_1 = \left(\frac{d(\ln(p))}{d(\ln(\rho))} \right)_{ad} \quad , \qquad 1.3.4$$

c is the local sound speed, p_0 and ρ_0 are the unperturbed pressure and density respectively, and g is the gravitational acceleration.

The frequency of oscillation for the g-modes is typically lower than those of the p-modes. The lowest possible frequency for the pressure modes is on the order of the time that is required for a sound wave to travel through the Sun, which is approximately one hour. On the other hand, gravity waves have an upper limit for the frequency at which they can oscillate, which is the Brunt-Vaisala frequency given in Equation 1.3.2. Since a gas becomes convective when $N^2 < 0$, gravity waves cannot exist in the convection zone.

Figure 1.1 shows the regions of the Sun, as a function of depth for the gravity modes and L_ℓ for the acoustic modes, in which the p-modes and g-modes can exist. Therefore, by studying the behavior of the eigenfunctions that exist in the region of interest, observational information of the internal structure of the Sun becomes available.

1.4 Current Observational Techniques

Since the birth of helioseismology, there has been a considerable amount of controversy generated over the widespread disagreement of the results obtained using different observational techniques for measuring solar oscillations. Currently, the primary methods of observation include Doppler shift measurements, total irradiance measurements, and differential radius measurements.

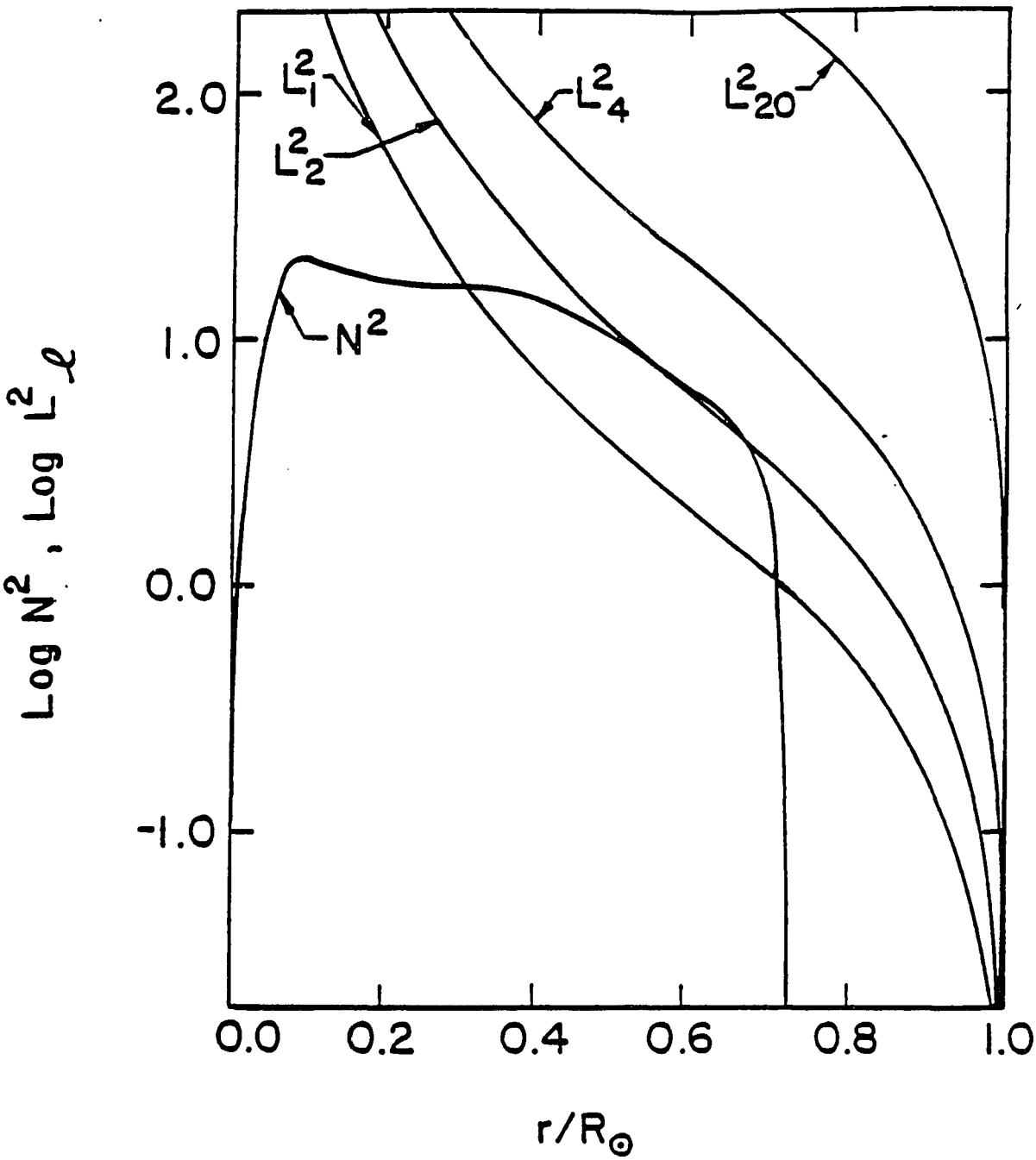

Figure 1.1 Propagation diagram for the solar interior.

Using available spectroscopic techniques, Doppler shift measurements detect velocities of the solar surface. Since this technique measures the velocity of a gas cell in the line of sight, these measurements are sensitive to vertical displacements near the center of the solar disk and are sensitive to horizontal displacements near the limb. Several groups have obtained data using this technique while using different spatial filtering. For example, the Birmingham group (Claverie et al., 1979) has published results from whole solar disk velocity measurements. This integration has the same effect as making the Sun appear as a star, and therefore, their observations are inherently sensitive to modes of oscillation with low ℓ. On the other hand, the Crimean group has developed a technique of Doppler shift measurements where the outer annular part of the solar disk ($\sim$ 50% in brightness) is used as a reference for measuring the Doppler shift in the inner disk (Severny, Kotov and Tsap, 1976). This technique has the added advantage of removing the effects due to the Earth's rotation.

The Active Cavity Radiometer Irradiance Monitor (ACRIM) experiment on the **Solar Maximum Mission** (SMM) has provided total irradiance measurements from a satellite based instrument. This experiment was designed to provide solar irradiance information during the last part of the maximum solar active period in 1980 and the first part of the solar minimum in 1984. The instrument used on the SMM consists of three independent self-calibrating pyroheliometers developed at the Jet Propulsion Laboratory. The primary cavity that is used for solar observations is maintained 0.5° K above the reference cavity by an electrical heater. A shutter alternately opens and closes with a two-minute time

resolution allowing sunlight to enter the instrument. The measurement of the solar irradiance is then determined by the difference between the shutter open and shutter closed power requirements. The response of the cavity as an effective absorber in the vacuum UV to the mid IR has been predicted to be ≈0.999 (Willson and Hudson 1981). Some of the results obtained from this mission are discussed in Section 7.2.

Another technique employed to detect solar oscillations is that of diameter measurements and differential radius measurements. It was the use of this technique that led to the first announcement of the detection of global solar oscillations (Hill and Stebbins, 1975). Diameter measurements have also been obtained by Caudell (1980) and some of those results are presented in Section 6.8. In 1979, SCLERA began a program of obtaining differential radius measurements. It has been determined that the differential radius measurements are less sensitive, by a factor of approximately 600 in amplitude, to differential refraction effects in the Earth's atmosphere than the diameter measurements. The differential radius observations consist of measuring a functional of intensity of three pairs of diametrically opposed positions near the solar limb. The functional of the intensity is determined by measuring the difference of two positions on the limb which were defined by the Finite Fourier Transform Definition (Hill, Stebbins, and Oleson 1975). Making use of the symmetry properties inherent in the geometry of the differential radius observations enabled Hill to classify solar modes of oscillation (Hill 1984) that are discussed extensively in this work.

CHAPTER 2

THEORETICAL BACKGROUND FOR THE OBSERVATIONAL METHOD

The amplitudes of solar modes of oscillation are clearly small, which is evident from the fact that they have only recently been detected. Certainly larger amplitudes of oscillation would have been discovered long ago. The mere fact that these amplitudes are small leads to difficulty in detecting solar oscillations. Current techniques, such as the differential radius measurements obtained at SCLERA, have proven successful in providing strong observational evidence in favor of the existence of solar normal modes of oscillation. As a result of these observations, one expects to observe changes in the solar radiation intensity near disk center. However, attempts in detecting oscillations through the measurements of the latter type have been unsuccessful. Negative results have been reported by Beckers and Ayres (1977) when searching for brightness fluctuations near disk center in the Ca K-line wings. Musman and Nye (1976) have also studied solar oscillations by monitoring the intensity at 32 different positions on the solar disk near disk center. They monitored the continuum intensity fluctuations, line center intensity fluctuations of the Fe I 5576 line, and the ratio of the line center to continuum fluctuations also for Fe I 5576. Musman and Nye found no long period brightness fluctuations greater than they expected from a 0.3 K fluctuation in temperature.

As pointed out by Beckers and Ayers (1977) and Musman and Nye (1976), fluctuations in the Earth's atmospheric transparency introduced noise in the signal. When measuring the radiation intensity over a limited spectral range (or integrated intensity in wavelength in the continuum), it is impossible to distinguish between brightness fluctuations due to changes in the transparency of the Earth's atmosphere or brightness fluctuations that are solar in origin. However, in the work of Hill and Logan (1984) and Hill, Tash, and Padin (1986), it was shown that perturbations in the solar radiation intensity due to solar normal mode oscillations are quite wavelength dependent with a unique signature. Since most fluctuations in the Earth's atmospheric transparency are wavelength independent (Elder and Strong, 1953; cf. Chapter 5), events that are terrestial in origin can be distinguished from events that are solar in origin. Therefore, by measuring the solar radiation intensity over a wide spectral range, solar oscillations near disk center should be detectable.

2.1 Radiative Transport in the Photosphere

Enormous amounts of energy are produced in the central region of the Sun ($r \lesssim \frac{1}{4}R_\odot$, where $R_\odot$ is the solar radius), called the core. The density and temperature of the core are sufficient to allow thermonuclear fusion to occur. Most of the energy released in the core results from the main proton-proton cycle. In a series of three steps, four protons are converted to a helium nucleus. This process occurs through

$$
\begin{aligned}
{}^{1}H + {}^{1}H &\rightarrow {}^{2}H + e^{+} + \nu \\
{}^{2}H + {}^{1}H &\rightarrow {}^{3}He + \gamma \\
{}^{3}He + {}^{3}He &\rightarrow {}^{4}He + {}^{1}H + {}^{1}H \quad .
\end{aligned}
\qquad 2.1.1
$$

For every gram of hydrogen, 0.007 grams of matter are converted to energy. This energy is transferred toward the surface through radiative transport. In its journey to the surface, the photon energy decreases by being absorbed and reemitted by the intervening solar material. At approximately 80% of the solar radius, the gas properties have changed so that energy transport occurs through turbulent convection (cf. Section 1.3). This region of the Sun is known as the convection zone. Finally, the energy produced in the core reaches the photosphere. The density scale height of the photosphere is approximately 100 km, and in this region there is only a small probability of a photon interacting with the solar material before being radiated into space.

Since the Sun is to be studied by measuring the intensity of the radiation as a function of wavelength, it is necessary to study the physical principles of how this radiation is transported through a medium. When being transported through a medium, a photon experiences scattering, absorption, and emission which all contribute to changing the specific intensity, I_λ. Allowing for these effects in the derivation of a radiation transport equation, two coefficients are introduced. These are the opacity, κ_λ, which considers the effects of absorption, and the emission coefficient, j_λ, which includes the effects of scattering and emission. Hence, the change in specific intensity, I_λ, in a

cylinder of length ds, containing a material of density ρ, is the excess of emission, ρj_λ, over absorption, $\rho \kappa_\lambda I_\lambda$,

$$dI_\lambda = (j_\lambda - \kappa_\lambda I_\lambda)\rho ds \quad . \qquad 2.1.2$$

The specific intensity, $I_\lambda(\mathbf{r},\mathbf{n},t)$, at position $\mathbf{r}$, traveling in direction $\mathbf{n}$ per unit solid angle and per unit wavelength is defined by

$$\frac{dE}{dt} = I_\lambda(\mathbf{r},\mathbf{n},t) \cos\theta \, dA \, d\lambda \, d\omega \quad . \qquad 2.1.3$$

where the amount of energy, dE, is being transported across an effective area, $\cos\theta \, dA$, in time dt into a solid angle $d\omega$ and wavelength interval $d\lambda$.

Equation 2.1.2 can be stated in a more useful form by defining a source function, S_λ, where

$$S_\lambda = \frac{j_\lambda}{\kappa_\lambda} \qquad 2.1.4$$

so that Equation 2.1.2 becomes

$$dI_\lambda = (S_\lambda - I_\lambda)\rho \kappa_\lambda ds \quad . \qquad 2.1.5$$

The $\rho \kappa_\lambda$ in Equation 2.1.5 is used to define another quantity called the optical depth, τ_λ, where

$$d\tau_\lambda = -\rho\kappa_\lambda dz \qquad 2.1.6$$

where z is the distance along the normal to the surface. If θ is the angle between the outward normal and the cone of radiation (see Figure 2.1), then Equation 2.1.5 becomes

$$\mu \frac{dI_\lambda(\tau_\lambda,\theta)}{d\tau_\lambda} = I_\lambda(\tau_\lambda,\theta) - S_\lambda(\tau_\lambda) \qquad 2.1.7$$

with $\mu = \cos\theta$. Here, the opacity has been written for a plane-parallel atmosphere with axial symmetry.

Equation 2.1.7 is a linear first order differential equation that can be solved by using an appropriate integrating factor. Choosing $e^{-\tau_\lambda/\mu}$ as the integrating factor, Equation 2.1.7 can be written as

$$\mu \frac{d}{d\tau_\lambda} I_\lambda(\tau_\lambda,\theta)e^{-\tau_\lambda/\mu} = -S_\lambda(\tau_\lambda)e^{-\tau_\lambda/\mu} \qquad 2.1.8$$

Integrating this from $\tau_\lambda = u_1$ to $\tau_\lambda = u_2$, we arrive at

$$I_\lambda(u_1,\theta) = I_\lambda(u_2,\theta)e^{-(u_2 - u_1)/\mu} + \int_{u_1}^{u_2} S(t)e^{-(u - u_1)/\mu}\frac{du}{\mu} \qquad 2.1.9$$

If we define $u_1 = 0$ as the top of the atmosphere, and take the limit as $\tau_2 \dashrightarrow \infty$, then

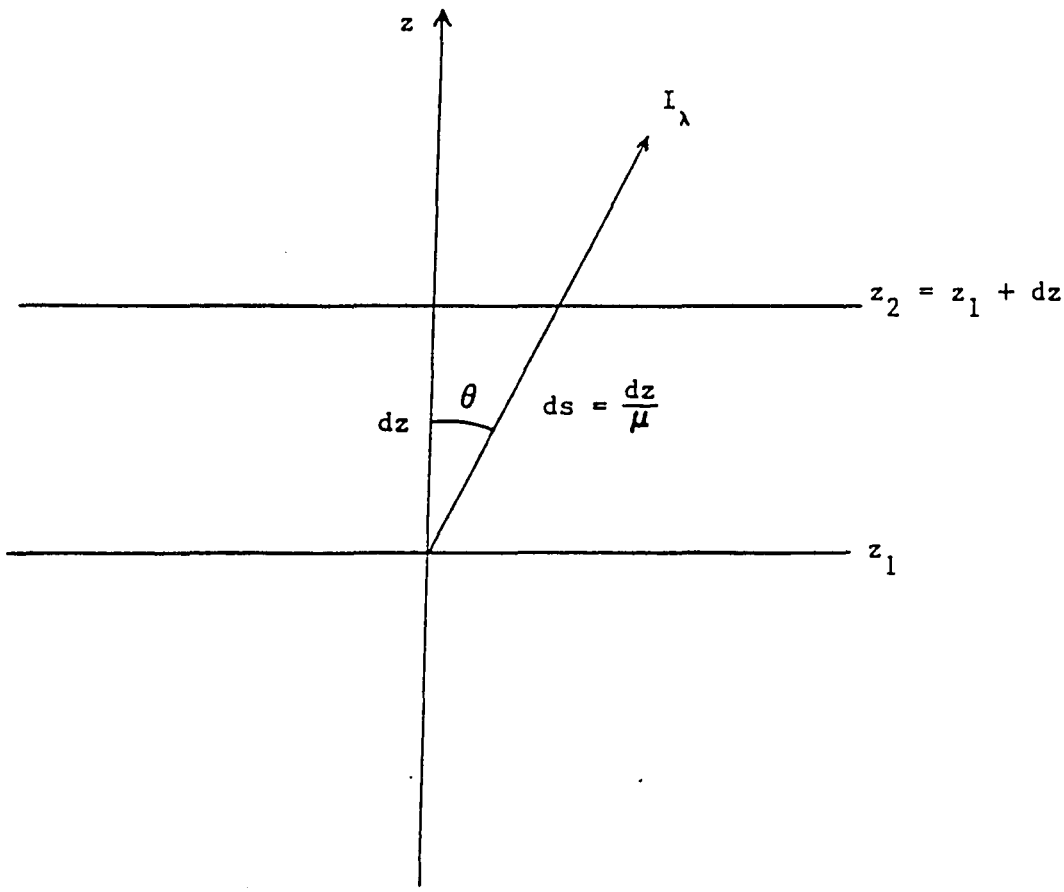

Figure 2.1. Model illustrating radiative attenuation.

$$I(0,\mu) = \int_0^\infty S(t)e^{-u/\mu}\,\frac{du}{\mu} \qquad 2.1.10$$

where we have required

$$\lim_{\tau_\lambda \to \infty} I_\lambda(\tau_\lambda,\theta)e^{-\tau_\lambda/\mu} = 0 \qquad 2.1.11$$

for the semi-infinite atmosphere.

If the system is in local thermodynamic equilibrium (LTE) with no scattering, the source function is equal to the Planck function, B_λ, with

$$S_\lambda = B_\lambda = \frac{c_1}{\lambda^5(e^{c_2/(\lambda T)} - 1)} \qquad 2.1.12$$

and

$$c_1 = 2\pi hc^2 = 3.74 \times 10^{-12} \text{ Watts-cm}^2 \quad ,$$

$$c_2 = hc/k = 1.44 \text{ cm°K} \quad .$$

The assumption of LTE is a statement that the ratio of the emission to absorption coefficients, $\frac{j_\lambda}{\kappa_\lambda}$, is only dependent on the local value of temperature and is equal to the Planck function.

One immediate result of the solution in Equation 2.1.10 becomes apparent when considering the case of limb darkening, which is the fact that in visual wavelengths, the Sun is brighter at the center than near

the limb. From the properties of Equation 2.1.10, little radiation emerges from deeper than $u/\mu = 1$. Therefore, when observing the solar surface near disk center ($\mu = 1$) one sees deeper into the brighter, hotter regions, whereas near the solar limb ($\mu \rightarrow 0$) one sees into the higher cooler regions of the Sun.

2.2 Opacity in the Solar Photosphere

Since the temperature of the photosphere is much lower than the interior regions of the Sun, it is possible for hydrogen ions to recombine and form neutral hydrogen. Furthermore, due to its large polarizability, hydrogen can form a negative ion, H^-, consisting of one proton and two electrons. Since this ion has a single bound state with a binding energy of 0.754 eV, this ion cannot exist at high temperatures. H^- is the dominant contributor to the opacity in the atmosphere of cooler stars with temperatures $T \lesssim 10^4$ K (Mihalas, 1978).

Photons travel through the photosphere via both bound-free and free-free processes. In particular, these reactions are

$$h\nu + H^- \underset{\leftarrow}{\overset{\rightarrow}{}} H + e \qquad 2.2.1$$

and

$$H + e + h\nu \underset{\leftarrow}{\overset{\rightarrow}{}} H + e \qquad 2.2.2$$

respectively. In these relations $h\nu$ is the photon energy.

The threshold for the bound-free process is at about 1.65μ which corresponds to the detachment energy. In the free-free process an electron passes near a neutral hydrogen atom and in doing so it temporarily induces a dipole moment. This dipole can interact with the radiation field leading to other absorption and emissions.

The relative contributions of the bound-free, H^-_{bf}, and free-free, H^-_{ff}, processes to the opacity change in the spectral region under study. For example, at 0.5 μ, ≈ 90% of the opacity is due to the bound-free process, and at 1.65 μ, the contribution of H^-_{bf} is zero and H^-_{ff} dominates by contributing ≈ 80% to the opacity (Vernazza, Avrett, and Loeser, 1976).

The H^- free-free absorption coefficient is given by (Vernazza, Avrett, and Loeser, 1976)

$$\kappa(\lambda) = 4.5791\times10^{-40} n_e n_{H1} \lambda [1 + 10.631\lambda(1 - 594.15/T)] \qquad 2.2.3$$

where n_e is the electron density and n_{H1} is the density of hydrogen. The H^- bound-free absorption coefficient is given by (Vernazza, Avrett, and Loeser, 1976)

$$\kappa(\lambda) = n_{H^-}\sigma(\lambda)\times10^{-17}\left[1 - \frac{1}{b_{H^-}} e^{-(c_2/\lambda T)}\right] \qquad 2.2.4$$

where

$$n_{H^-} = 1.0354\times10^{-16}\, b_{H^-}\, n_e n_{H1} T^{-3/2}\, e^{-8762/T} \qquad 2.2.5$$

$\sigma(\lambda)$ is the photoionization cross section and is zero for $\lambda \geq 1.65\ \mu$, which corresponds to the energy required to ionize the hydrogen ion. b_{H^-} is the departure coefficient and is essentially unity in all regions where H^- is an important absorber. That is, the assumption of LTE is valid in this region since the source function and the Planck function are essentially the same.

2.3 The Wavelength Dependence of I'_λ in the Continuum

When measuring the solar radiation intensity, fluctuations in the optical transmission of the Earth's atmosphere introduce fluctuations in the measured radiation intensity at all wavelengths of the visible to near infrared spectrum. As previously mentioned, other researchers have been unsuccessful in detecting solar oscillations by measuring intensity fluctuations near disk center. Difficulty arises in measurements of this type because of the contributions of the Earth's atmosphere to the measured value of intensity. If the solar radiation intensity is measured in the visible to near infrared continuum, fluctuations in the optical transmission of the terrestrial atmosphere would give rise to changes in the spectral curve that are distinctly different from the changes in the radiation intensity due to perturbations in the temperature of the Sun. The changes that are solar in nature would give rise to an increase or decrease in the slope of the logarithm of the radiation intensity vs. wavelength curve. However, fluctuations in the optical transmission of the Earth's atmosphere do not lead to changes in the slope of the ln(I) vs. λ curve (Elder and Strong, 1953; cf. Chapter

5). Therefore, the undesirable atmospheric effects can be reduced by making use of this information.

Solar oscillations are typically described through the basic equations by introducing a small perturbation of the fluid parameters. One way of describing this method is known as the Eulerian perturbation. The Eulerian perturbation, denoted by a prime ('), is the difference between the perturbed and unperturbed fluid flow at a given position and time. If a physical quantity is denoted by f, the Eulerian perturbation of that quantity is expressed by

$$f'(\mathbf{r},t) = f(\mathbf{r},t) - f_0(\mathbf{r}) \qquad 2.3.1$$

where the subscript 0 refers to the unperturbed quantity.

Using this as a basis, the linearized perturbation of Equation 2.1.7 can be written in Eulerian form as

$$\mu \frac{dI'_\lambda}{d\tau_\lambda} = (I' - S') + \frac{(\rho\kappa)'}{\rho\kappa}(I - S) \qquad 2.3.2$$

where products of the perturbed quantities have been neglected. The solution of this equation is obtained by using the same integrating factor, $e^{-\tau_\lambda/\mu}$, that was used to solve Equation 2.1.6. Thus, the solution to Equation 2.3.2 is

$$I'_\lambda = \int_0^\infty \left[S'_\lambda - \frac{(\rho\kappa)'}{\rho\kappa}(I_\lambda - S_\lambda)\right] e^{-\tau_\lambda/\mu} \, d\tau_\lambda/\mu \qquad 2.3.3$$

The integral in Equation 2.3.3 has been evaluated using one-point Gaussian quadrature and written in terms of T'/T:

$$I' = \left[S_\lambda S_T\left(\frac{T'}{T}\right)\right]_{u_1} - \frac{(\kappa_\lambda \rho)}{\kappa_\lambda \rho}\left[S_\lambda(u_1) - S_\lambda(u_2)\right] \qquad 2.3.4$$

with

$$\frac{(\kappa_\lambda \rho)'}{\kappa_\lambda \rho} = (\kappa_T - \delta_T)\frac{T'}{T} + (\kappa_P + \alpha)p \qquad 2.3.5$$

where $u_1/\mu = 1$ and $u_2/\mu = 2$ are the roots for the two one-point Gaussian quadrature integrations. The following definitions apply for Equations 2.3.4 and 2.3.5:

$$S_T = \left[\frac{d(\ln S_\lambda)}{d(\ln T)}\right] \quad , \qquad 2.3.6$$

$$\kappa_T = \left[\frac{\partial(\ln \kappa_\lambda)}{\partial(\ln T)}\right]_P \quad , \qquad 2.3.7$$

$$\kappa_p = \left[\frac{\partial(\ln \kappa_\lambda)}{\partial(\ln P)}\right]_T \quad , \qquad 2.3.8$$

$$\delta_T = \left[\frac{\partial(\ln \rho)}{\partial(\ln T)}\right]_P \quad , \qquad 2.3.9$$

$$\alpha = \left[\frac{\partial(\ln \rho)}{\partial(\ln P)}\right]_T \quad , \qquad 2.3.10$$

$$p = \frac{P'}{\rho g r} \qquad 2.3.11$$

where ρ and P are the equilibrium density and pressure.

The wavelength dependence of the Eulerian perturbation in the radiation intensity is primarily through the interference of the source function and the opacity terms in Equation 2.3.4. Since $\kappa_T > 0$ in the low photosphere, and $S_\lambda(u_1) - S_\lambda(u_2) > 0$, then clearly the S_T and κ_T are competing in Equation 2.3.4 tending to make I' small. However, if the temperature dependence of S_T and κ_T changes as λ changes from 0.5 μ to 1.6 μ, then the interference of the two terms will lead to an I' that has an enhanced sensitivity to changes in wavelength.

If an instrument is to be designed to measure these changes, it becomes necessary to determine the magnitude of I'. In order to evaluate I', the magnitudes of T'/T and p must be known. The relative values have been obtained theoretically through the work of Logan (1984). The results of that work show that $\frac{p}{T'/T} \sim 10^{-4}$ so that the second term on the right hand side of Equation 2.3.5 can be neglected to the accuracy of the calculations desired here. The magnitude of T'/T has been determined at SCLERA to be $\sim 10^{-4}$ (Hill, 1984; Hill and Rosenwald, 1986). Evaluating I' at $\lambda = 0.5\ \mu$ and $\lambda = 1.6\ \mu$ yields

$$\frac{I'_{0.5}}{I} \approx 7.4 \times 10^{-5} \quad , \qquad 2.3.13$$

$$\frac{I'_{1.6}}{I} \approx -5.3 \times 10^{-5} \quad .$$

The striking feature about this result is that the changes in I' are in opposite directions at the two different wavelengths. This, of course, is not surprising if the properties of S_T and κ_T are taken into consideration. Assuming LTE, S_T is given by

$$S_T = B_T = \frac{d(\ln B_\lambda)}{d(\ln T)} = \frac{c_2}{\lambda T}\left(1 - e^{-c_2/\lambda T}\right)^{-1} \qquad 2.3.14$$

where B_λ is the Planck function given in Equation 2.1.11. At 0.5 μ, $S_T = 5.02$, and at 1.6 μ, $S_T = 1.97$. The logarithmic derivative of the opacity, κ_T, is determined from Figure 2.2 and Equations 3.2.4 and 3.2.5. For $\lambda = 0.5$ μ, at a height in the solar atmosphere where the optical depth $\tau_{0.5} = 1$, the log of the pressure, log P = 5.12 (Gingerich, et. al., 1971), so that from Figure 2.2, $\kappa_T = 8$ at $\lambda = 0.5$ μ. At $\lambda = 1.6$ μ, $\kappa_T = 11$. Therefore, in going from $\lambda = 0.5$ μ to $\lambda = 1.6$ μ, the temperature dependence of S, S_T, decreases by more than three while the temperature dependence of κ, κ_T, increases by approximately three. This effect will give rise to wavelength dependent changes in I' (described quantitatively in Equation 2.3.4) that are plainly different from the changes in the signal measured at the Earth's surface due to fluctuations in the transparency of the Earth's atmosphere (cf. Chapter 5).

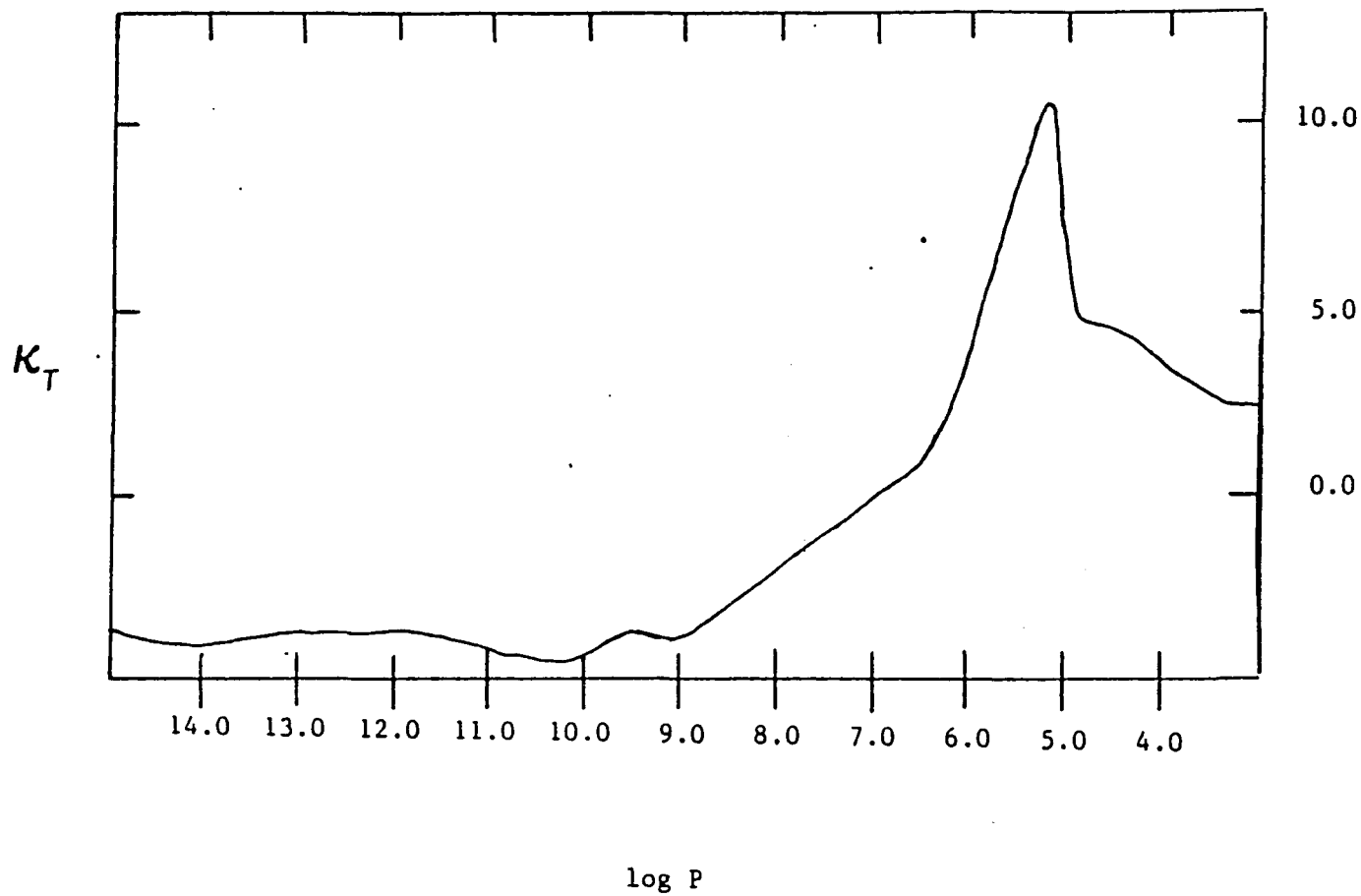

Figure 2.2. The logarithmic derivative of opacity by temperature, κ_T. (Reproduced from Ando and Osaki, 1975).

CHAPTER 3

INSTRUMENTAL DESIGN

To design and build an instrument to measure the changes in the Eulerian perturbation of the solar radiation intensity, J', where

$$J' = I'(\mu) Y_{\ell}^{m}(\theta, \phi) \quad , \qquad 3.1$$

several factors must be considered. One of the most important considerations comes from the discussion of Chapter 2. From that chapter it was demonstrated that perturbations in the radiation intensity along the continuum give rise to wavelength dependent shifts in the spectral curve distinctly different from that produced by the Earth's atmosphere. Since a clear distinction can be made between these two effects, changes in the signal due to atmospheric effects can be significantly reduced, thereby increasing the probability of successfully measuring solar oscillations near disk center. However, in order to measure changes in slope of the logarithm of the intensity vs. wavelength curve, it is necessary to design an instrument capable of scanning a wide spectral range. On the other hand, since a general trend in the changes of slope along this curve are sought, a relatively low spectral resolution is adequate.

Of course, cost and compactness must also be considered in the design of this instrument. In this case it is of particular interest

that this design be one that is reasonably small and lightweight since it is to be mounted on an existing telescope (cf. Section 4.1).

3.1 Choice of Dispersing Element

Because of the need to scan a very large wavelength range, $0.5 \leq \lambda \leq 1.7$ μ, a conventional diffraction grating spectrometer was ruled out. This is due to the overlapping of the shorter wavelengths of a higher order of diffraction with the longer wavelengths of a lower order of diffraction. The order of diffraction is given by

$$m = (d/\lambda)\sin(\theta) \qquad 3.1.1$$

where d is the groove spacing, λ is the wavelength, and θ is the angle of diffraction with respect to the undiffracted beam. The overlap for a typical grating in this wavelength range is illustrated by Table 3.1. This difficulty could possibly be circumvented by using a combination of filters and multiple gratings. However, this would be at the risk of greatly complicating the design and increasing the cost.

A prism-type spectrometer was found to possess all of the desirable characteristics previously mentioned which are required to successfully measure J'. Since the problem of overlapping spectral orders is non-existent when using a prism, a wide spectral range may be scanned provided the transmission properties of the prism material remain favorable in the region of interest.

Since the Sun radiates approximately like a blackbody, especially in the spectral region considered in this dissertation, the

Table 3.1. Overlapping orders of diffraction for a 300 grove/mm diffraction grating.

θ degrees	Wavelength (μ) m = 1	m = 2	m = 3	m = 4
10	0.58			
15	0.86			
20	1.14	0.57		
25	1.41	0.70		
30	1.67	0.83	0.56	
35		0.96	0.64	
40		1.07	0.71	0.54
45		1.18	0.79	0.59
50		1.28	0.85	0.64
55		1.37	0.91	0.68
60		1.44	0.96	0.72
65		1.51	1.01	0.76
70		1.57	1.04	0.78

solar radiation intensity decreases by about a factor of six from 0.5 to 1.7 μ. From the discussion in Chapter 5, it would be more favorable if the time-averaged signal remained approximately constant over this wavelength range. This feature would also be desirable from a design standpoint. The light signal is converted to a voltage via a lead sulfide detector and digitized on an analog-to-digital converter, A/D (cf. Section 4.1). However, if the detector properties of the system are chosen such that the time-averaged voltage did not change appreciably over the wavelength range of $0.5 \leq \lambda \leq 1.7$ μ, higher AC gains may be used in the electronics at the frequencies of the solar oscillations. This would result in a greater sensitivity to the changes in the radiation intensity.

3.2 Discussion of Operation

The basic design of the telescope/spectrometer is given in Figure 3.1. The portion of the schematic drawing that is enclosed in bold lines is the spectrometer. Care should be taken to isolate this part of the instrument from undesirable light sources. Therefore, the inside walls of the spectrometer were covered with black velvet to reduce the level of scattered light. Furthermore, the detectors, D_1 and D_2, were baffled in order to limit their fields of view.

Light from the Sun enters the Newtonian telescope at A_1. The image is then focused by the primary mirror onto the entrance pupil of the spectrometer, A_2, after passing through an image rotator, R . The size of aperture A_2 was selected so that a 200 x 400 arcsec slice of the central region of the Sun is allowed to enter the spectrometer (see

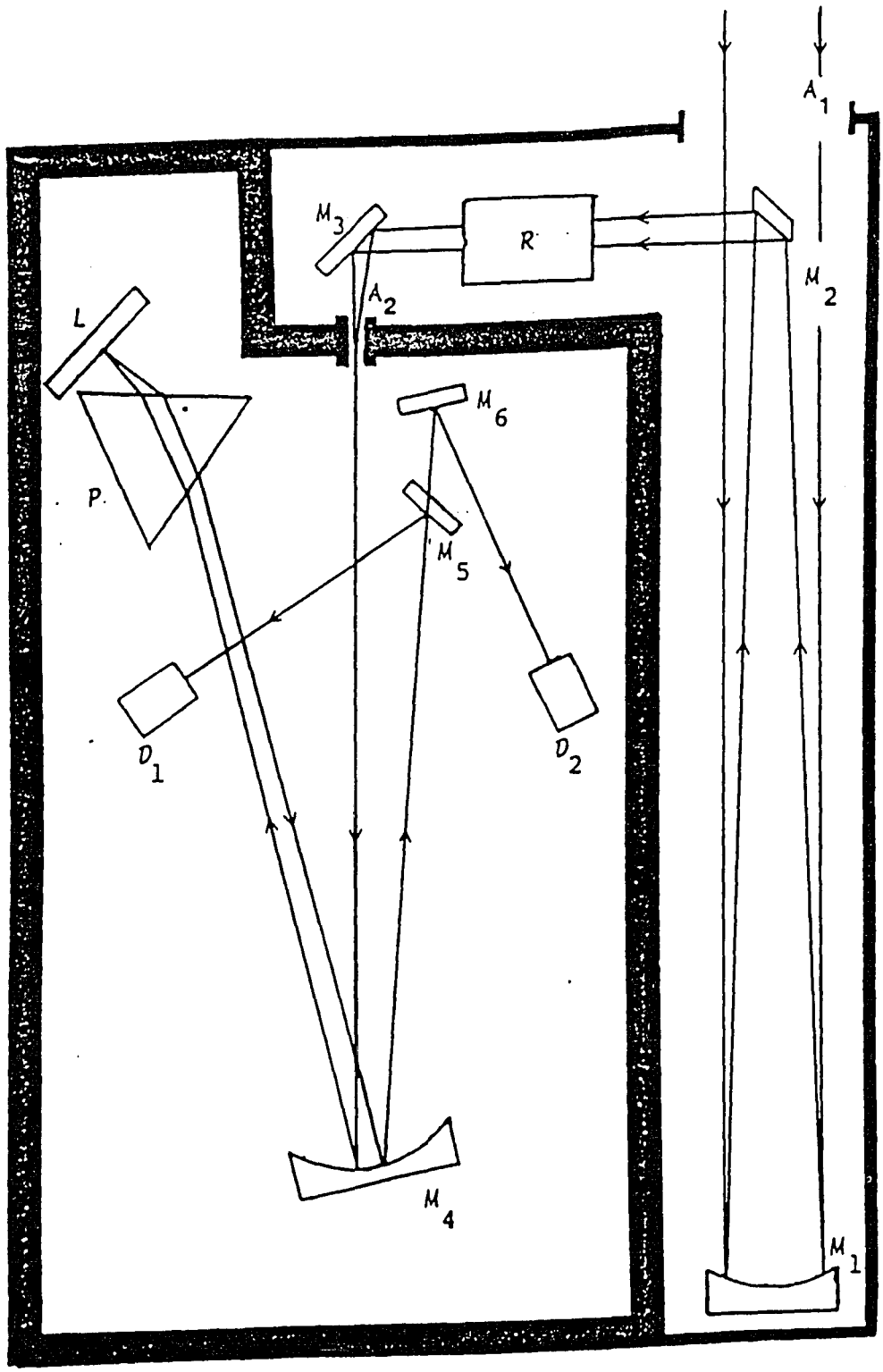

Figure 3.1. Schematic diagram of the telescope/spectrometer.

Figure 3.2). This light is collimated by a spherical mirror, M_4, and doubly dispersed by passing through the prism twice. The wavelengths from 0.5 to 1.7 μ are selected by rotating the Littrow mirror, M_5 through an angle θ. To scan the appropriate spectral range mentioned above, a rotation through an angle $\theta \approx 1.75^{\circ}$ was required. Finally the light returns to the collimator and the image of A_2 is focused on the two lead sulfide detectors, D_1 and D_2. The detectors are positioned such that a 200 x 200 arcsec section of the image of the solar disk enters each detector. This is illustrated in Figure 3.2, where the shaded area falls on D_1 and the unshaded area falls on D_2.

Upon careful inspection, one may notice this design is not free from secondary reflections that will cause a mixing of the shorter wavelengths with the longer ones. For example, suppose the Littrow mirror, L, is positioned such that a particular wavelength λ_0 is selected to enter the two detectors. Because the index of refraction of the prism increases with decreasing wavelength, there will exist another wavelength λ_1 (with $\lambda_1 < \lambda_0$) such that λ_1 will return to the collimator at the appropriate angle to be reflected back to the prism a second time. Upon leaving the prism once more, λ_1 will follow the same path as λ_0. For this particular arrangement it was calculated that if $\lambda_0 \approx 1.5$ μ then $\lambda_1 \approx 0.5$ μ. Of course, the contamination at the shorter wavelengths would be small for two reasons: 1) the radiation has passed through the prism two more times thereby increasing the dispersion, and 2) the radiation at these shorter wavelengths would not be in focus at the focal plane. However, this problem was avoided by simply designing the spectrometer so that M_5 and M_6 do not lie in the plane defined by

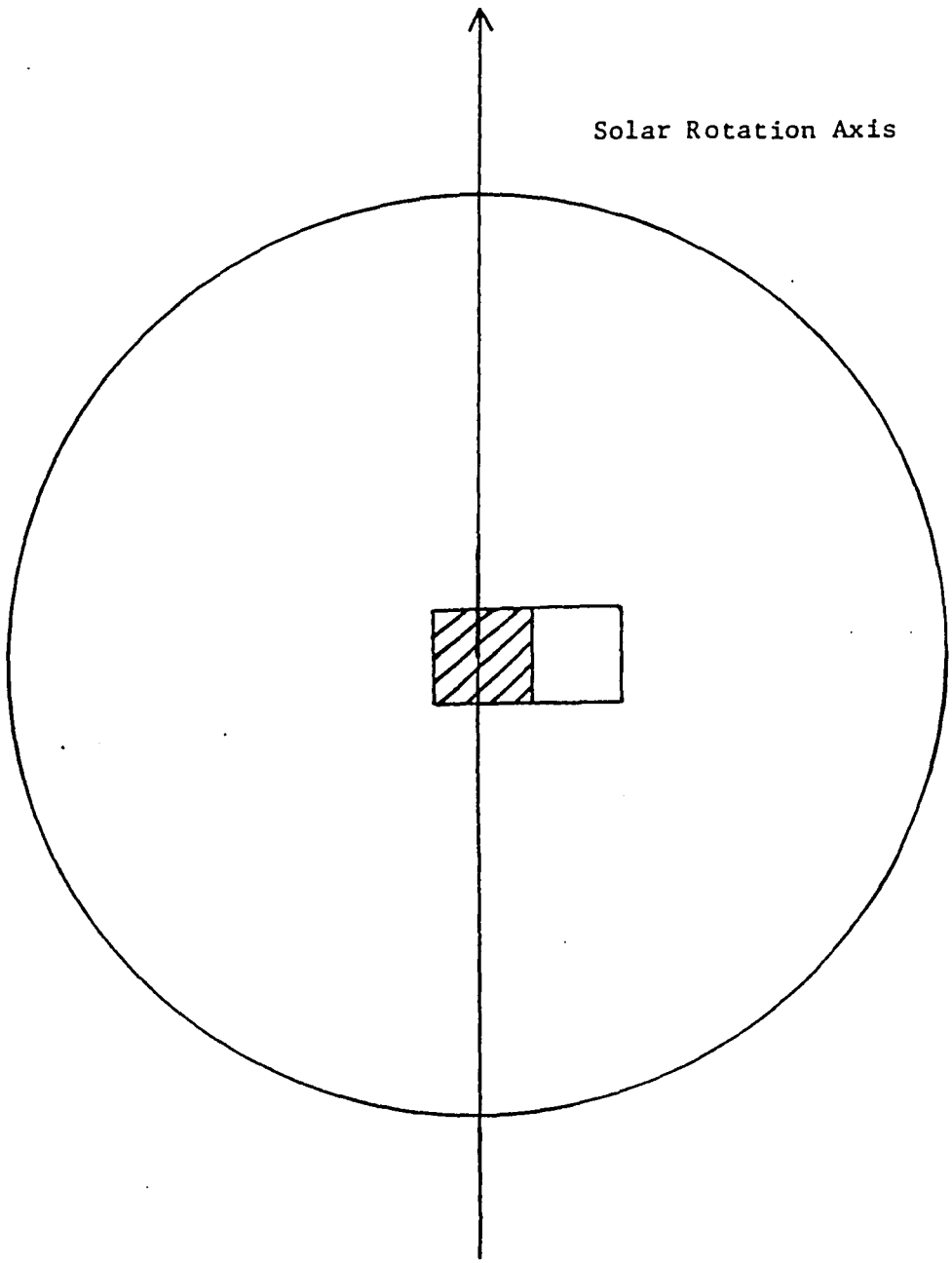

Figure 3.2 1985 detector geometry.

A_2, M_4, and the normal to M_4. With this configuration, the shorter wavelengths that returned to the prism were blocked by a black absorber placed on top of the prism.

3.3 Resolution

The width of the 200 x 400 arcsec aperture is intimately related to the resolution of the spectrometer. Indeed, it is precisely this width coupled with the dispersion of the prism that determines the resolution. The resolution, $\Delta\lambda$, at a given wavelength, λ, is given by

$$\Delta\lambda = \frac{w}{f_c (d\theta/d\lambda)_\lambda} \qquad 3.3.1$$

where w is the width of the aperture, f_c is the focal length of the collimator, and $(d\theta/d\lambda)_\lambda$ is the angular dispersion of the prism at a particular wavelength λ. As previously mentioned, it would be desirable to "flatten" the signal curve in the region of interest. By choosing the proper prism material, it would be possible to have a higher dispersion at the shorter wavelengths relative to that at the longer wavelengths, thereby decreasing the net energy entering a fixed aperture at the shorter wavelengths relative to that at the longer wavelengths. Several materials were considered and BK-7 was determined to have a dispersion with the desired wavelength dependence as well as a transparency to the radiation in the visible to near-infrared. Referring to Table 3.2 we see that BK-7 does have the required dispersion mentioned above. The percent transmission through 10 mm of

Table 3.2. Index of refraction and dispersion for BK-7.

Wavelength (μ)	Index of Refraction (n)	$\frac{dn}{d\lambda}$ (μ^{-1})
0.5	1.5214	0.0665
0.6	1.5163	0.0395
0.7	1.5131	0.0266
0.8	1.5108	0.0198
0.9	1.5090	0.0161
1.0	1.5075	0.0140
1.1	1.5062	0.0128
1.2	1.5049	0.0122
1.3	1.5037	0.0120
1.4	1.5025	0.0120
1.5	1.5013	0.0122
1.6	1.5001	0.0125
1.7	1.4988	0.0129

BK-7 is shown in Figure 3.3. The dip in the transmission curve at approximately 1.38 μ is attributed to an OH bond resonance which corresponds to the atmospheric water vapor absorption line observed in the data (cf. Chapter 4, Figure 4.2)

3.4 Theoretical Limit to the Resolution of the Spectrometer

For any spectrometer it is important to determine the limit to its resolution. To determine the resolution here we will use Rayleigh's criterion.

The angular separation of the first diffraction minima is

$$\omega = 2\lambda/D \qquad 3.4.1$$

where λ is the wavelength of the incident radiation, and D is the clear aperture (see Figure 3.4). The angle subtended by a slit, Δx, at a distance f from the collimating mirror is given by

$$\gamma = \Delta x/f \qquad 3.4.2$$

Next, the quantity α is defined by

$$\alpha \equiv \gamma/\omega = \frac{\Delta x/f}{2\lambda/D} = \frac{\Delta x}{2\lambda}\frac{1}{F} \qquad 3.4.3$$

where F is the f-number of the collimator. Of course, when $\alpha = 1$ the geometric image of the slit just fills the principal diffraction

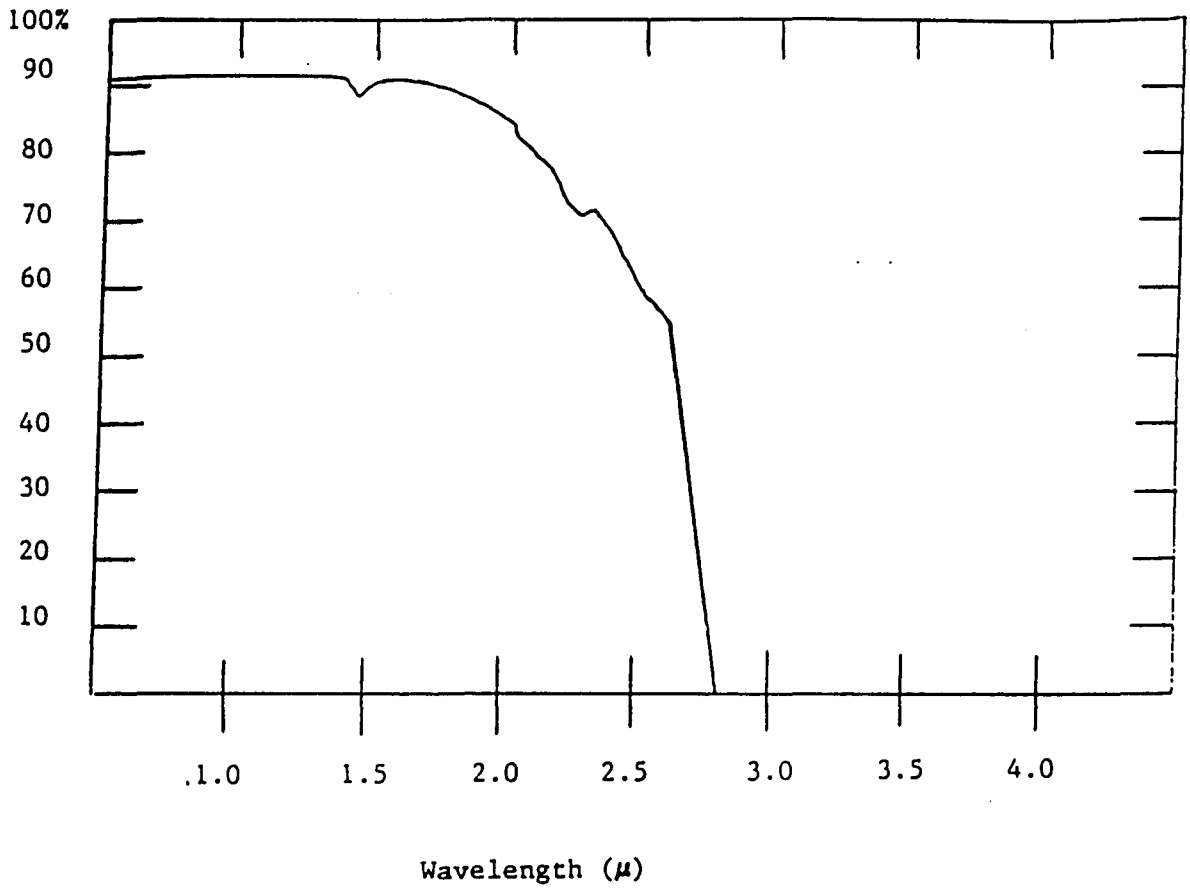

Figure 3.3. Transmission curve for BK-7.

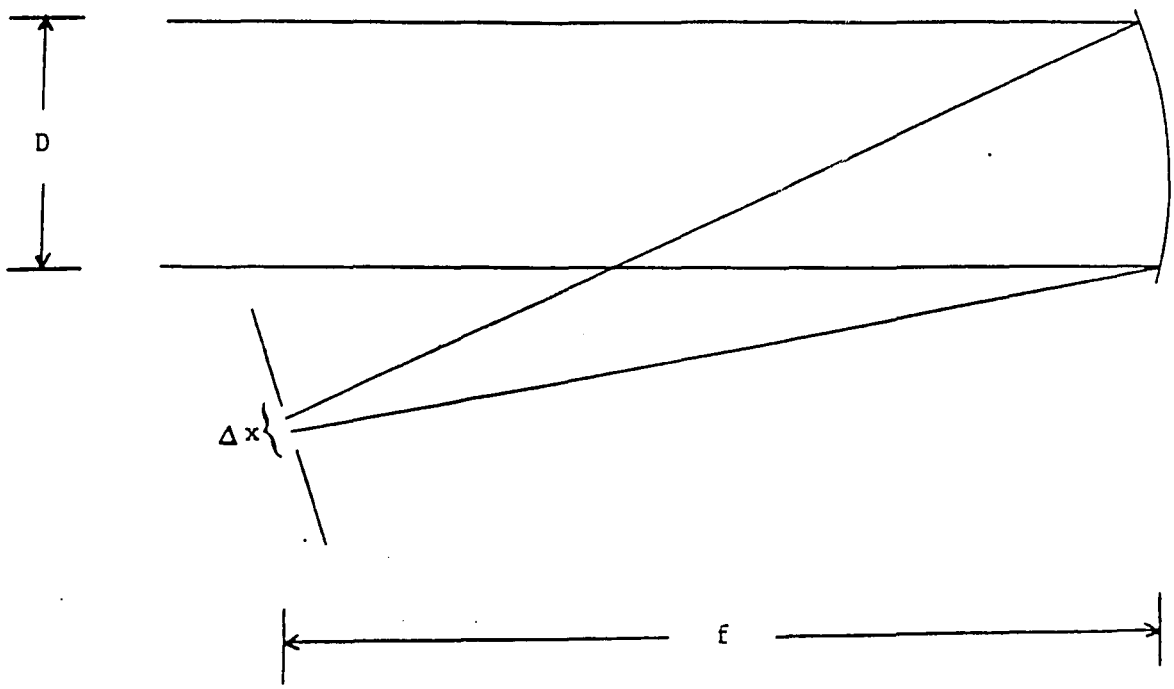

Figure 3.4. Simple model for determining resolution limit.

maximum, so that the geometric angular width of the slit image, $\Delta\theta$, at a distance f from the objective is

$$\Delta\theta = 2\lambda/D \quad . \qquad 3.4.4$$

Since α is just the measure of the angle subtended by the slit, α is by definition unaffected by diffraction. The angular width of the slit image at full width at half maximum is

$$\Delta\theta = 2\lambda\beta/D \qquad 3.4.5$$

where $\beta = \alpha + h(\alpha)$. The function β was introduced in order to allow for corrections in the extension of the slit image beyond the geometric image of the slit arising from diffraction so that $h(\alpha) << \alpha$ when $\alpha >> 1$. Therefore, the range of wavelengths entering the aperture, $\Delta\lambda$, can be obtained by letting

$$\Delta\lambda = (\Delta\lambda/\Delta\theta)\Delta\theta = D(\Delta\theta/R) \qquad 3.4.6$$

where R is defined by

$$R \equiv D(\Delta\theta/\Delta\lambda) \quad . \qquad 3.4.7$$

Thus, the expression for $\Delta\lambda$ becomes

$$\Delta\lambda = 2\lambda\{\alpha + h(\alpha)\}/R \quad . \qquad 3.4.8$$

Using Rayleigh's criterion, we require that the principal diffraction maximum of a particular wavelength, λ_1, fall at the same angle as the first diffraction minimum of wavelength λ_2. In this case, for a square aperture, the angular separation between the principle maximum and the first minimum in the diffraction pattern is

$$\delta\theta = \lambda/D \quad . \qquad 3.4.9$$

When $\Delta\lambda/2 = \delta\lambda$, we see from Equation 3.4.7 that

$$\delta\lambda = \lambda\{\alpha + h(\alpha)\}/R \quad , \qquad 3.4.10$$

or

$$\lambda/\delta\lambda = pR \quad , \qquad 3.4.11$$

where

$$p \equiv \{\alpha + h(\alpha)\}^{-1} \quad . \qquad 3.4.12$$

The value of p, of course, depends on the width of the aperture and its dependence is determined by integrating over the principal diffraction maximum. However, if α is sufficiently large (typically $\alpha \geq 2$; Conn, 1956), then

$$p = 1/\alpha \quad . \qquad 3.4.13$$

For the instrument described in Section 3.2, p and $pR = \lambda/\delta\lambda$ are tabulated for the spectral region under study in Table 3.3. From this we see that the spectrometer is operating well within the geometric limits.

3.5 Discussion of the Sensitivity of the Spectrometer and its Dependence on Wavelength

Because the changes in the Eulerian perturbation in the radiation intensity, , due to oscillations are very small (on the order of 1 part in 10^5) it is necessary to design a spectrometer with a relatively high sensitivity. The sensitivity is highly dependent on the detector used. The detectors chosen for this experiment were composed of lead sulfide which are classified as photoconductors. Clearly, the inverse of the noise equivalent power (NEP) should be larger than the oscillatory signal being measured. The NEP is defined as the signal power required to produce a signal-to-noise ratio of one, where the root mean square noise is measured in a 1 Hertz bandwidth. The NEP for the lead sulfide detectors used in this experiment is tabulated as a function of wavelength in Table 3.4.

One must exercise caution in using the NEP listed for determining the sensitivity of a particular detector. The lower limit to the detector's sensitivity is set by the fluctuations in the background radiation, B_{fl}. Using Poisson statistics, this lower limit is

$$B_{fl} \geq \frac{hc}{\lambda}(2\dot{n})^{1/2} \qquad 3.5.1$$

Table 3.3. Resolution for the spectrometer.

λ (μ)	R	p	$pR = \frac{\lambda}{\delta\lambda}$
0.5	5690	0.010	56.9
0.6	3257	0.012	39.1
0.7	2182	0.014	30.5
0.8	1622	0.016	26.0
0.9	1314	0.018	23.7
1.0	1139	0.020	22.8
1.1	1043	0.022	22.9
1.2	993	0.024	23.8
1.3	974	0.026	25.3
1.4	974	0.028	27.3
1.5	987	0.030	29.6
1.6	1007	0.032	32.2
1.7	1036	0.034	35.2

Table 3.4. D^* and NEP for the PbS detectors.

Wavelength (μ)	$D^* \left(= \frac{\sqrt{\text{Detector Area}}}{\text{NEP}}\right)$ $\left(\frac{\text{cm-(Hz)}^{1/2}}{\text{Watts}}\right)$ $(\times 10^{10})$	NEP $(\times 10^{-12})$ $\left(\frac{\text{Watts}}{(\text{Hz})^{1/2}}\right)$
0.5	0.40	5.6
0.6	0.44	5.1
0.7	0.48	4.7
0.8	0.52	4.3
0.9	0.56	4.0
1.0	0.60	3.8
1.1	0.64	3.5
1.2	0.68	3.3
1.3	0.72	3.1
1.4	0.76	3.0
1.5	0.80	2.8
1.6	0.84	2.7
1.7	0.88	2.6

where $\dot{n}$ is the number of background plus signal photons incident on the detector per second, h, c, and λ are Planck's constant, the speed of light, and wavelength respectively. Therefore, in order to determine if the spectrometer is subject to photon noise limitations, $\dot{n}$ must be calculated at the location of the lead sulfide detectors.

To facilitate this calculation we will refer to Figure 3.1. The irradiance at the entrance of the spectrometer, A_2, is

$$F_\lambda = (1-r)W_\lambda \frac{\pi(D^2 - d^2)}{\pi S^2} \qquad 3.5.2a$$

$$= \frac{(1-r)W_\lambda}{4F_{eff}^2 \tan^2 u} \qquad 3.5.2b$$

where r is the fractional loss due to reflectance, S is the image size of the Sun, W_λ is the irradiance at the Earth's surface, and u is the semi-diameter of the Sun in degrees. The quantity F_{eff} is the effective f-number of the system and is given by

$$F_{eff} = F(1 - (d/D)^2)^{1/2} \qquad 3.5.3$$

where d is the diameter of M_2, while F and D are the f-number and diameter of the primary M_1. If t is the fractional transmission through the spectrometer, then the irradiance at the detectors is given by

$$F_\lambda^{det} = \frac{t(1-r)W_\lambda}{4F_{eff}^2 \tan^2 u} \ell w \qquad 3.5.4$$

where ℓ and w are the length and width of the aperture. For this instrument, the magnification of the spectrometer is one, so that the values for ℓ and w are the dimensions of A_2. Therefore, the power at the detectors in a given wavelength range, $\Delta\lambda$, is

$$P_\lambda^{det} = \int F_\lambda^{det} d\lambda = \frac{t(1-r)}{4F_{eff}^2 \tan^2 u} \ell w \int_{\lambda_0 - \Delta\lambda/2}^{\lambda_0 + \Delta\lambda/2} W_\lambda d\lambda \qquad 3.5.5$$

where $\Delta\lambda$ is determined by Equation 3.3.1. Since $\Delta\lambda$ is typically small, the integral in Equation 3.5.5 is approximated by letting

$$I = \int W_\lambda d\lambda \approx W_\lambda \Delta\lambda \qquad 3.5.6$$

so that the power at the detectors for a given wavelength is

$$P_\lambda^{det} \approx \frac{t(1-r)}{4F_{eff}^2 \tan^2 u} lw^2 \frac{d\lambda}{f_c d\theta} W_\lambda \qquad 3.5.7$$

Therefore, $\dot{n}$ is determined by

$$\dot{n} = \frac{\lambda}{hc} P_\lambda^{det} \qquad 3.5.8$$

which, from Equation 3.5.1 we have

$$B_{fl} \geq \left(2 \frac{hc}{\lambda} P_\lambda^{det}\right)^{1/2} \qquad 3.5.9$$

The solar radiation intensity very closely approximates that of a blackbody radiating at 5770°K (cf. Section 2.1). Therefore, the Planck function, $B_\lambda(T)$, can be used to estimate W_λ. Then

$$W_\lambda = B_\lambda(T)\ (R_s/R_{es}) = \frac{c_1}{\lambda^5(e^{c_2/(\lambda T)} - 1)}\ (R_s/R_{es})^2 \qquad 3.5.10$$

where R_s is the radius of the Sun and R_{es} is the distance between the earth and the Sun. Atmospheric extinction is not considered since it does not affect the results to the accuracy of the calculations necessary.

The value of $d\theta/d\lambda$ in Equation 3.5.7 is determined (for a 60° prism) using

$$d\theta/d\lambda = \frac{\sqrt{3}/2\ n_\lambda}{\cos(r)(n_\lambda^2 - \sin^2 i)^{1/2}}\ dn/d\lambda \qquad 3.5.11$$

where

$$\sin(r) = .5\ (\ [3(n_\lambda^2 - \sin^2 i)]^{1/2} - \sin(i)\ ) \qquad 3.5.12$$

where $dn/d\lambda$ is given in Table 3.2 and n_λ is the index of refraction at wavelength λ. The quantity i is the angle of incidence of the incoming ray, while r is the angle of the ray exiting the prism. Both angles are measured with respect to their respective surface normals. Since Equation 3.5.11 is the dispersion of one passage through the prism, the

value of $d\theta/d\lambda$ in Equation 3.5.7 is approximately twice the dispersion given in Equation 3.5.12. Therefore, from Equations 3.5.7, 3.5.9, 3.5.10, and 3.5.11 the lower limit to the sensitivity of the detectors, B_{fl}, can be calculated. Using these results, B_{fl} is tabulated (cf. Table 3.5). Comparing this with Table 3.4, we note that the spectrometer is indeed photon noise limited, where the effects of the Earth's atmosphere have been neglected.

Table 3.5. Magnitude of the fluctuations in the background intensity.

Wavelength (μ)	B_{fl} ($\times 10^{-9}$) $\frac{\text{Watts}}{(\text{Hz})^{1/2}}$
0.5	5.2
0.6	3.8
0.7	3.1
0.8	2.8
0.9	2.6
1.0	2.6
1.1	2.7
1.2	2.8
1.3	3.0
1.4	3.1
1.5	3.3
1.6	3.7
1.7	4.0

CHAPTER 4

OBSERVATIONS

The main purpose of this work is to establish the effectiveness of detecting changes in the radiation intensity along the continuum. In later chapters the results from these observations will be presented along with some observational results from diameter measurements taken in 1978. For this reason, a brief description of the 1978 observations is included in Section 4.3.

4.1 Location of Equipment

The location selected for the testing of the telescope/spectrometer described in Chapter 3 was the Tumamoc Hill Observatory located approximately one mile west of Tucson, Arizona. This facility is 650 feet above the valley floor. The instrument for measuring the solar radiation intensity was mounted "piggyback" on the 21" f/5 reflecting telescope located at the Tumamoc Hill Observatory and the telescope driving system was used for tracking the Sun.

The existing system at the Tumamoc Observatory utilized the signals from a frequency generator to establish the motor speeds of the telescope drive for tracking purposes. For this experiment, it was desirable for the tracking system to be computer-controlled. Therefore,

the necessary interfacing was done so that the tracking could be completely controlled by a Digital Equipment Corporation LSI 11/02 computer.

A lead sulfide (PbS) detector monitored the radiation intensity near the center of the solar disk. This detector is a photoconductor (described in Section 3.5) and the radiation intensity was measured as a voltage across a load resistor mounted in series with the PbS detector. This signal was preamplified and then digitized by a 12-bit analog-to-digital, A/D, converter for use by the computers.

The expected fractional changes in the radiation intensity due to Eulerian perturbations were approximately one part in one hundred thousand. A 12-bit A/D is sufficient for measuring these changes to the required accuracy since the fluctuation in the intensity is greater than the one bit accuracy of the A/D.

Since the Sun was viewed through the Earth's atmosphere, signal changes which are solar in origin as well as changes due to fluctuations in the optical transmission of the Earth's atmosphere were measured. However, most atmospheric effects occur on a time scale typically much shorter than the period of the solar oscillations under study. Therefore, a low pass filter can be designed to discriminate against the undesirable higher frequencies and favor the lower frequency components of the signal which are solar in origin. The residual systematic atmospheric effects remaining in the data can be reduced by noting that changes in the solar signal are uniquely manifested as changes in the slope of the intensity vs. wavelength spectral curve; whereas changes in the intensity caused by fluctuations of the optical transmission of the

Earth's atmosphere give rise to essentially wavelength independent shifts of the entire spectral curve (cf. Chapters 2 and 5).

4.2 Observing Program

The data was collected over a 65-day period spanning March 23 to May 26, 1985. A total of 35 days of data were obtained and are listed in Table 4.1.[1] Two 200x200 arsec apertures were placed on the image of the solar disk. The first aperture was positioned on the center of the image, and the second aperture was positioned adjacent to the first along a line perpendicular to the solar rotation axis.[2] This arrangement is illustrated in Figure 3.2 and is described in more detail in Section 3.2.

The solar spectrum was scanned in the visible to near infrared region. A total of 48 data points were collected between $0.5 \leq \lambda \leq 1.7$ μ along the spectrum, and the intensity at each of the points was recorded as a function of the wavelength step. A single spectral curve consists of these 48 data points. A typical spectral curve is shown in Figure 4.1.

Each wavelength step along the spectrum required approximately 0.24 seconds. For each of these steps, the signal was sampled 16 times and the average intensity was recorded. Therefore, it required 11.52 seconds to complete a single spectral scan.

---

1. Additional data was accumulated until July 1, 1985, however, a detector failure occurred near June 1, 1985, and the quality of the data obtained after the failure has not been determined.

2. Only the information obtained from the aperture positioned near the center of the solar disk was used in this dissertation.

Table 4.1. Observations used for the 1985 data.

Day no.	Date	Length (hrs)	Starting Time (MST)
1	3/23/85	9.667	8.717
2	3/24/85	8.633	8.218
5	3/27/85	4.517	7.917
6	3/28/85	8.417	8.567
8	3/30/85	10.133	7.800
10	4/01/85	10.300	7.683
11	4/02/85	10.050	7.416
13	4/04/85	5.397	12.536
14	4/05/85	8.853	8.587
15	4/06/85	9.303	8.635
16	4/07/85	10.283	7.616
17	4/08/85	6.267	7.240
18	4/09/85	9.025	7.107
19	4/10/85	5.250	7.201
20	4/11/85	6.712	11.288
21	4/12/85	5.824	7.177
22	4/13/85	9.795	8.221
23	4/14/85	9.674	8.539
24	4/15/85	7.505	7.164
32	4/23/85	11.241	6.959
33	4/24/85	11.211	7.006
34	4/25/85	6.279	7.538
40	5/01/85	7.906	7.533
41	5/02/85	9.149	6.639
50	5/11/85	11.381	6.819
51	5/12/85	9.682	6.676
52	5/13/85	11.477	6.773
53	5/14/85	10.849	6.743
56	5/17/85	2.826	9.728
57	5/18/85	11.962	6.428
59	5/20/85	11.928	6.696
60	5/21/85	8.806	6.547
63	5/24/85	7.225	8.613
64	5/25/85	10.675	7.438
65	5/26/85	10.938	7.349

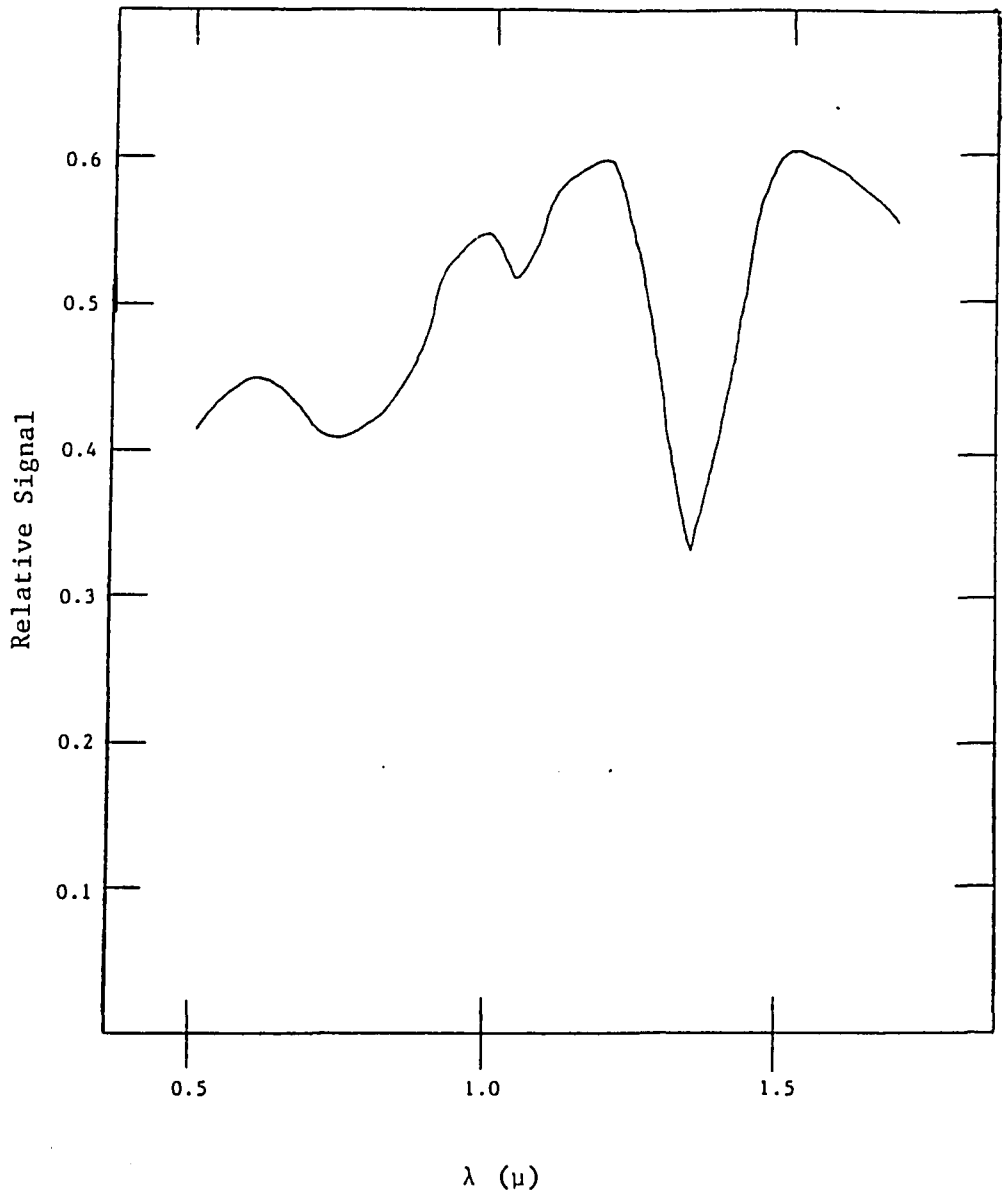

Figure 4.1. Typical Spectral Curve.

The cycling of the assembly language program that controlled the tracking of the telescope was used to calculate the length of time between each successive Littrow mirror step (or wavelength step). During each cycle a 32 bit register, R_1, was incremented and after 200 cycles the motor driving the Littrow mirror was stepped. To determine the cycling time of the assembly program, the total time of data acquisition for each day was divided by the number of counts accumulated in R_1 for that particular day. From this analysis, it was determined that the program cycled every 1.21 ms and, hence, the time required for each mirror step was 0.24 s. This result was calculated using the information obtained in the 18 days of observations between March 23 and April 23, 1985.

4.3 The 1978 Solar Diameter Observations

The 1978 observations have been described extensively in other works; therefore, only a brief description is offered here. The 1978 observations consist of 18 days of equatorial diameter measurements taken between May 21 and June 12, 1978. The diameter measurements consist of recording the relative separation between the positions of two diametrically opposed solar limbs. These positions were defined by the finite Fourier transform definition (FFTD) of an edge of the solar limb (Hill, Stebbins and Oleson 1975). More complete descriptions of the observations are given by Caudell et al. (1980) and Caudell (1980).

4.4 Spatial Filter Functions

Most of the tests performed in the following sections are comparisons of the 1985 data set with the 1979 observations (cf. Chapters 6, 7 and 8; Bos 1982; Hill 1984). For the low-degree gravity modes studied in Chapter 8, it is especially important to know how the detector sensitivity for these modes of oscillation depends on the detector geometry. Hill, Alexander, and Caudell (1985) have extensively studied the spatial filter function, w(m), for the 1979 differential radius observations and the results for $\ell \leq 5$ are given in Table 4.2.

From the 1985 detector geometry, the spatial filter function F is proportional to

$$F \propto \overline{Y_\ell^m}(\pi/2,0) \int_{-\Phi/2}^{+\Phi/2} \cos(m\phi)\, d\phi \qquad 4.4.1$$

where Φ is the heliocentric azimuthal angle that is subtended by the aperture of the instrument described in Chapter 3; and $\overline{Y_\ell^m}(\pi/2,0)$ is the average of the standard spherical harmonic over the heliocentric angle θ for the geometry of the aperture. For the instrument used in the 1985 observations, a 200 x 200 arcsec aperture was centered on the solar disk (cf. Section 3.2), so that in Equation 4.4.1, $\Phi \approx 0.2$.

From the work of Hill, Alexander, and Caudell (1985) we are able to write the ratio of the 1979 differential radius amplitudes to the 1985 intensity amplitudes as

Table 4.2. Spatial filter functions for the 1979 and 1985 observations.

m	w	sinc(m/10)	$\frac{w(m)}{w(0)} \frac{1}{\text{sinc}(\frac{m}{10})}$	$\frac{\overline{Y_{\ell}^{m}}}{\overline{Y_{\ell}^{m}}}\Big\|_{79}^{85}$
0	4.61	1.000	1.429	
1	5.23	0.998	1.596	
2	7.03	0.993	2.198	
3	9.87	0.985	3.101	
4	13.49	0.974	4.382	
5	17.60	0.959	5.782	

$$R(m) = k \frac{w(m)}{W(m)} \frac{\overline{Y_\ell^m(\pi/2,0)}\,|_{79}}{\overline{Y_\ell^m(\pi/2,0)}\,|_{85}} \qquad 4.4.2$$

where k is a proportionality constant and the integral in Equation 4.4.1 yields:

$$W(m) = \mathrm{sinc}(m/10) = \frac{\sin(m/10)}{(m/10)} \qquad 4.4.3$$

Since this ratio is proportional to w(m), and w(m) exhibits a strong dependence on m, it is meaningful to compare the expected behavior of R predicted by Equation 4.4.2 with that observed. Such a comparison should allow us to test the mode classifications by Hill (1984), Rabaey, Hill, and Barry (1986), and Rabaey and Hill (1987). If, for example, the m classifications are incorrect, no m dependence should be observed.

Using the results obtained from the 1985 observations, the tests in the m classifications are valid only for low ℓ values. This, of course, stems from the fact that the aperture was centered on the solar disk and not the solar equator (cf. Section 3.2). Therefore, for lower ℓ values, the radiation intensity measurements would be sensitive to even (ℓ+m), whereas for higher ℓ values, the measurements would be sensitive to both even and odd (ℓ+m). For this reason, the p- and f-modes, which consist of mostly high ℓ values, do not exhibit the symmetry properties that the low ℓ g-modes do.

CHAPTER 5

DATA REDUCTION

One major advantage inherent in measuring J' in the continuum in order to detect solar oscillations is its insensitivity to atmospheric effects as measured with the instrument developed here. The atmospheric attenuation of the radiation intensity is given by Beer's Law:

$$I_\lambda = I_{0\lambda} e^{-\tau_\lambda} \qquad 5.1$$

where $I_{0\lambda}$ is the radiation intensity outside of the Earth's atmosphere,

$$\tau_\lambda = \int k_\lambda ds \quad , \qquad 5.2$$

k_λ is the absorption coefficient per unit length, and s is the pathlength through the atmosphere in the direction of the line of sight. The work of Elder and Strong (1953) found that the dependence of τ_λ on wavelength is negligible outside of resonant absorption bands of the atmospheric gases for a clear day in the visible (i.e. no fog, mist, clouds, or smoke), so that most atmospheric effects are wavelength independent. Therefore, the effect of a change in atmosphere would give rise to an upward (or downward) shift of the entire spectral curve that is proportional to I_λ, or in other words,

$$\frac{dI_\lambda}{I_\lambda} = -d\tau_\lambda = \text{const.} \qquad 5.3$$

or

$$\frac{d(\ln I_\lambda)}{d\lambda} = 0 \quad . \qquad 5.4$$

On the other hand, the effects due to J' would be manifested as changes in the slope, $\frac{d(\ln I_\lambda)}{d\lambda}$, (cf. Chapter 2). However, there is one atmospheric effect that must be considered in this analysis. This is the resonant absorption of atmospheric gases, which is discussed in detail in the next section.

5.1 The Effects of the Earth's Atmosphere on the Observed Spectral Curve

In the spectral region under study, $0.5 \leq \lambda \leq 1.7$ μ, the water vapor absorption lines are of primary concern. The main reason for concern lies in the fact that the water vapor content in the atmosphere varies with time, which could introduce noise in the signal, while the contents of most other gases remain approximately constant (Goldberg, 1954) on the time scale of the daily observations. Furthermore, the major absorption bands evident in the spectral curve obtained in the 1985 data (see Figure 4.1) are identified as the 0.74, 0.94μ, 1.14μ, and 1.38μ water absorption lines.

Since the Eulerian perturbation in the radiation intensity, J', depends on wavelength, the solar oscillations will be observed in the

visible to near infrared continuum. These oscillations would give rise to changes in the slope, $\frac{d(\ln I_\lambda)}{d\lambda}$, of the spectral curve. The temporal changes in the slope along this curve due to J' could then be Fourier transformed to decompose the signal into its individual frequency components.

As previously mentioned, if the received signal s_λ by the observer is $I_\lambda g_\lambda$, it is possible to design g_λ such that s_λ is flattened, i.e.

$$\frac{d(\ln s_\lambda)}{d\lambda} = 0 \qquad 5.5$$

when $J' = 0$. Under these conditions, any changes in $\frac{d(\ln s_\lambda)}{d\lambda}$ due to would be straightforward to measure. However a typical spectral scan yields a curve with at least three major absorption lines. These absorption lines are due to terrestrial water vapor and should certainly be avoided when searching for changes in the radiation intensity that occur because of solar physics. Therefore, the first step must be to remove these unwanted lines from the spectral curve. Typically, this procedure involved determining where the wings of an individual line "ended" and then extending two or three more data points on both sides of the line as a conservative measure. Once these values have been determined, the unwanted absorption line plus the extra values on either side were removed. After this is performed on a given spectral curve for a particular day, a computer program could be implemented and given

this information to remove the absorption lines in all of the spectra obtained on that day.

5.2 Decomposition of the Data into its Frequency Components

Once the terrestrial water vapor lines were removed, the remaining portions of the spectral curves, s_λ, obtained on a particular day were fit with a polynomial using the least-squares method. In this analysis, a fourth order polynomial was fit to the data, with

$$s_\lambda = \sum_{i=1}^{4} a_i \lambda^i \qquad 5.2.1$$

where s_λ is the measured signal at wavelength λ, and the a_i's are determined from the fit. Upon completion of the above procedure, a method for quantifying the changes in s_λ with wavelength must be developed. Since slope changes are predicted due to the changing radiation intensity at different wavelengths (cf. Chapter 2), the expected course of action would be to decompose either the first or third order coefficients of the polynomial curve fit into a frequency spectrum. Consequently, the time series formed by the coefficient of the linear term was filtered, as described in the following paragraph, and then finally Fourier analyzed.

After performing the least-squares curve fits to the s_λ, the time series of the linear coefficients of those fits for each day were passed through two low pass rectangular filters. In the low pass filtering process, the data was averaged in a window containing 21 data

points. Next, the window was shifted three data points and another average was calculated. This procedure continued until the end of the data set was reached. Using this filtered data set, the data was then averaged in a window containing 7 data points. This window was then shifted 4 data points to obtain the average for the next point in the time series. As above, this procedure continued until the end of the data set was reached. The effective bandpass for both of these filters is 2.05 mHz.

For the analysis of the p- and f-modes discussed in Chapters 6 and 7, the data was additionally high pass filtered twice. A moving average of each successive 417 points was obtained using a rectangular window and this result was subtracted from the input data. This identical process was then repeated. The effective passband frequency in this case was 103.5 μHz. The high pass filtering described here was not done for the lower frequency g-mode analysis in Chapter 8. The resulting time series were then Fourier analyzed and the power spectra generated from this analysis (cf. Figures 5.1-5.9) are analyzed in the following sections.

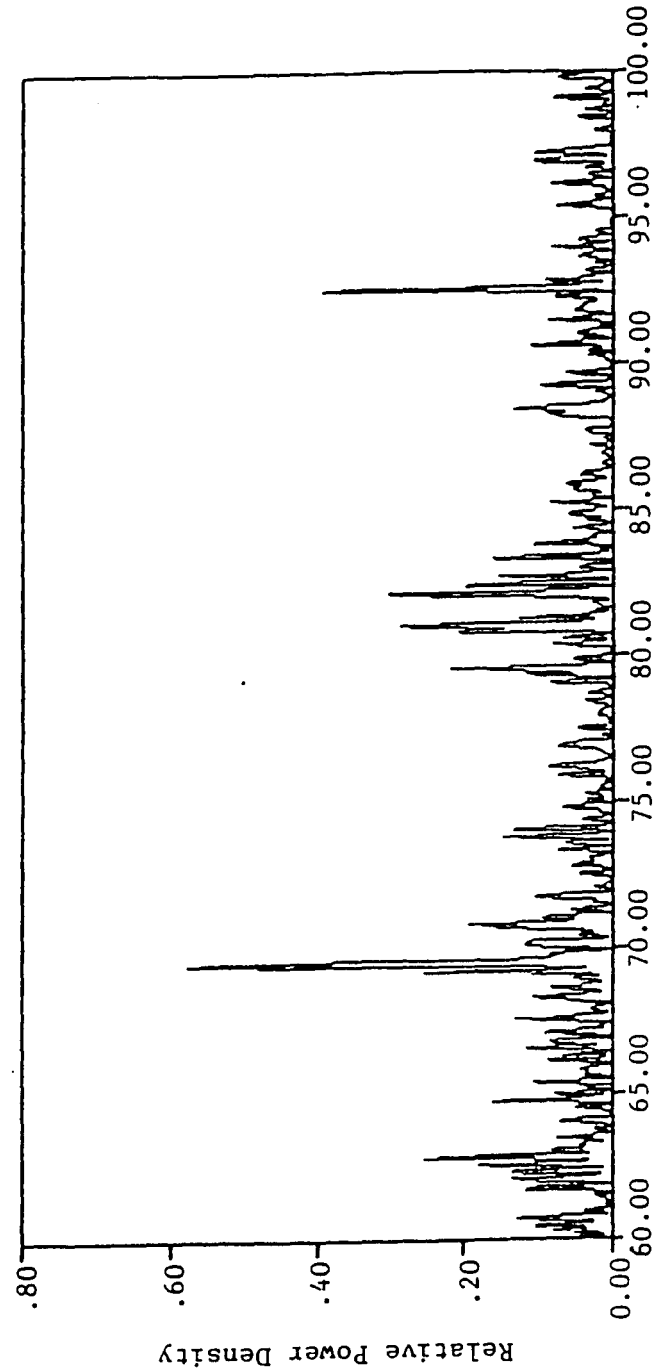

Fig. 5.1 Portion of the 1985 Power Spectrum between 60 and 100 μHz.

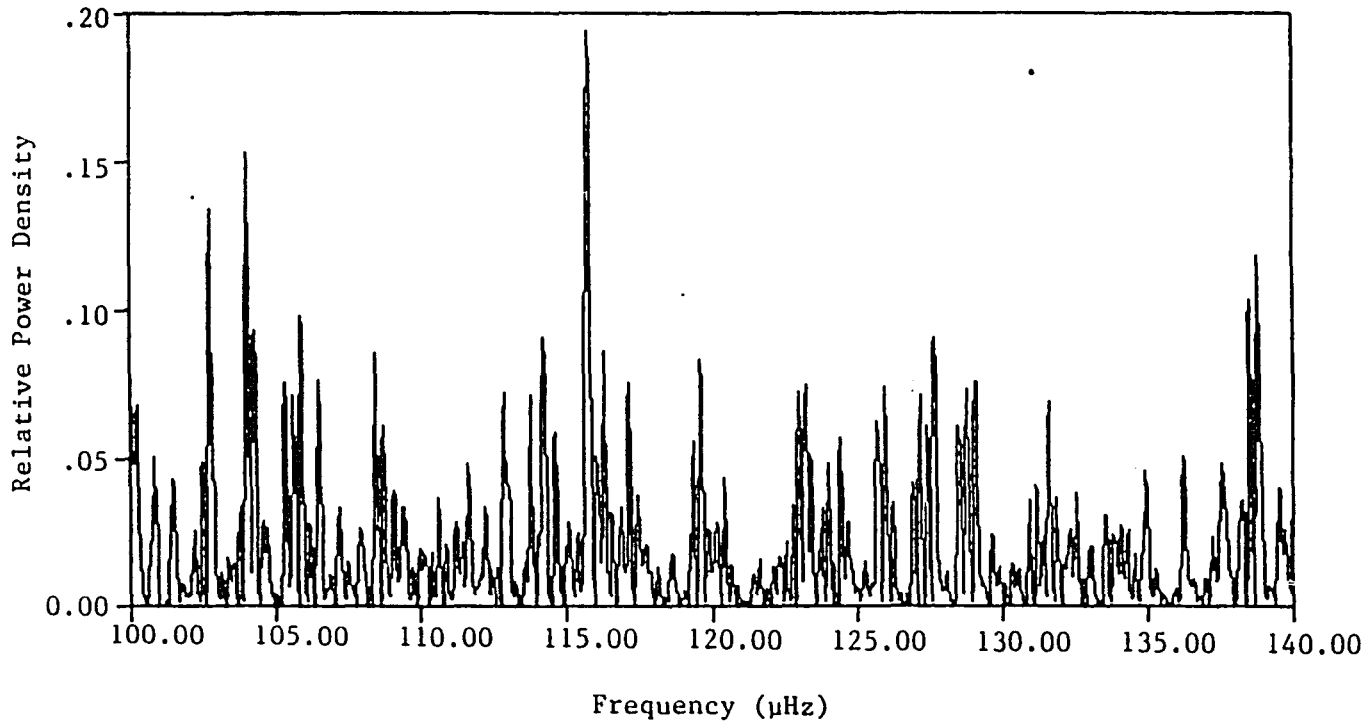

Fig. 5.2 Portion of the 1985 Power Spectrum between 100 and 140 μHz.

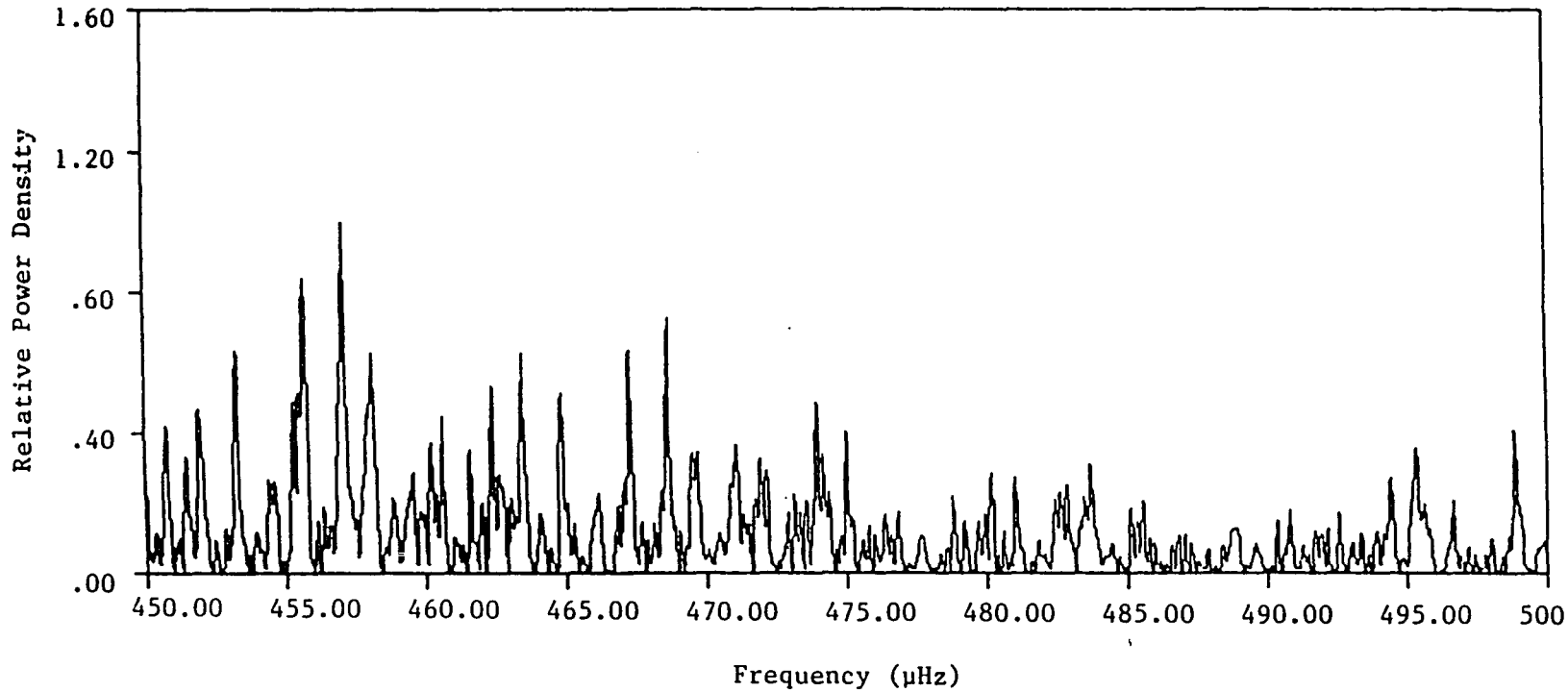

Fig. 5.3 Portion of the 1985 Power Spectrum between 450 and 500 μHz.

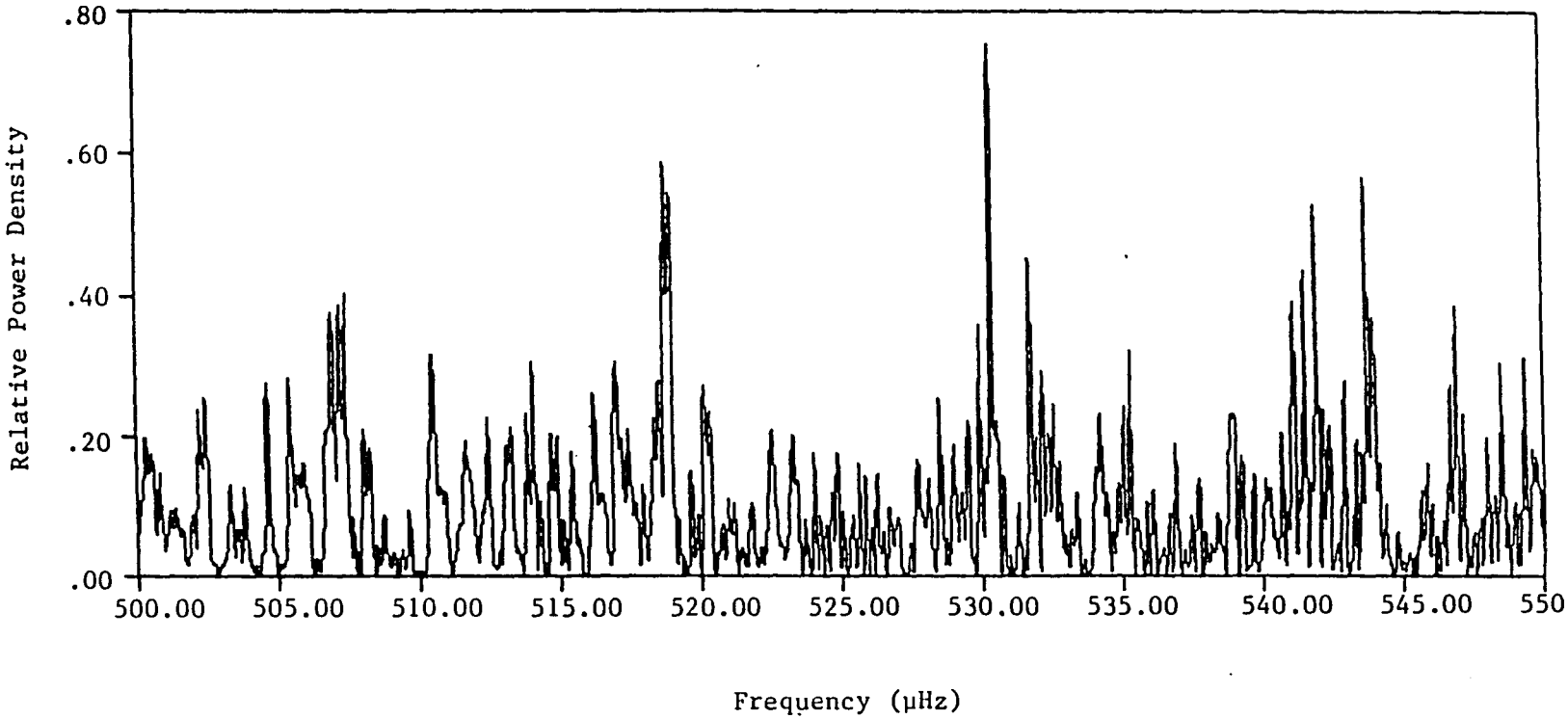

Fig. 5.4 Portion of the 1985 Power Spectrum between 500 and 550 μHz.

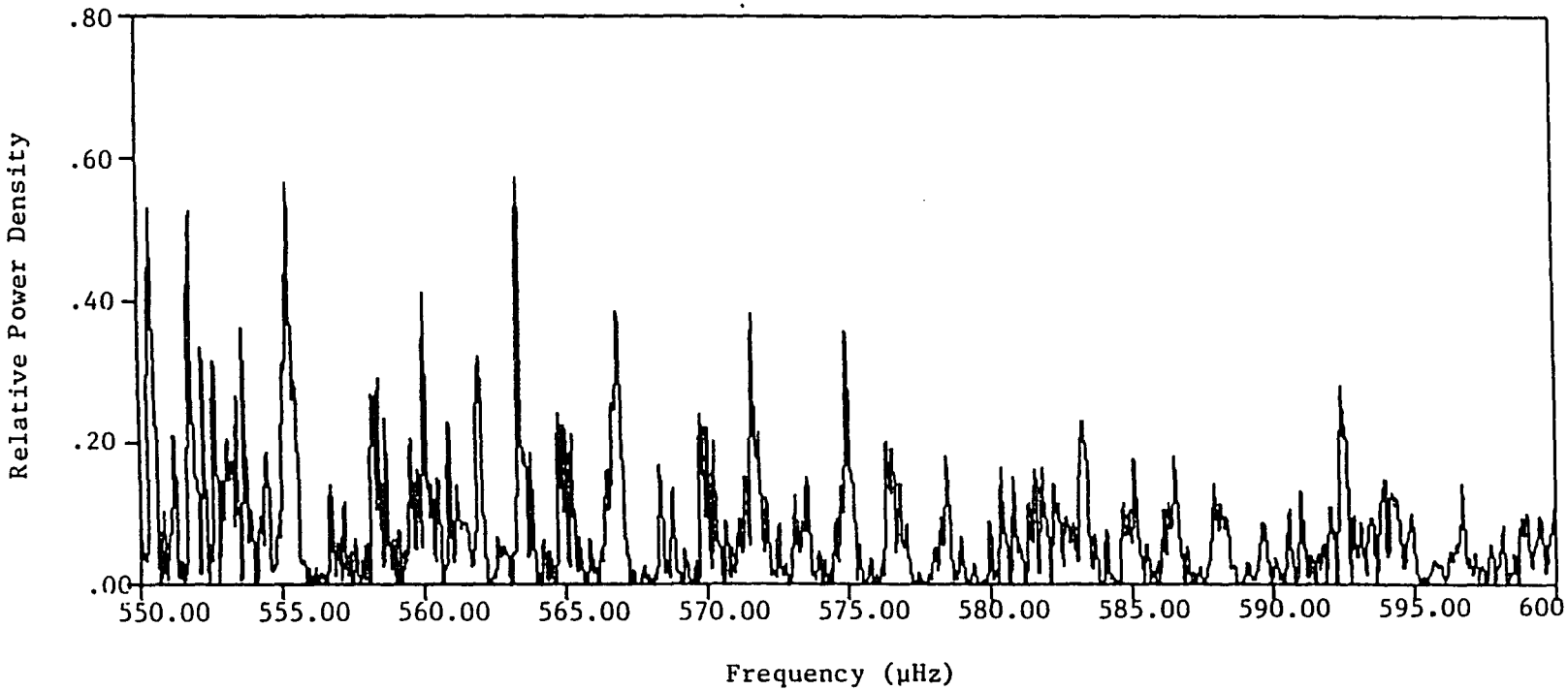

Fig. 5.5 Portion of the 1985 Power Spectrum between 550 and 600 μHz.

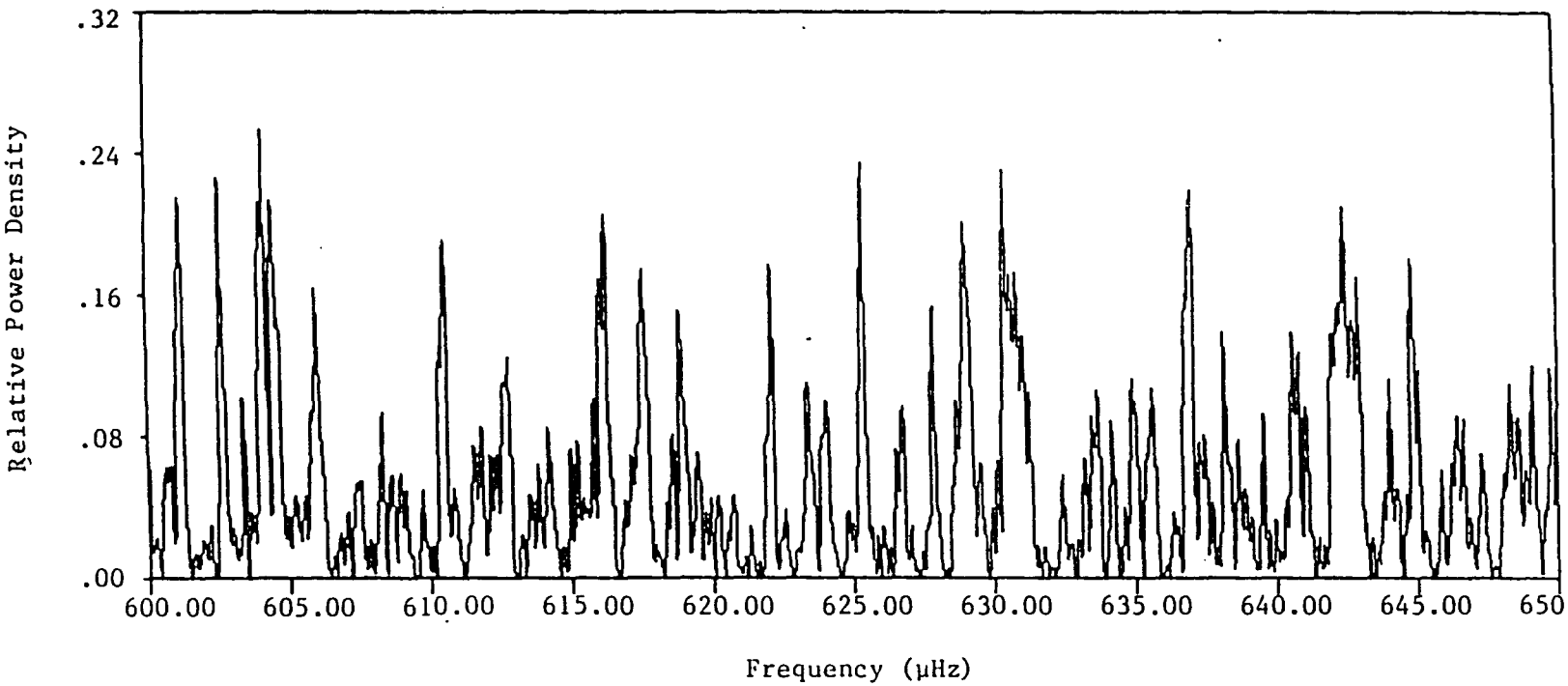

Fig. 5.6 Portion of the 1985 Power Spectrum between 600 and 650 μHz.

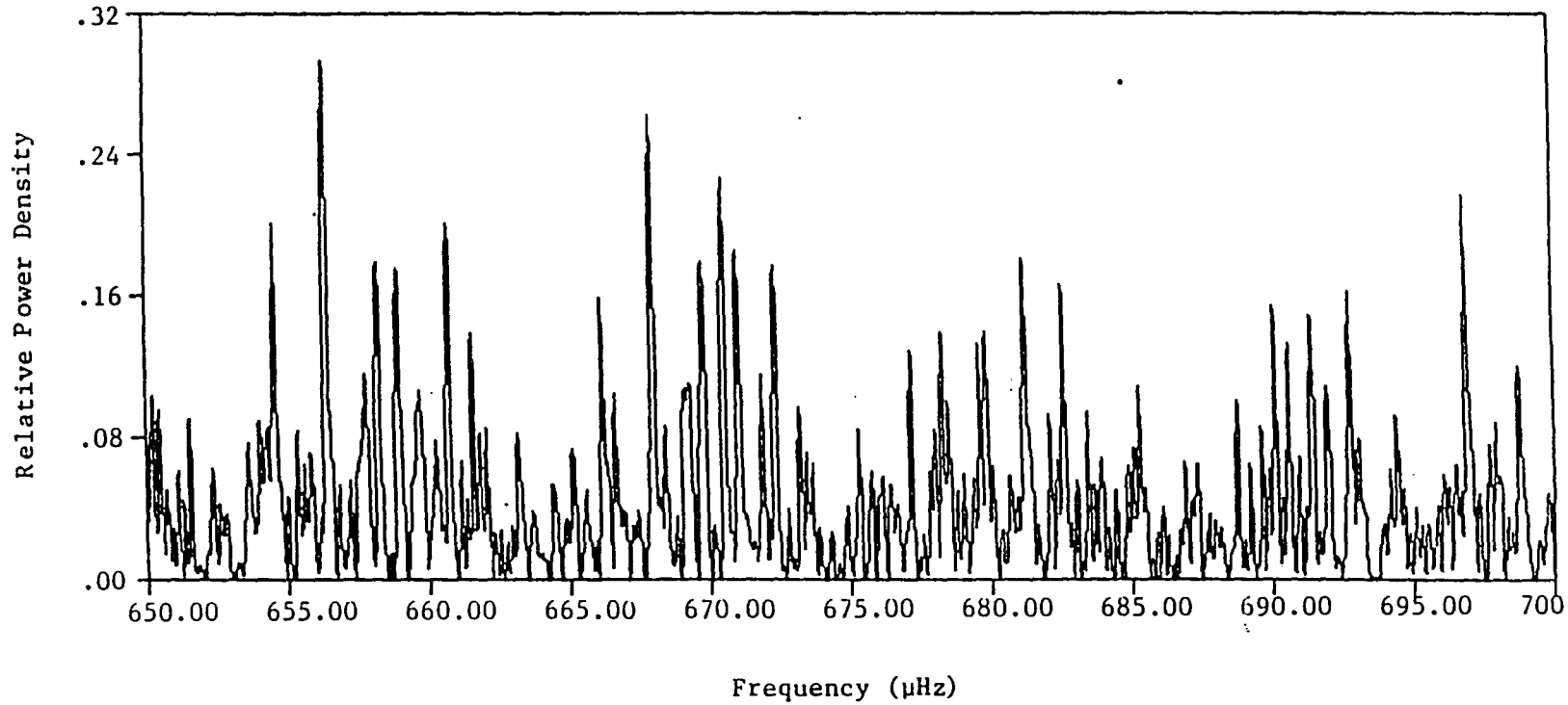

Fig. 5.7 Portion of the 1985 Power Spectrum between 650 and 700 μHz.

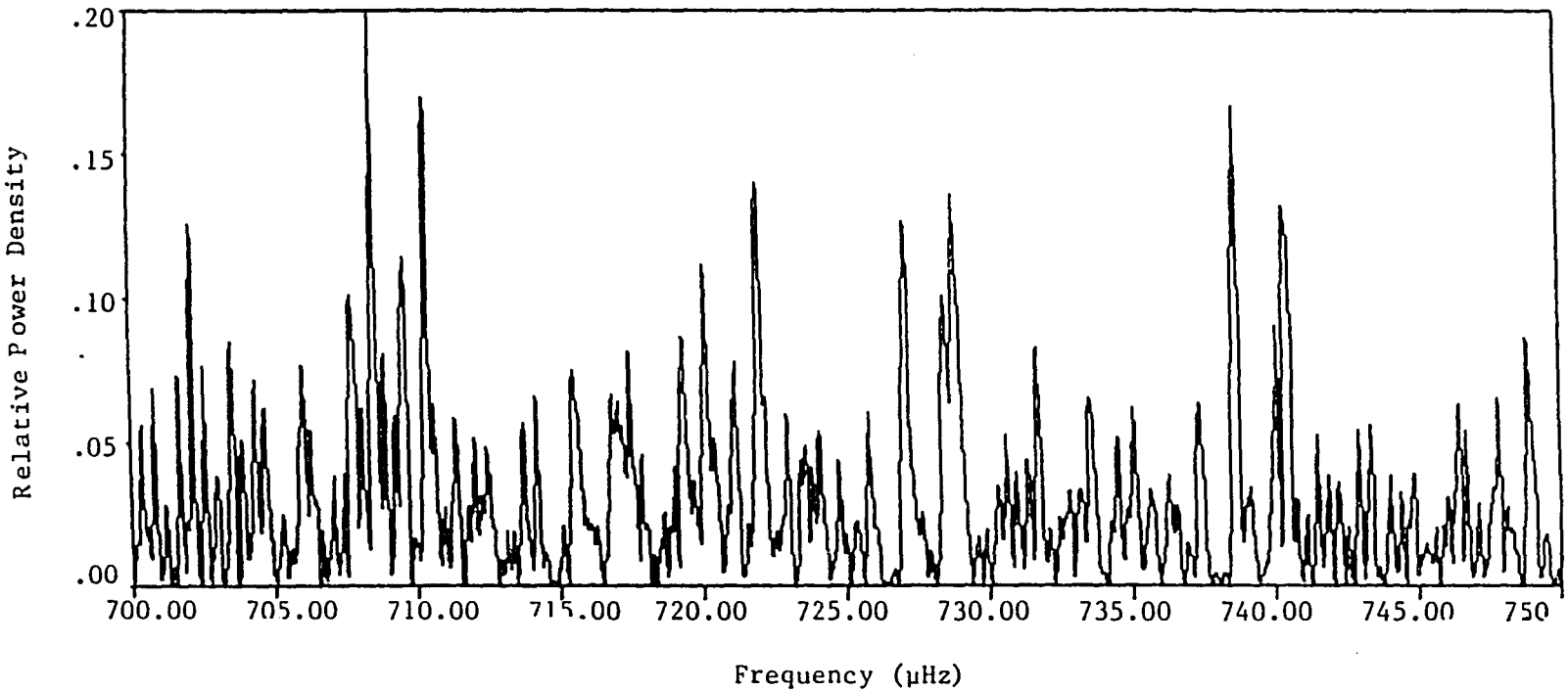

Fig. 5.8 Portion of the 1985 Power Spectrum between 700 and 750 μHz.

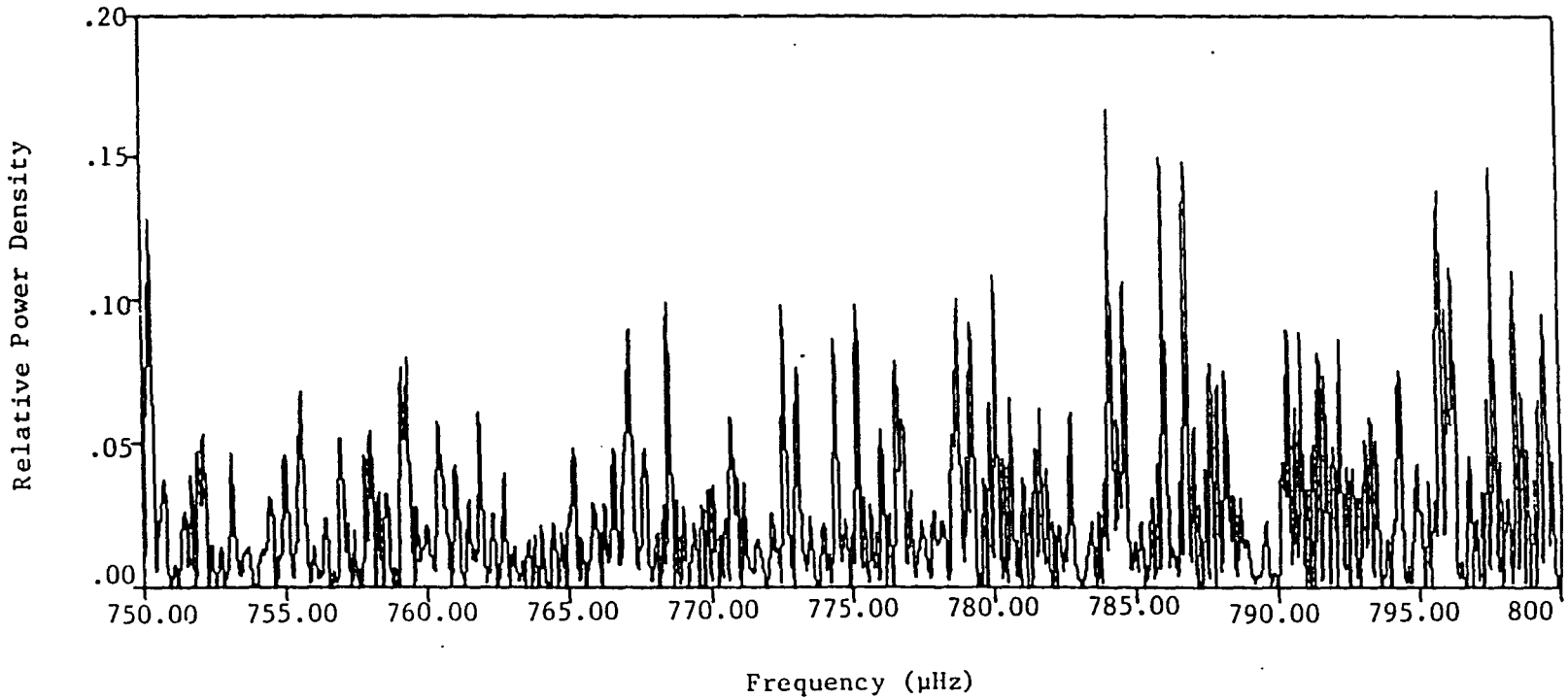

Fig. 5.9 Portion of the 1985 Power Spectrum between 750 and 800 μHz.

CHAPTER 6

RESULTS FOR THE ACOUSTIC AND f-MODES

The solar low-order, low-degree acoustic modes of oscillation play a vital role in the understanding of the Sun's interior. By inverting the observed rotational splitting results for these modes, the approximate outer half of the Sun's internal rotation may be studied (Hill, Bos, and Goode 1982; Campbell et al. 1983; and Duvall et al. 1984). However, there is little agreement about the rotational effects. Conflicting results are generally being reported between two findings when using two different observational techniques. Therefore, the significance of the agreement between the results obtained using two different observational techniques should not be understated.

Once the linear term of the polynomial fit to the observed spectral curve (cf. Section 5.2) has been Fourier analyzed, it is necessary to decide what information can be extracted from the power spectrum. Certainly, there are many terrestrial events, discussed earlier, that could introduce a false signal in the data. Our primary interest is that of investigating the power spectrum in order to find signals that are solar in origin.

One approach to identify the signature of solar oscillations in the very complex power spectrum would be to start from scratch, i.e. rely on the information contained in the 1985 power spectrum to demonstrate the presence of signals due to solar oscillations and to

classify these modes of oscillation using these signals. However, almost all reliable methods of mode classification rely on some sort of spatial information. The amount of spatial information in the 1985 data is limited. Furthermore, the aperture was positioned on the center of the solar disk adding a great deal of complexity to the spatial information that is available. However, it is possible to test a particular set of mode identifications with the 1985 data. Indeed, this instrument was designed and implemented to test whether or not solar oscillations could be detected due in the Eulerian perturbation of the radiation intensity in the continuum. Therefore, a successful confirmation of an independently classified set of mode classifications would be sufficient to not only determine if the power spectrum contains signals due to modes of oscillation, but also furnish a very important independent confirmation based on observations using a different observational technique.

6.1 Comparison of the 1985 Data to Classified Solar Normal Modes of Oscillation

Since many oscillatory modes have been identified, the most logical and straightforward approach to testing whether perturbations of the radiation intensity in the continuum have been measured, would be to statistically compare the peaks in the 1985 power spectrum with those predicted from another data set. Of course, a statistically significant positive result from such a test demonstrates that the new technique to detect global solar oscillations developed in this dissertation is valid. From the perspective of the present discrepancies encountered in

helioseismology, a positive result would have far-reaching implications as a consequence of the agreement between independent data sets taken using different observational techniques.

6.2 Solar Normal Modes Classified at SCLERA

Since SCLERA has been involved in detecting solar oscillations for fifteen years, a ready source is available for use in a statistical comparison of the 1985 data with an independent data set. In 1979, solar differential radius observations were obtained by Bos (1982). Using this data, Hill (1984; 1985), Rabaey, Hill, and Barry (1986), Rabaey and Hill (1987) have classified approximately 823 modes of oscillation. This dissertation will be primarily concerned with testing these reported detections and classifications of the low-order, low-degree acoustic modes; the f-modes; and the low-order g-modes. The comparison will be performed on the multiplets listed in Table 6.1.

6.3 Determination of the Statistical Significance of the Comparison of the 1985 Power Spectrum with the Classified Eigenfrequencies

Before a comparison between the 1985 data and an independent data set can be done, we must do some preliminary work to ensure that the results obtained are not likely to be due to random fluctuations. We must address the question: what results would be expected from a random distribution of peaks?

Under the hypothesis the 1985 power spectrum is randomly distributed relative to a classified spectrum, the probability of a coincidence between a classified eigenfrequency and a peak in the 1985

Table 6.1. List of multiplets used in this analysis.

f-modes		
n=0	$21 \leq \ell \leq 36$	
p-modes		
n=1	$4 \leq \ell \leq 22$	
n=2	$3 \leq \ell \leq 10$	
n=3	$2 \leq \ell \leq 4$	
g-modes		
ℓ=1	$4 \leq n \leq 7$	
ℓ=2	$7 \leq n \leq 12$	
ℓ=3	$11 \leq n \leq 18$	
ℓ=4	$15 \leq n \leq 21$	
ℓ=5	$18 \leq n \leq 29$	$n \neq 19$, 20, or 23

power spectrum where the two, if they are accepted as being in coincidence, cannot be separated in frequency by more than $\pm\Delta\nu$ is easily determined by

$$p(\Delta\nu) = 2\bar{\rho}\Delta\nu \qquad 6.3.1$$

with

$$\bar{\rho} = \frac{N}{\nu_1 - \nu_0} \qquad 6.3.2$$

where N is the number of peaks in the frequency range $\nu_1 - \nu_0$. Alternatively, this quantity can be empirically determined by comparing randomly generated frequencies to the peaks in the power spectrum. In the g-mode region, $60 \leq \nu \leq 130$ μHz, 3×10^5 randomly generated peaks were compared to the data and the results were in agreement with the value predicted by Equation 8.1.1 (cf. Section 8.1).

The treatment for the p- and f-modes will be slightly different from that used on g-modes. This is because the p- and f-modes are analyzed by comparing subgroups of multiplets, instead of comparing all multiplets as one set as in the case of the g-modes (cf. Chapter 8). The motivation for approaching the p- and f-modes in this manner lies in the fact that over a period spanning the time that the modes were classified until 1985, the eigenfrequencies may slightly change for the p- and f-modes, whereas no significant changes are expected for the g-modes.

In order to obtain an estimate of the probability of an accidental coincidence for the p- and f-modes, 10^5 random peaks were generated in the frequency range of 400-850 μHz. Next, the absolute value of the distance from a randomly generated peak to the nearest peak in the 1985 power spectrum was determined. As above, peaks from the two different spectra were not considered to be coincident unless their separation was less than or equal to $\Delta\nu = 0.07$ μHz. The probability density function was then approximated by

$$P(\Delta\nu) = \bar{\rho}[1.0 + \alpha(\bar{\rho}\Delta\nu)^2] \qquad 6.3.3$$

where $\bar{\rho}$ is the average peak density in the frequency range of the multiplet under study. The integrated form of this equation is essentially the same as Equation 6.3.1, except for the addition of the small correction term which allows for the decreasing slope in the region where $\Delta\nu < \nu_1$ of the distribution shown in Figure 6.1. Due to the symmetry properties of the distribution, the linear term in the above equation is omitted. Upon performing a least-squares curve fit of the distribution obtained in the p- and f-mode region to the functional form of Equation 6.3.3, the value of α was determined to be

$$\alpha = -2.10 \qquad . \qquad 6.3.4$$

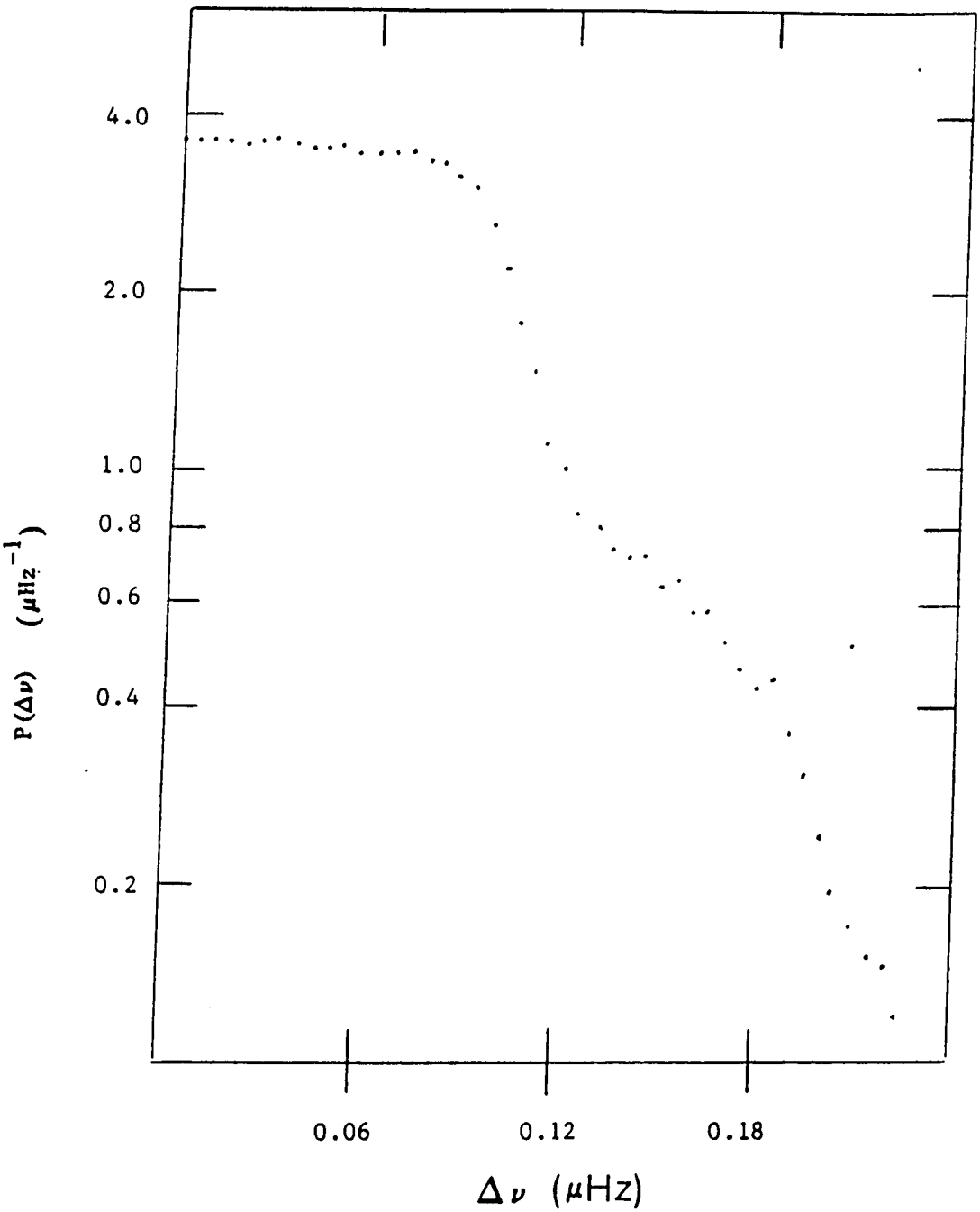

Figure 6.1. Probability density function, P(Δν) obtained by comparing 10^5 randomly generated peaks with the actual data.

The probability of finding one or more random peaks within $\pm\Delta\nu$ of ν, is found by integrating Equation 6.3.3 yielding

$$\int_{-\Delta\nu}^{+\Delta\nu} P(\Delta\nu)d(\Delta\nu) = p(\Delta\nu) = 2\bar{\rho}\Delta\nu[1.0 - 0.70(\bar{\rho}\Delta\nu)^2] \qquad 6.3.5$$

6.4 Formalism Used in Comparing the 1985 Observations With the Classified Modes

To begin this analysis, it will be necessary to calculate the coincidence rate, R_i, between a set of predetermined frequencies contained in a multiplet and the peaks observed in the 1985 power spectrum, where a frequency and peak are considered to be coincident if their separation is within ± 0.07 μHz. Then,

$$R_i = N_\ell / N_{max} \qquad 6.4.1$$

where N_ℓ is the number of coincidences for the multiplet in question, and N_{max} is the maximum number of coincidences possible. For the p- and f-mode analysis, the maximum number of coincidences possible is $(2\ell+1)$, which includes both even $(\ell+m)$ and odd $(\ell+m)$ (cf. Sections 6.5 and 6.7). In the study of the g-modes, the maximum number of modes accessible is $\approx (\ell+1)$, which only considers even $(\ell+m)$ (cf. Chapter 8). The reason for taking this approach is a consequence of detector geometry used in the 1985 observations (cf. Sections 3.2 and 4.4).

The square of the uncertainty in N_ℓ is determined from the binomial distribution and is given by

$$\sigma^2 = N_{max}p(1-p) \qquad 6.4.2$$

where p is estimated to be given by Equation 6.4.1. Clearly, then, the uncertainty of the results is heavily dependent on the maximum number of available states. Therefore, statistically speaking, the most significant results will occur for large ℓ.

The formal comparison of the 1985 power spectrum to the classified eigenfrequencies was made by calculating $\bar{d}$, where

$$\bar{d} = \langle R_i - p \rangle \qquad 6.4.3$$

is the weighted average of the difference between the observed coincidence rate and the coincidence rate expected under the null hypothesis.

6.5 Confirmation of the Detection and Classification of the Low-Order, Low-Degree, Acoustic Modes

The eigenfrequency spectrum for n=1, ℓ=4-22 was divided into four groups containing three to six multiplets each according to

Group 1	$4 \leq \ell \leq 6$
Group 2	$7 \leq \ell \leq 12$
Group 3	$13 \leq \ell \leq 17$
Group 4	$18 \leq \ell \leq 22$

For each group the location of a multiplet member was determined by a polynomial for the eigenfrequency $\nu_{n\ell m}$ given by

$$\nu_{n\ell m} = \nu_{n\ell} + \nu'_{n\ell} m + \frac{1}{2!}\nu''_{n\ell} m^2 + \frac{1}{3!}\nu'''_{n\ell} m^3 \quad . \qquad 6.5.1$$

In the search for evidence of p-modes in the 1985 radiation intensity measurements, the locations of the classified eigenfrequencies determined by Equation 6.5.1 were compared to peaks in the 1985 power spectrum. Very small shifts were introduced in the $\nu_{n\ell}$, $\nu'_{n\ell}$, and $\nu''_{n\ell}$ of the groups of multiplets. It should be noted that the shifts were performed on the groups of multiplets and not the individual multiplets themselves. For example, if $\nu_{n\ell}$ was shifted by $\Delta\nu_{n\ell}$ in Group 2, all multiplets listed in that group were shifted by the same $\Delta\nu_{n\ell}$. This procedure was undertaken in order to search for a maximum coincidence rate, with respect to $\nu_{n\ell}$, $\nu'_{n\ell}$, and $\nu''_{n\ell}$, between the 1985 power spectrum and the frequencies predicted by Equation 6.5.1, where the intial values for $\nu_{n\ell}$, $\nu'_{n\ell}$, $\nu''_{n\ell}$, and $\nu'''_{n\ell}$ were taken from Hill (1985). The study of the shifts in the ν'' term was motivated primarily as a result of the reported changes in the solar magnetic field (Roberts and Campbell, 1986). This will be discussed in detail in Section 7.2.

Each group of multiplets was allowed a maximum shift in $\nu_{n\ell}$ of typically ±0.10 μHz and in $\nu'_{n\ell}$ by typically ±0.01 μHz. Maxima in the coincidence rates were found for shifts of Groups 2, 3, and 4 of

$$\Delta\nu_{n\ell} = \begin{cases} -0.06 \pm 0.04 \ ; & 7 \leq \ell \leq 12 \\ -0.01 \pm 0.04 \ ; & 13 \leq \ell \leq 17 \\ 0.04 \pm 0.04 \ ; & 18 \leq \ell \leq 22 \end{cases} \qquad 6.5.2$$

A peak in the 1985 power spectrum was accepted as being in coincidence with a corresponding shifted classified eigenfrequency if the separation in their frequencies was ≤ 0.07 μHz. These results, as well as the results for $\Delta\nu'_{n\ell}$ are displayed as a function of $\bar{d}/\sigma$ in Figures 6.2-6.7. The values given in Equation 6.5.2 were estimated directly from the figures. No statistically significant positive correlations were found for $n=1$, $4 \leq \ell \leq 6$.

What is the likelihood that these results could occur if the relative distribution is random? To answer this, the mean difference, $\bar{d}_i$, between the observed coincidence rate and the expected rate due to a relative random distribution is calculated. This yields a value for each of the three groups of multiplets of

$$\bar{d}_i = \begin{cases} 0.219 \pm .040; & 7 \leq \ell \leq 12 \\ 0.161 \pm .038; & 13 \leq \ell \leq 17 \\ 0.110 \pm .034; & 18 \leq \ell \leq 22 \end{cases} \qquad 6.5.3$$

where the mean difference is weighted by the standard deviations of the $N_{n\ell}/N_{max}$. The individual $N_{n\ell}/N_{max}$ are displayed as a function of ℓ in Figure 6.8 for the shifts in Equation 6.5.2. The larger error bars for the lower ℓ values in this figure are a direct result of the smaller values of N_{max} (cf. Equation 6.4.3).

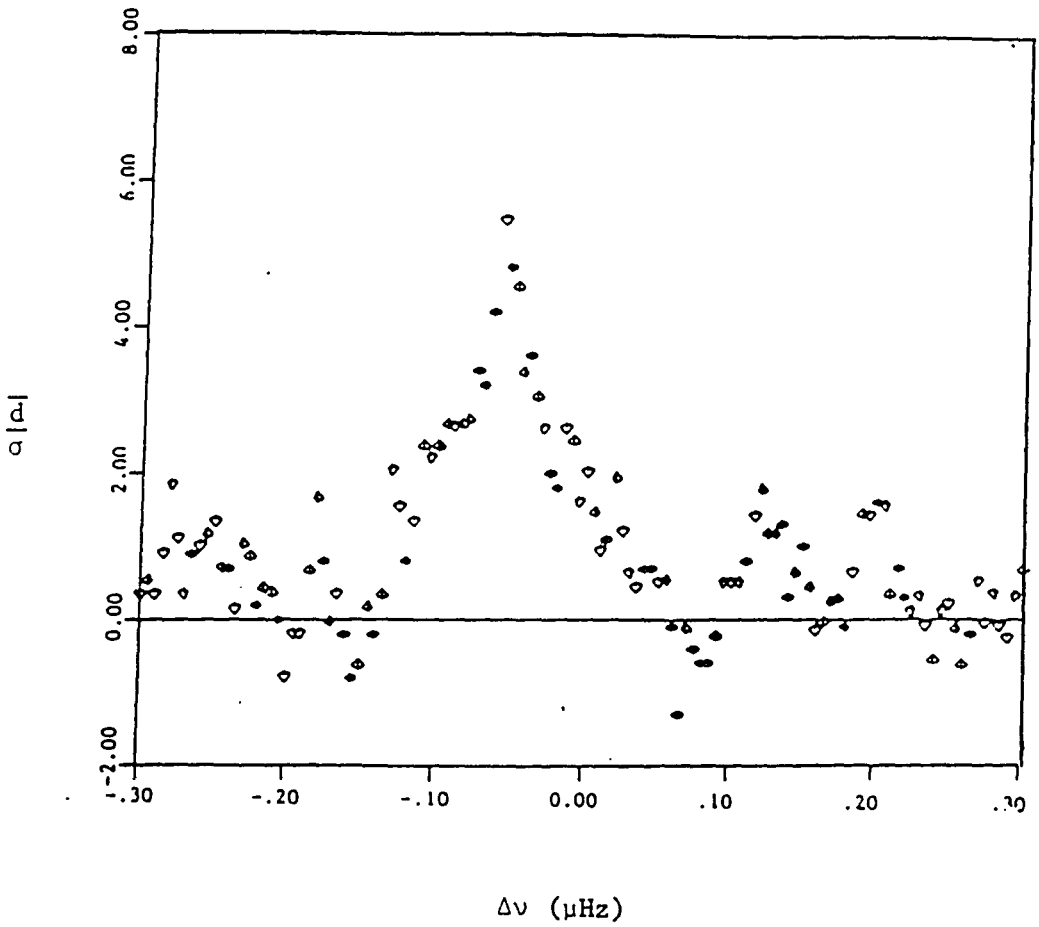

Figure 6.2 Coincidence rate between the 1985 power spectrum and the classified p-mode spectrum for $7 \leq \ell \leq 12$ with $\Delta\nu'$ held constant.

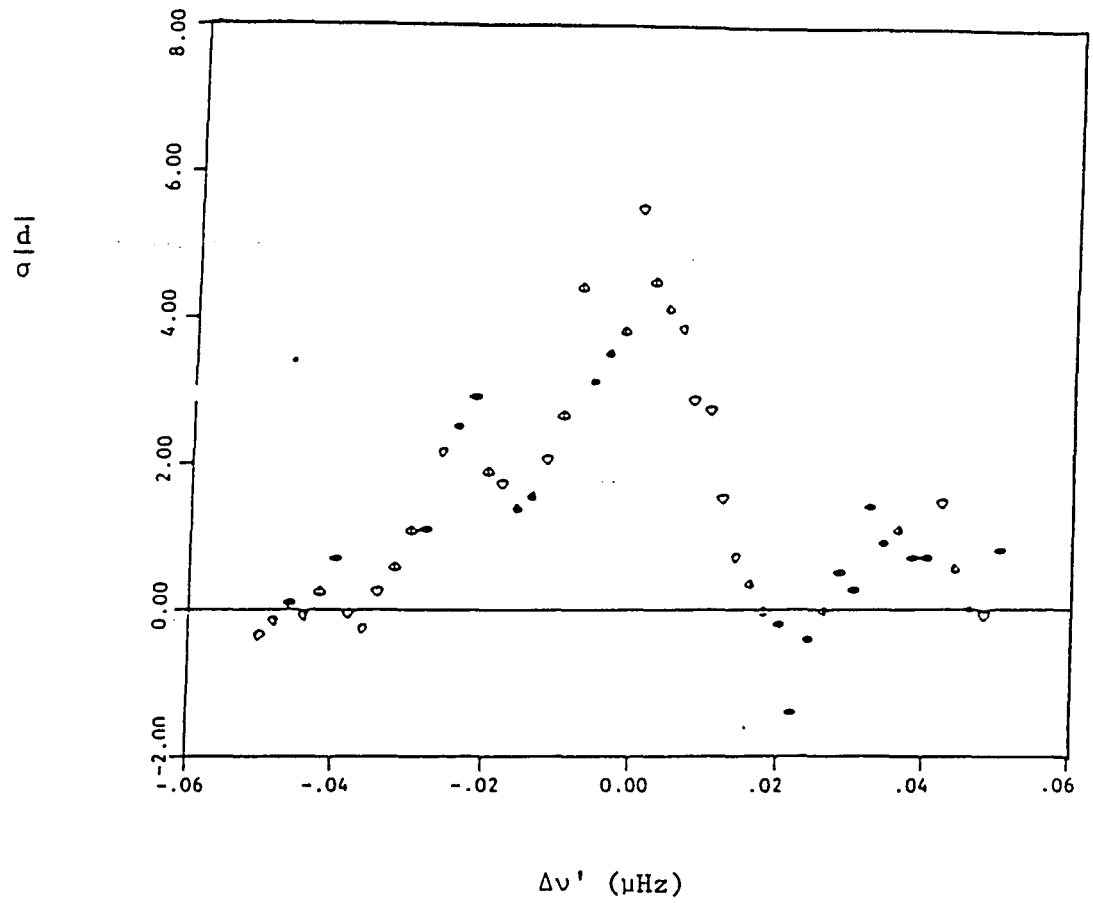

Figure 6.3. Coincidence rate between the 1985 power spectrum and the classified p-mode spectrum for $7 \leq \ell \leq 12$ with $\Delta\nu$ held constant.

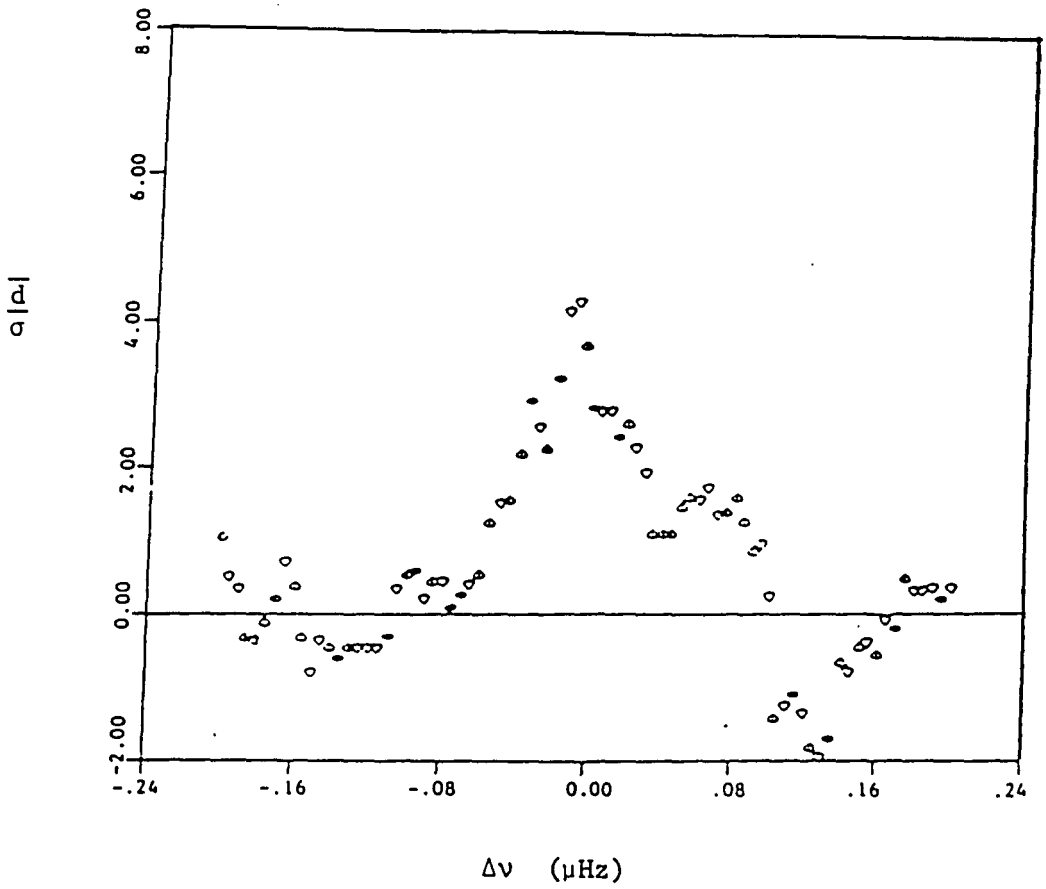

Figure 6.4 Coincidence rate between the 1985 power spectrum and the classified p-mode spectrum for $13 \leq \ell \leq 17$ with $\Delta\nu'$ held constant.

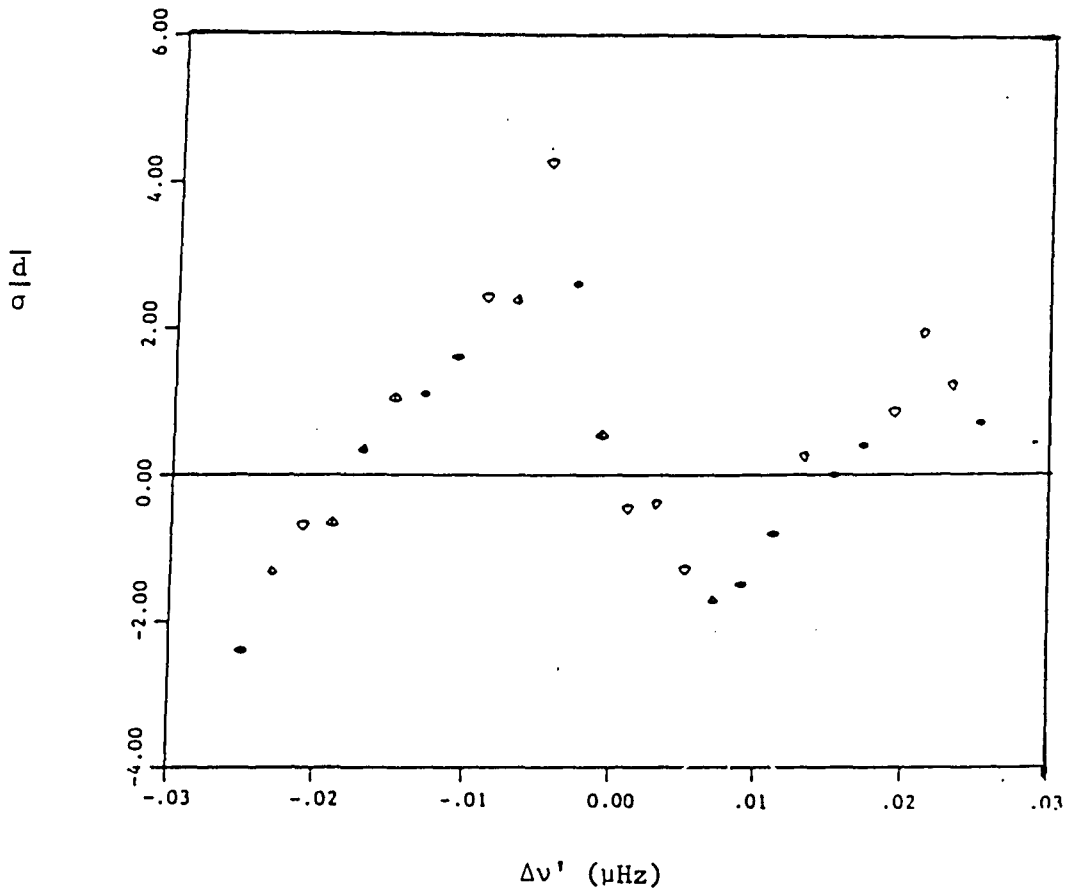

Figure 6.5. Coincidence rate between the 1985 power spectrum and the classified p-mode spectrum for $13 \leq \ell \leq 17$ with $\Delta\nu$ held constant.

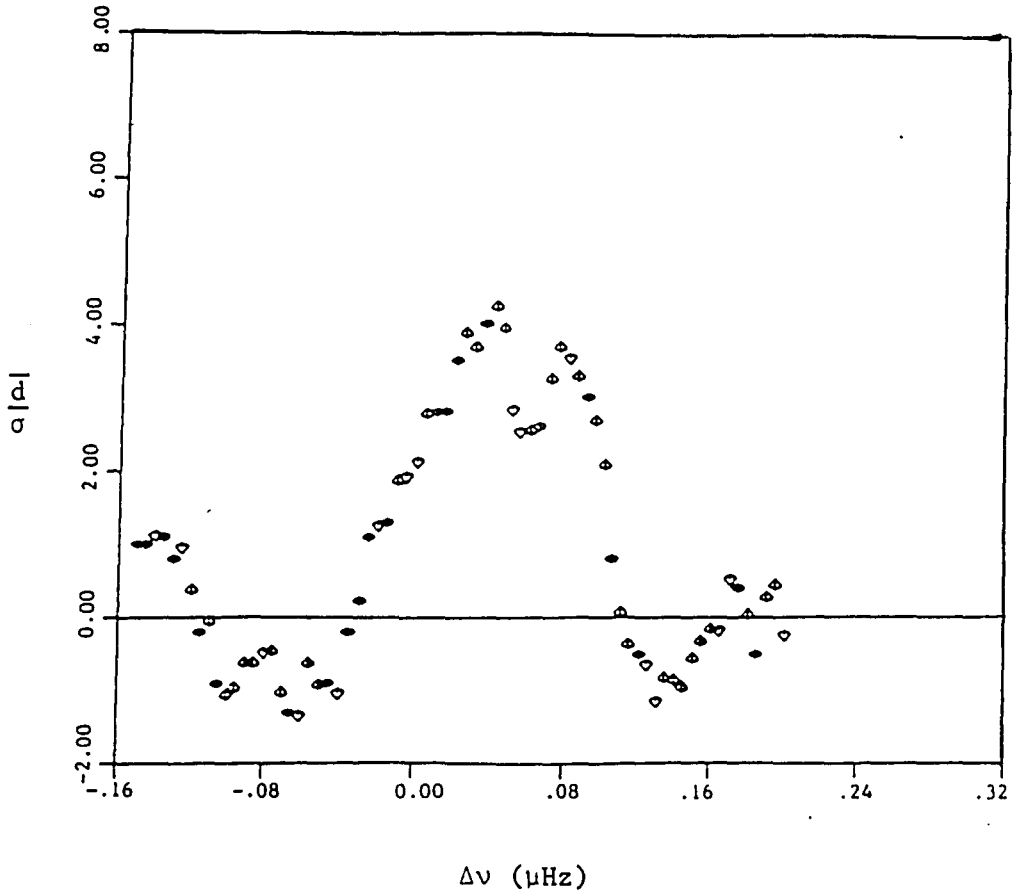

Figure 6.6 Coincidence rate between the 1985 power spectrum and the classified p-mode spectrum for $18 \leq \ell \leq 22$ with $\Delta\nu'$ held constant.

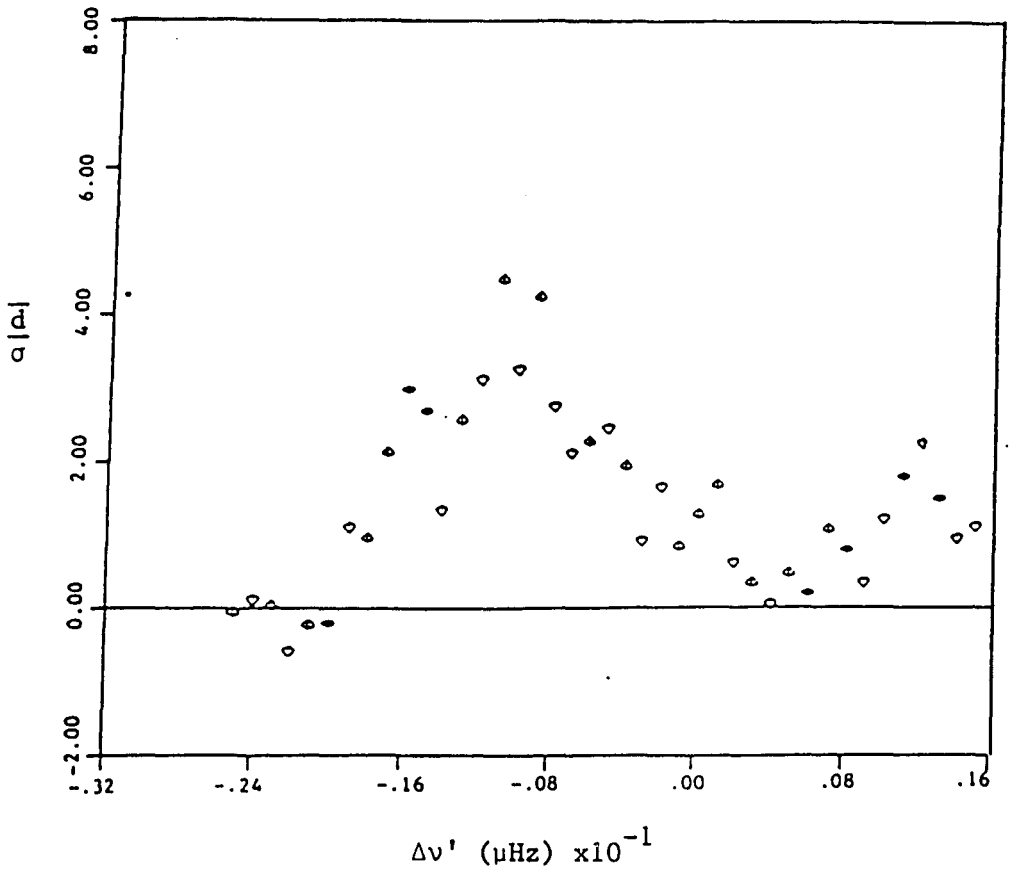

Figure 6.7. Coincidence rate between the 1985 power spectrum and the classified p-mode spectrum for $18 \leq \ell \leq 22$ with $\Delta\nu$ held constant.

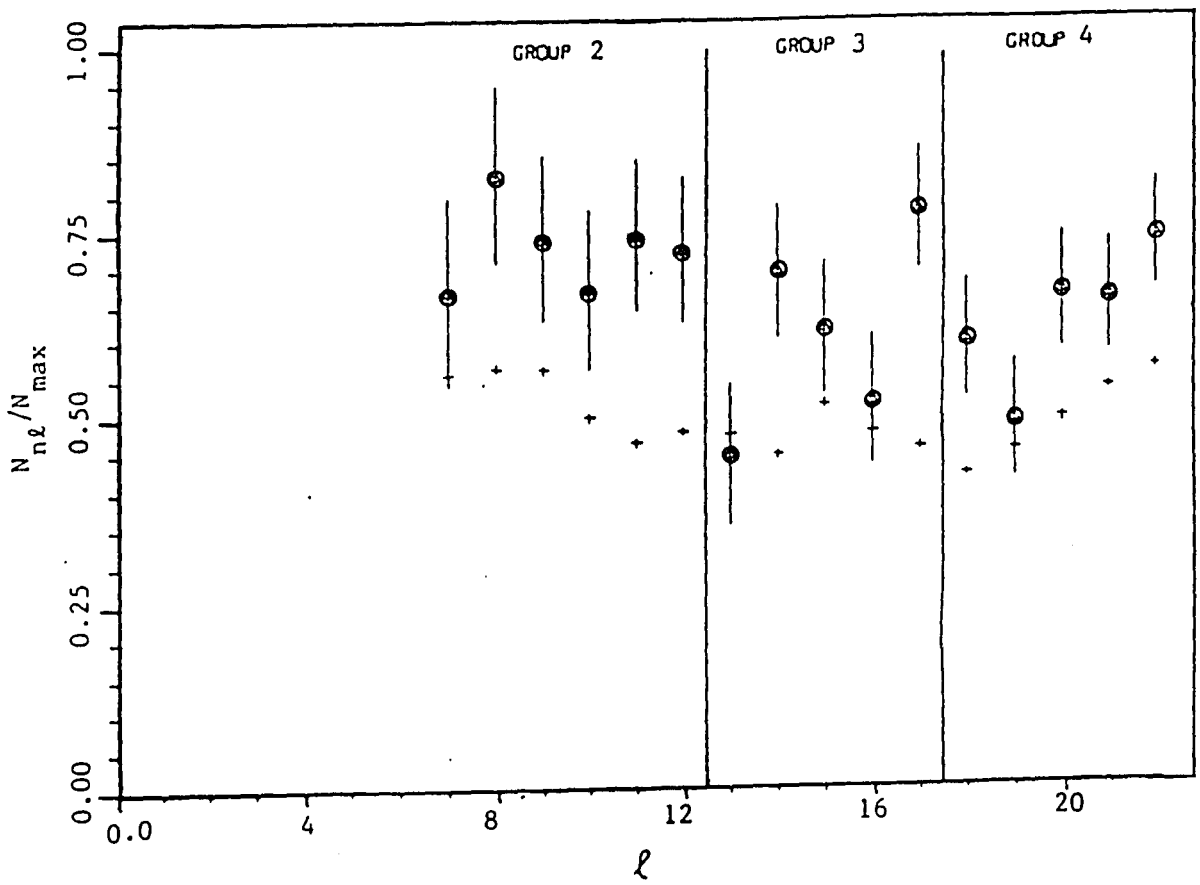

Figure 6.8. Observed coincidence rate, N_ℓ/N_{max}, for three groups of multiplets.

The $\bar{d}_i$'s in Equation 6.5.3 are 5.5, 4.3, and 3.3 standard deviations away from zero. The determination of the probabilities of obtaining these results is made on the assumption that the distributions of the $\bar{d}_i$ are nearly normal around zero. Strictly speaking, this is expected to be true if the 1985 power spectrum and the classified eigenfrequencies were random with respect to each other. Therefore, under the null hypothesis the probability of obtaining a particular $\bar{d}/\sigma$ is estimated to within two orders of magnitude[3] of

$$p_{erf} = [1 - erf(\bar{d}/\sqrt{2}\sigma)]/2 \qquad 6.5.4$$

where

$$erf(x) = \frac{2}{\sqrt{\pi}} \int_0^x e^{-t^2} dt \quad . \qquad 6.5.5$$

Thus, the probability of obtaining the above quoted $\bar{d}/\sigma$'s for each of the group of multiplets if no evidence of g-modes is present in the 1985 power spectrum and/or if the g-mode classifications are incorrect is estimated to be

$$p \lesssim \begin{cases} 2 \times 10^{-6} & ; \quad 7 \leq \ell \leq 12 \\ 1 \times 10^{-3} & ; \quad 13 \leq \ell \leq 17 \\ 5 \times 10^{-2} & ; \quad 18 \leq \ell \leq 22 \end{cases} , \qquad 6.5.6$$

---

3. Since $\Delta\nu$ and $\Delta\nu'$ were allowed to slightly vary, an order of magnitude was allowed for each of these degrees of freedom.

for groups 2, 3, and 4 respectively. Therefore, this indicates the hypothesis that the 1985 peaks are randomly distributed in frequency with respect to the multiplets identified by Hill is very unlikely.

The n=2 modes were treated in the same manner as those above. The observed $\bar{d}$ for n=2, $3 \leq \ell \leq 10$ is

$$\bar{d} = 0.212 \pm 0.040 \qquad 6.5.7$$

where the coincidence rates between the peaks in the 1985 power spectrum and the classified eigenfrequencies were maximized for a shift of

$$\Delta\nu_{n\ell} = -0.27 \pm 0.05 \quad \mu\text{Hz} \quad . \qquad 6.5.8$$

No statistically significant positive correlation was found for the n=3 modes with $2 \leq \ell \leq 4$.

6.6 Comparison of the 1978 Diameter Observations to the Low-Order Low-Degree Acoustic Modes

The 1978 diameter observations were compared to the low-order, low-degree, acoustic modes in the same manner as was done for the 1985 in Section 6.5. From the detector geometry used in 1978, the diameter observations will be sensitive to modes that are of even ℓ and even m, and should not be sensitive to modes with odd $(\ell+m)$.[4]

---

4. Measurements of this type are also sensitive to odd ℓ, odd m. However, Hill (1984) has shown that the average power of the signals with odd ℓ, odd m, is 4% of the average power of modes with even ℓ, even m.

Therefore, the maximum number of accessible modes is reduced by approximately a factor of 2. The weighted $\bar{d}$ for n=1, $6 \leq \ell \leq 12$, with ℓ and m both even is

$$\bar{d}_a = 0.235 \pm 0.076 \quad . \qquad 6.6.1$$

A shift of the classified eigenfrequencies of $\Delta\nu_{n\ell} = 0.01 \pm 0.10$ μHz maximized the coincidence rate. Since the 1978 data spanned only 18 days, a window larger than the $\Delta\nu = \pm 0.07$ used for the 1985 observations was used for accepting a coincidence between a peak in the 1978 power spectrum and a classified frequency. In this case a window of $\Delta\nu = \pm 0.12$ μHz was used.

The $\bar{d}$ given in Equation 6.6.1 is 3.1 standard deviations away from the null hypothesis compared to the 2.7σ (for the same multiplets) obtained by Hill and Caudell (1985) in comparing the 1978 and 1979 observations. Since Hill and Caudell did not consider any shifts of the eigenfrequencies to maximize the coincidence rates, the 2.7σ result is quoted for a $\Delta\nu_{n\ell} = 0$. The values for the shifts in $\Delta\nu_{n\ell}$ and $\Delta\nu'_{n\ell}$ are given as a function of $\bar{d}/\sigma$ in Figures 6.9 and 6.10. No statistically significant positive correlation was found for the other n=1 modes.

6.7 Comparison of the Peaks in the 1985 Power Spectrum to the Classified f-modes

Using data obtained in 1979 by Bos (1982), Rabaey, Hill, and Barry (1986) classified a series of intermediate-degree f-modes, n=0 for ℓ=18-36. In an extension of the work done in Section 6.5, the 1985

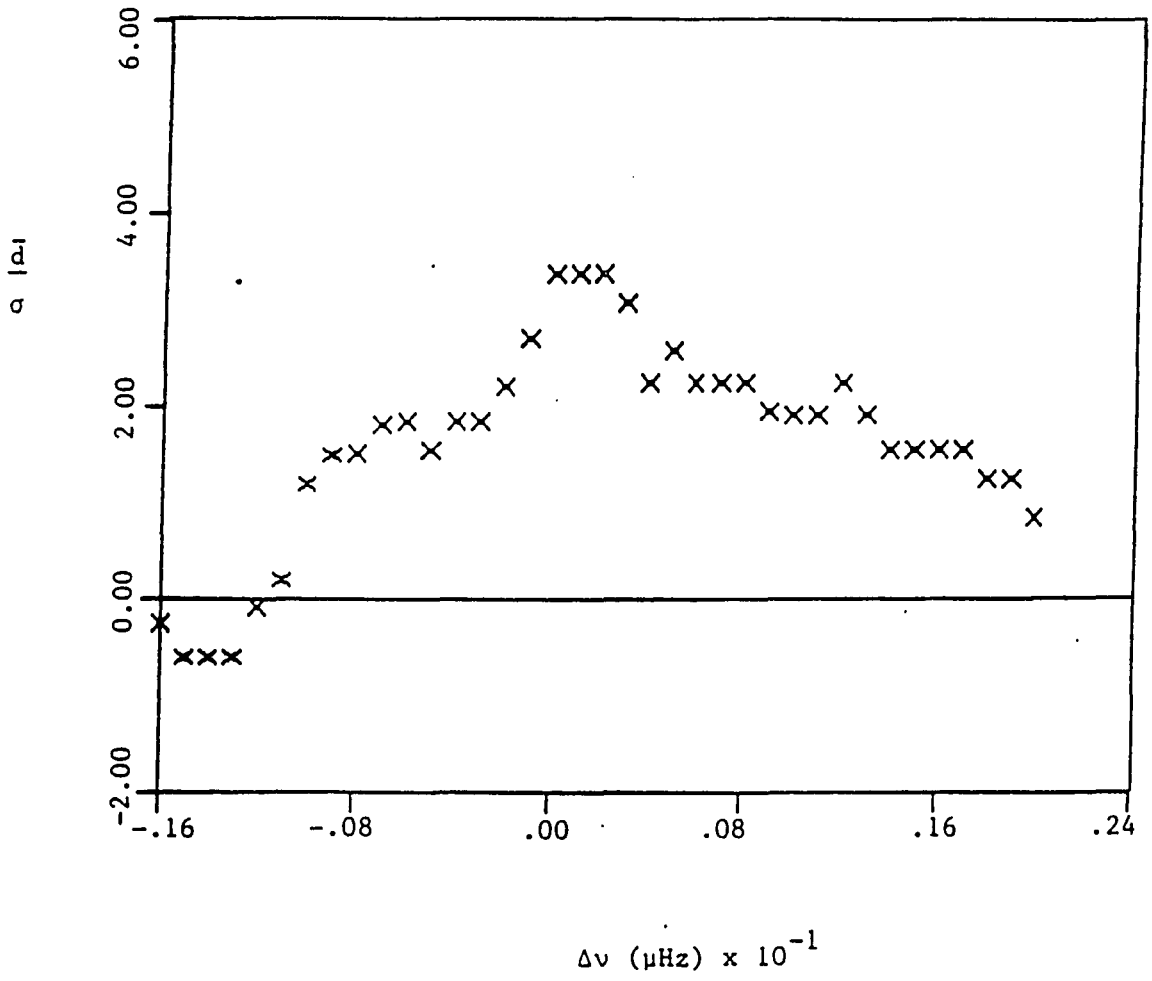

Figure 6.9. Coincidence rate between the 1979 power spectrum and the classified p-mode spectrum for $6 \leq \ell \leq 12$ with $\Delta\nu'$ held constant.

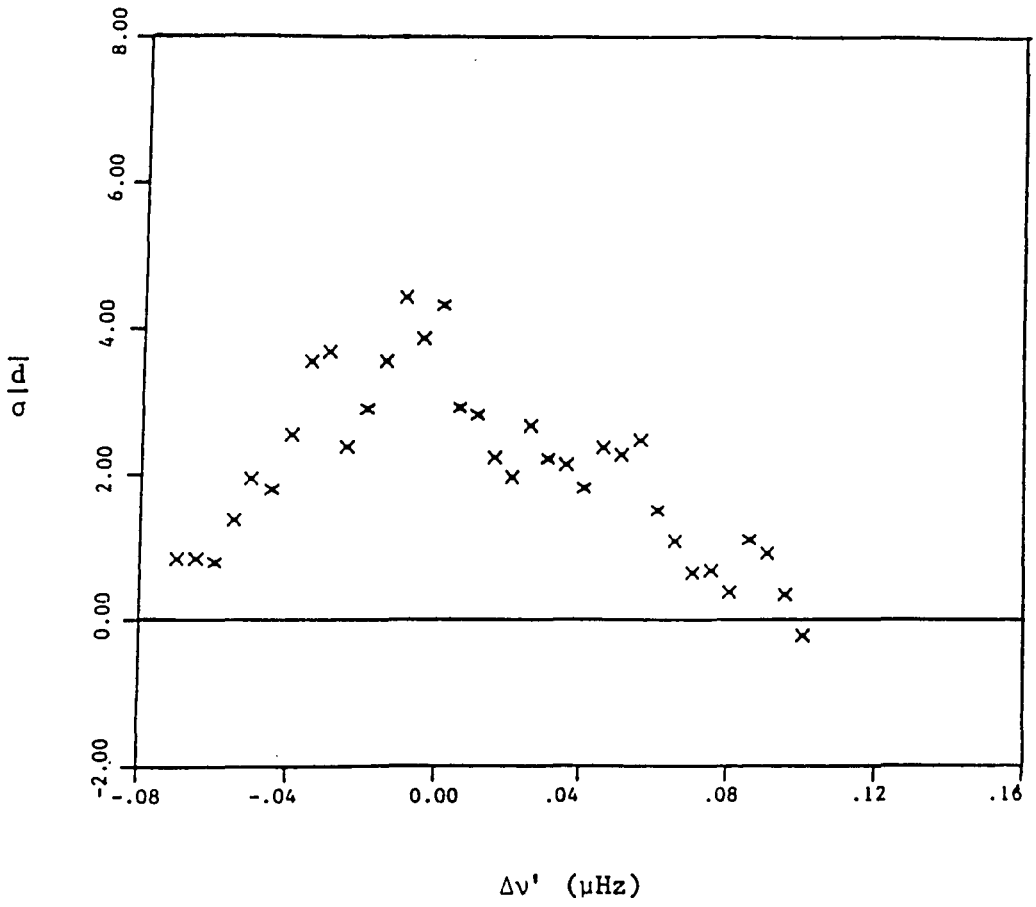

Figure 6.10. Coincidence rate between the 1979 power spectrum and the classified p-mode spectrum for $6 \leq \ell \leq 12$ with $\Delta\nu$ held constant.

power spectrum can be compared to these modes, which are sensitive mainly to the outer 5% of the Sun.

Continuing with the analysis in the same spirit of Sections 6.5 and 6.6, the eigenfrequency spectrum for n=0, ℓ=21-36 was divided into three bins:[5] $21 \leq \ell \leq 26$, $27 \leq \ell \leq 31$, and $32 \leq \ell \leq 36$. The test for secular changes in the f-mode $\nu_{n\ell}$ for the multiplets contained in a given bin was made by shifting in frequency, as a group, the classified spectrum and identifying the shift generating the maximum coincidence rate.

It should be mentioned at this point that there is a slight difference in the calculation of the locations of the members of a multiplet for the f-modes. It was determined that for the f-modes, fifth-order terms in m should be kept in calculating the eigenfrequencies (Rabaey, Hill, and Barry 1986). Therefore, Equation 6.5.1 of Section 6.5 is modified for the f-mode analysis to retain the fifth-order term.

As in the case of the low-order, low-degree acoustic modes, if the separation between a shifted classified frequency and a corresponding peak in the 1985 power spectrum was within $\pm\Delta\nu$, they were accepted as being in coincidence. The coincidence rates for $\Delta\nu$ = 0.07 μHz were found to be maximized for shifts in the classified f-mode spectrum of

---

5. Since this analysis, Rabaey and Hill have additionally classified f-modes (n=0) for $18 \leq \ell \leq 20$.

$$\Delta\nu_{n\ell} = \begin{cases} 0.040 \pm 0.040 \ \mu\text{Hz}; & 21 \leq \ell \leq 26 \\ 0.030 \pm 0.040 \ \mu\text{Hz}; & 27 \leq \ell \leq 31 \\ 0.060 \pm 0.040 \ \mu\text{Hz}; & 32 \leq \ell \leq 36 \end{cases} . \qquad 6.7.1$$

These results and those of $\Delta\nu'_{n\ell}$ are shown in Figures 6.11-6.16.

The formal comparison of the 1985 power spectrum to the classified eigenfrequencies is made through the calculation of the weighted mean difference, $\bar{d}$, between the observed coincidence rate, $N_{n\ell}/N_{max}$, and the coincidence rate expected from a relative random distribution. For the three groups of multiplets the $\bar{d}_i$ are

$$\bar{d}_i = \begin{cases} 0.105 \pm 0.028; & 21 \leq \ell \leq 26, \\ 0.085 \pm 0.028; & 27 \leq \ell \leq 31, \\ 0.094 \pm 0.027; & 32 \leq \ell \leq 36, \end{cases} \qquad 6.7.2$$

where the mean difference is weighted by the standard deviations of the $N_{n\ell}/N_{max}$. These values are 3.76, 3.04, and 3.54 standard deviations above zero, respectively. The probability of obtaining a positive $\bar{d}$ under the null hypothesis is estimated to be

$$p \lesssim \begin{cases} 5 \times 10^{-5} ; & 21 \leq \ell \leq 26 \\ 2 \times 10^{-3} ; & 27 \leq \ell \leq 31 \\ 5 \times 10^{-4} ; & 32 \leq \ell \leq 36 \end{cases} . \qquad 6.7.3$$

Therefore, these results indicate that the hypothesis that peaks in the 1985 power spectrum are randomly distributed in frequency with respect

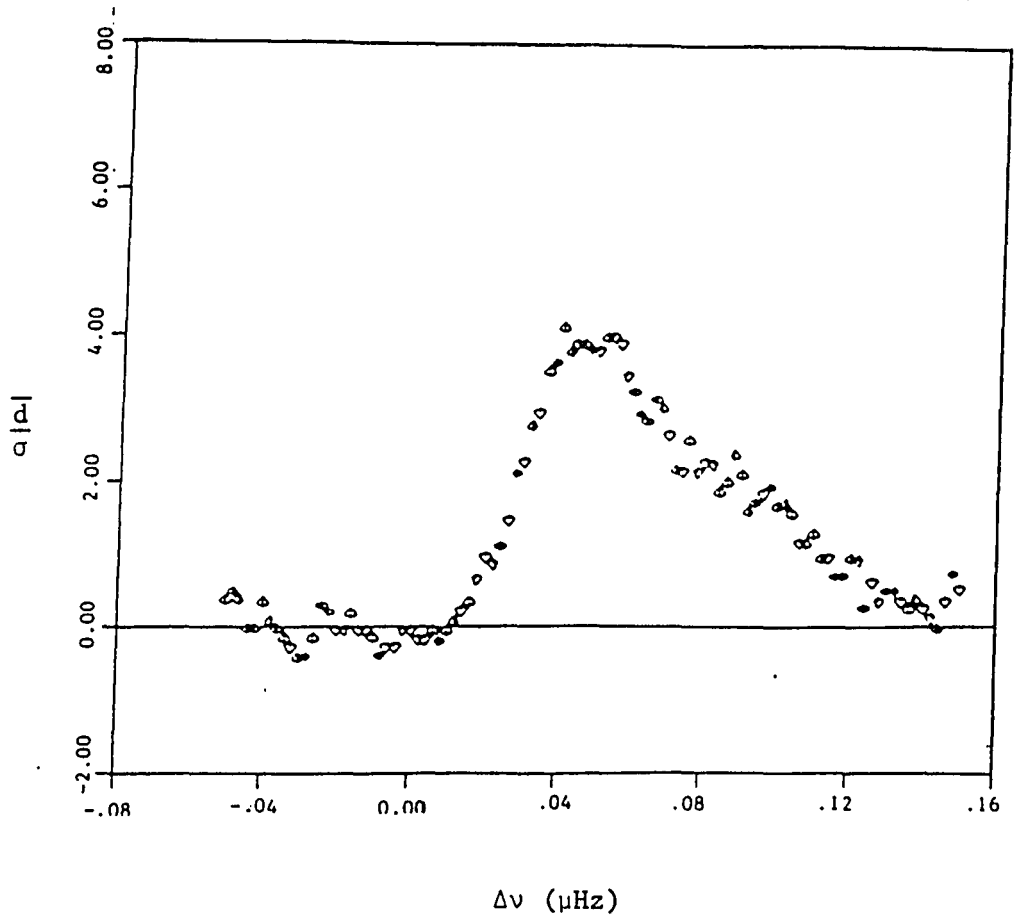

Figure 6.11. Coincidence rate between the 1985 power spectrum and classified f-mode spectrum for $21 \leq \ell \leq 26$ with $\Delta\nu'$ held constant.

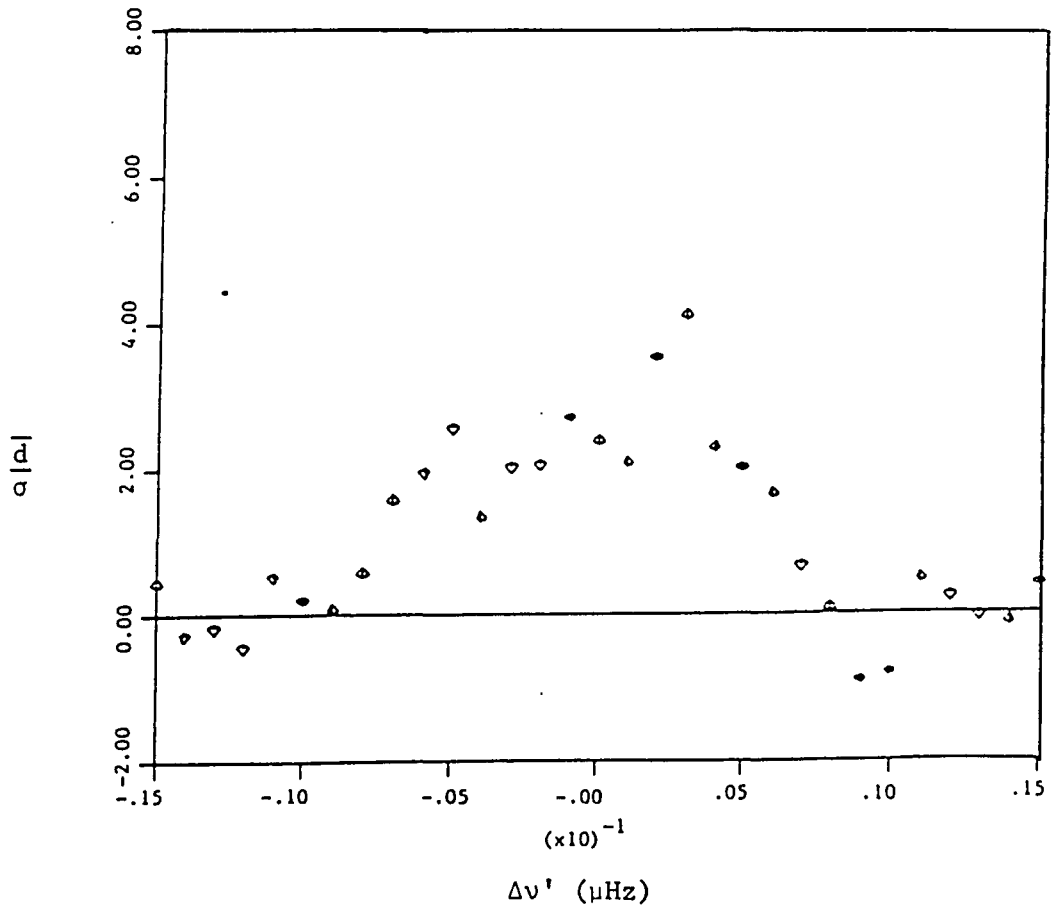

Figure 6.12. Coincidence rate between the 1985 power spectrum and the classified f-mode spectrum for $21 \leq \ell \leq 26$ with $\Delta\nu$ held constant.

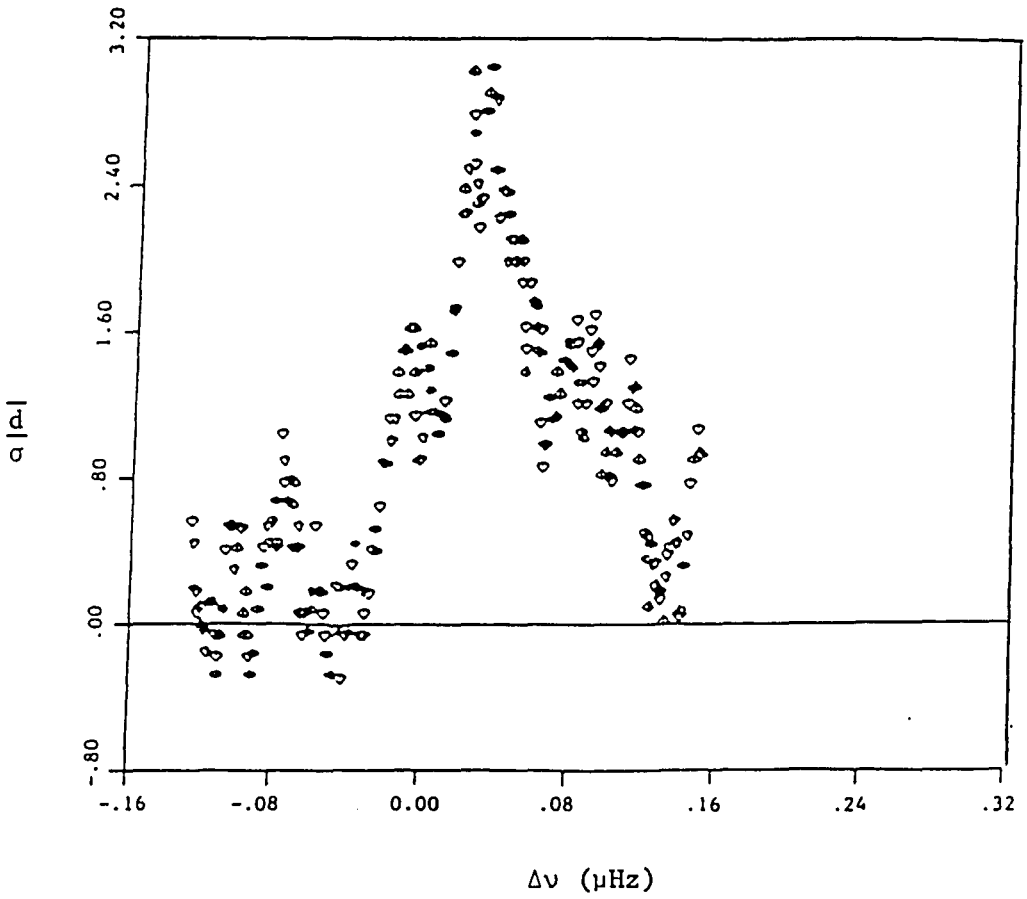

Figure 6.13. Coincidence rate between the 1985 power spectrum and the classified f-mode spectrum for $27 \leq \ell \leq 31$ with $\Delta\nu'$ held constant.

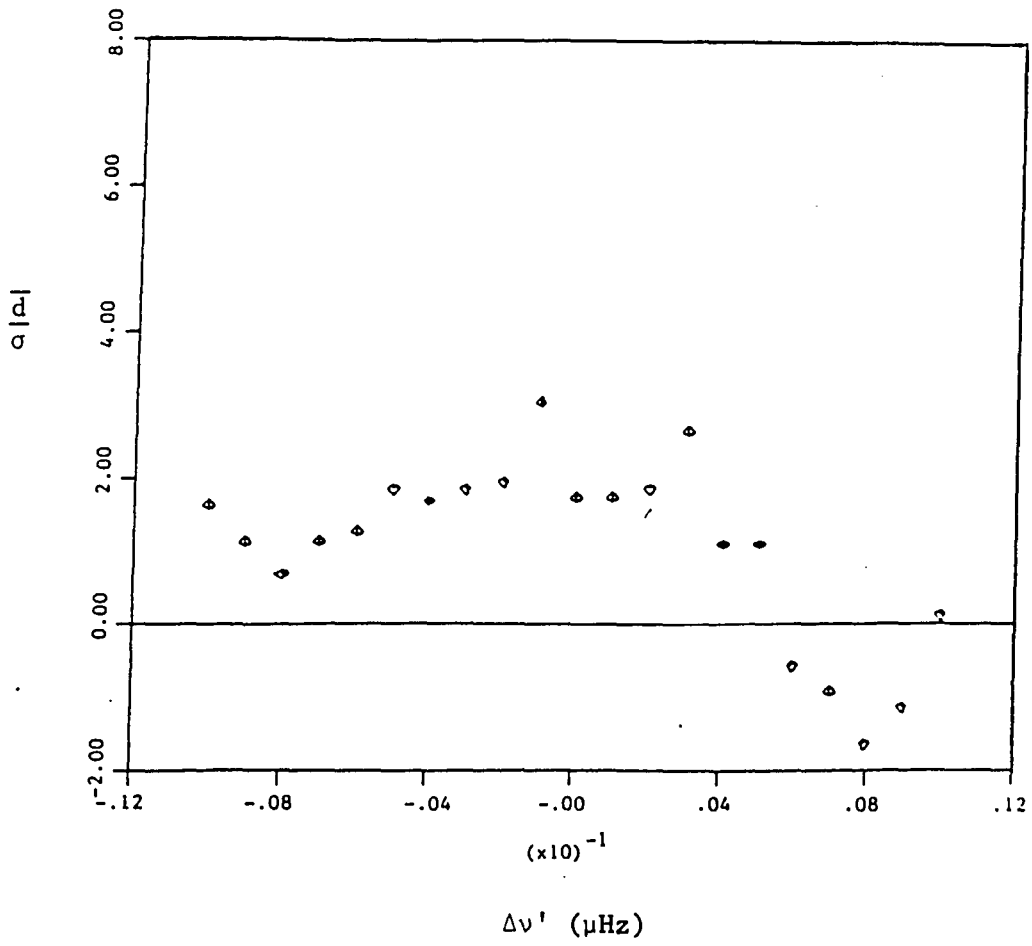

Figure 6.14. Coincidence rate between the 1985 power spectrum and classified f-mode spectrum for $27 \leq \ell \leq 31$ with $\Delta\nu$ held constant.

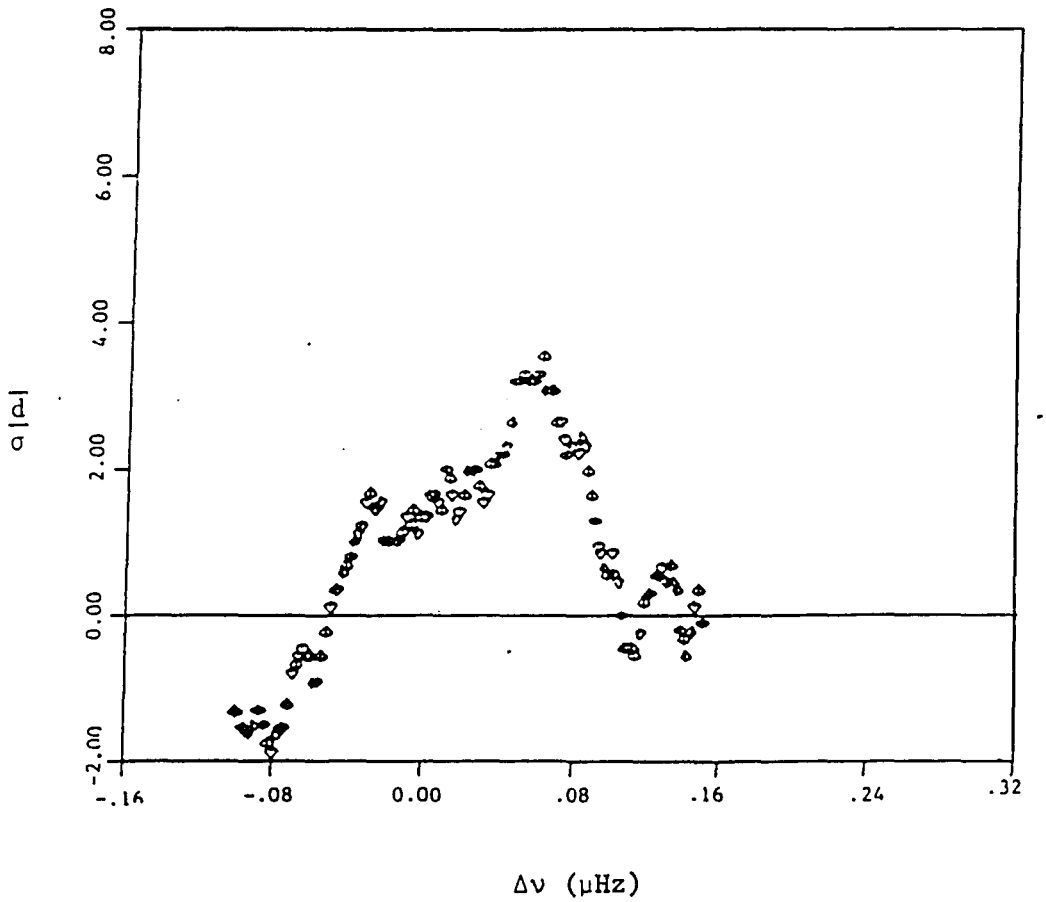

Figure 6.15. Coincidence rate between the 1985 power spectrum and the classified f-mode spectrum for $32 \leq \ell \leq 36$ with $\Delta\nu'$ held constant.

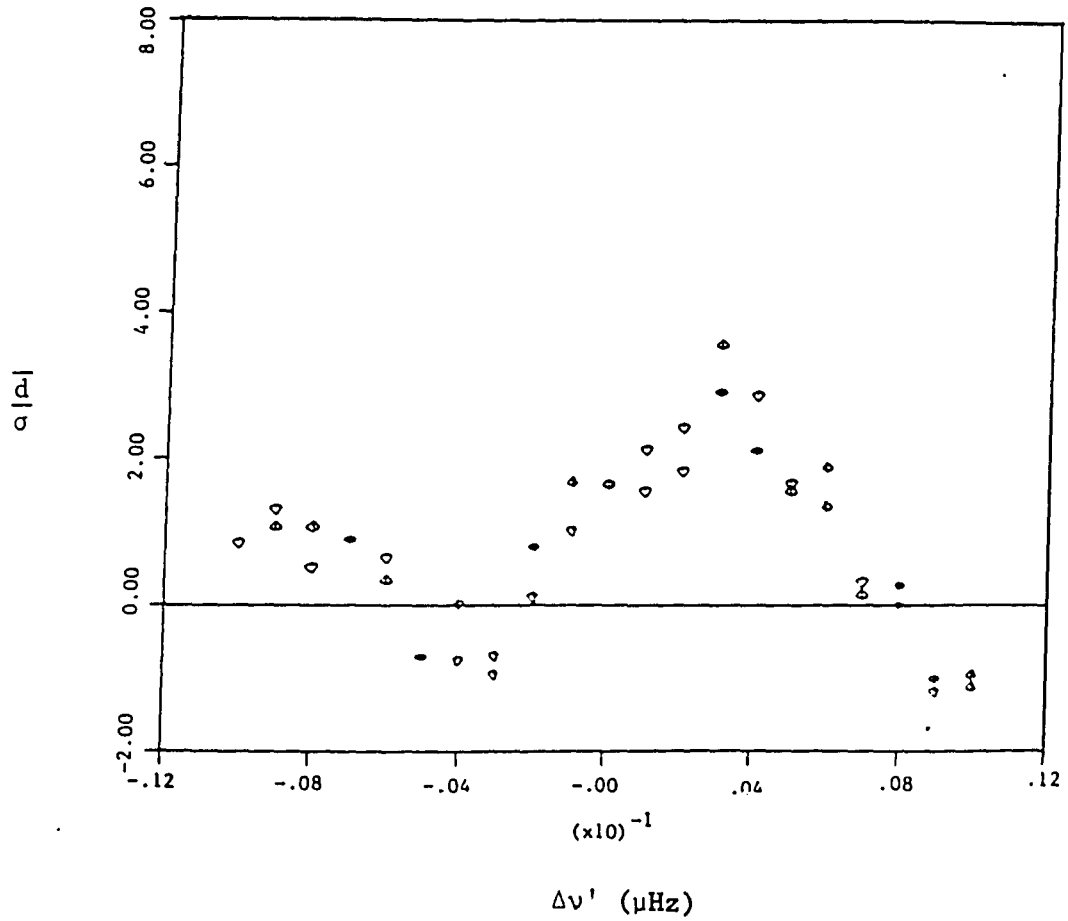

Figure 6.16. Coincidence rate between the 1985 power spectrum and the classified f-mode spectrum for $32 \leq \ell \leq 36$ with $\Delta\nu$ held constant.

to the eigenfrequencies of the n=0 modes identified by Rabaey, Hill, and Barry (1986) is very unlikely.

6.8 Comparison of the Peaks in the 1978 Power Spectrum to the Classified f-modes

The observed value of $\bar{d}$ from the 1978 observations for the $21 \leq \ell \leq 36$ f-modes is

$$\bar{d}_f = 0.098 \pm 0.032 \qquad 6.8.1$$

where a shift of the classified eigenfrequencies of $\Delta\nu_{n\ell} = 0.02 \pm 0.08$ μHz maximized the coincidence rate. The probability of obtaining this $\bar{d}$ under the null hypothesis is

$$p_f \lesssim 1.0 \times 10^{-2} \qquad . \qquad 6.8.2$$

CHAPTER 7

SECULAR CHANGES OBSERVED IN THE SOLAR NORMAL MODE FREQUENCIES OF OSCILLATION

Certainly, the Sun is not as constant in time as once had been thought. A very well-known example of this is the eleven-year sunspot cycle. Also the magnetic field is known to reverse polarity over an eleven-year period. Therefore, it may be expected that the characteristic eigenfrequencies of the normal modes of oscillation that are sensitive to the physical properties of the convection zone may change. Indeed evidence of this has been demonstrated in Chapter 6.

Any changes observed in the eigenfrequencies of modes that are sensitive to the properties of the convection zone are naturally a result of changes in, for example, density and temperature in that region of the Sun. Therefore, knowledge of the secular changes in the eigenfrequencies brings us closer to more fully understanding the Sun.

7.1 Frequency Shifts Observed in the Solar Normal Modes

Thus far it has been demonstrated by the results of Chapter 6, that changes have occurred over the past six years in the convection zone and that these changes are dependent on depth. Additionally, the most drastic change in eigenfrequency has been for modes that are sensitive to internal properties near the bottom of the convection zone.

The shifts in the eigenfrequencies of the normal modes of oscillation are an important result. As seen in Chapter 6, shifts in the classified eigenfrequencies were observed in the 1985 data set.

Since the low-order, low-degree acoustic modes and the intermediate-degree f-modes reside principally in the convection zone, the observed shifts will play an important role in determining how that region of the Sun is changing. The observed shifts obtained in Chapter 6 for the classified eigenfrequencies are displayed as a function of ℓ in Figure 7.1. These shifts amount to changes in the properties of the convection zone of the order of one part in 10^3. Furthermore, we have the added advantage of calculating how these changes occur as a function of depth, since lower ℓ values are sensitive at the top and bottom of the convection zone, while higher ℓ values are sensitive only to the top of the convection zone.

7.2 Comparison of Secular Changes in Solar Normal Modes with Changes Reported in Other Observations

Woodard and Noyes (1985) have analyzed data from the ACRIM total irradiance satellite on the **Solar Maximum Mission** in 1980 and 1984. They report that near solar maximum in 1980 the low-degree acoustic mode eigenfrequencies (in the 5-min p-mode region) were ≈ 0.4 μHz higher than those near the solar minimum in 1984. Roberts and Campbell (1986) have further suggested that the changes observed by Woodard and Noyes could be due to changes in the solar magnetic field. Roberts and Campbell (1986) have obtained an expression relating the change in

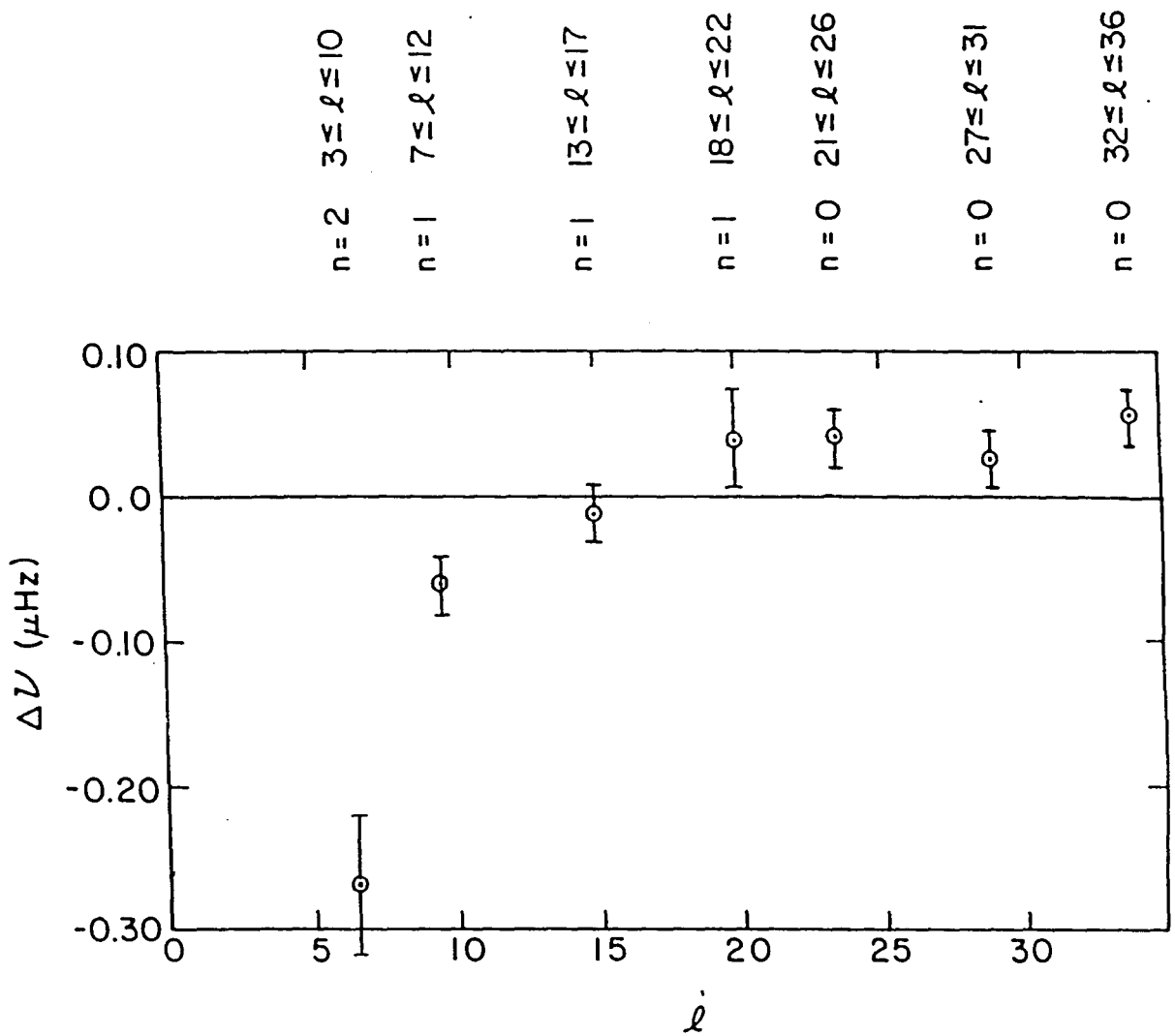

Figure 7.1. Observed frequency shift for the classified eigenfrequencies as a function of ℓ.

eigenfrequencies to a change in the square of the magnetic field from B' to B:

$$B^2 - B'^2 = 8\pi\bar{\rho}\overline{c^2}\frac{\Delta\nu_B}{\nu_0} \qquad 7.2.1$$

where $\bar{\rho}$ is the mean gas density and $\overline{c^2}$ is the mean squared sound speed where the means were taken over the integration range r = 0 to r = $R_\odot$. $\Delta\nu_B$ is the change in frequency due to a change in magnetic field, and ν_0 is the oscillation frequency. For the modes analyzed by Roberts and Campbell (1986), the average frequency was $\nu_0 \approx 3.1$ mHz.

From Equation 7.2.1, Roberts and Campbell (1986) concluded that assuming a peak field strength of $\approx 7\times10^5$ G, a change in magnetic field strength of $\approx 2\times10^5$ G would be required to produce the frequency shift reported by Woodard and Noyes (1985), assuming that the entire frequency shift was attributable to the change in the magnetic field.[6]

The eigenfrequencies studied by Woodard and Noyes (1985) and Roberts and Campbell (1986) are sensitive to the physical properties throughout the entire Sun. Changes in the magnetic field should also be detectable in the low-order, low-degree acoustic mode eigenfrequency spectrum such as those analyzed in Chapter 6. However, since these

---

6. Roberts and Campbell went further to add at the end of their analysis that recent data presented by Elsworth et al. (1986) has "cast some doubt on the trend in the p-mode frequencies" reported by Woodard and Noyes (1985).

modes are sensitive primarily to the internal properties of the convection zone, the expressions obtained by Roberts and Campbell (1986) cannot be used here. For this, the work of Dziembowski and Goode (1984) may be used, where they have also estimated the effect of a magnetic field on the fine structure of solar oscillations. The quadratic part of the fine structure splitting quadratic in m, ν_1 , due to the magnetic field is given in Equation 3.29 of Dziembowski and Goode (1984),

$$\nu_1 \approx \frac{1}{4[\ell(\ell+1)] - 3} \left\langle \frac{P_M}{P} \right\rangle \nu_0 m^2 \qquad 7.2.2$$

where P_M is the magnetic pressure. Returning to the polynomial used to calculate $\nu_{n\ell m}$ (cf. Equation 6.5.1), changes in the magnetic field should appear as changes in the coefficient of the second order term. This analysis is similar to the study of the shifts observed in the zeroth order and linear terms observed in Section 7.2. Therefore, information may be available for placing constraints on the magnitude of the magnetic field changes from 1979 to 1985.

Performing shifts in $\nu''_{n\ell}$ for the groups of multiplets delineated in Section 6.5 yields (in μHz)

$$\Delta(\nu''_{n\ell}/2) = \begin{cases} -0.0002 \pm 0.0004 & 7 \leq \ell \leq 12 \\ 0.0002 \pm 0.0001 & 13 \leq \ell \leq 17 \\ 0.0000 \pm 0.0002 & 18 \leq \ell \leq 22 \end{cases} \qquad 7.2.3$$

which is consistent with the hypothesis that no major shifts in ν'' are observed in the 1985 data. These results are presented as a function of $\bar{d}/\sigma$ in Figures 7.2 - 7.4.

Using Equation 7.2.2, an upper limit may be placed on the change in the magnetic field over a six year period (assuming that the contribution to the change in splitting is entirely due to magnetic field effects). At the bottom of the convection zone, $|\Delta B| \lesssim 25 \times 10^5$ G if the average of B over the six year period is 50×10^3 G. If the intial or final magnetic field is assumed to be zero, then $|\Delta B| \lesssim 55 \times 10^3$ G, which is one-tenth of value obtained by Roberts and Campbell (1986).

Changes in the magnetic field can also give rise to a shift in the zeroth order term, $\nu_{n\ell}$, of the expansion of the multiplet eigenfrequency spectrum. From Equation 3.11 of Dziembowski and Goode (1984), we find that in addition to the m^2 term given in Equation 7.2.2, there is a zeroth order term which is related to ν_1 in the following manner:

$$\nu_1 \propto \nu_0 \frac{\ell(\ell+1) - 3m^2}{4\ell(\ell+1) - 3} \quad . \qquad 7.2.4$$

Using this relationship, and the larger $\langle \frac{P_m}{P} \rangle$ inferred from the m^2 term, the shift in $\nu_{n\ell}$ due to magnetic field effects is estimated to be

$$\Delta\nu_{n\ell_{mag}} \approx 0.007 \ \mu\text{Hz} \quad . \qquad 7.2.5$$

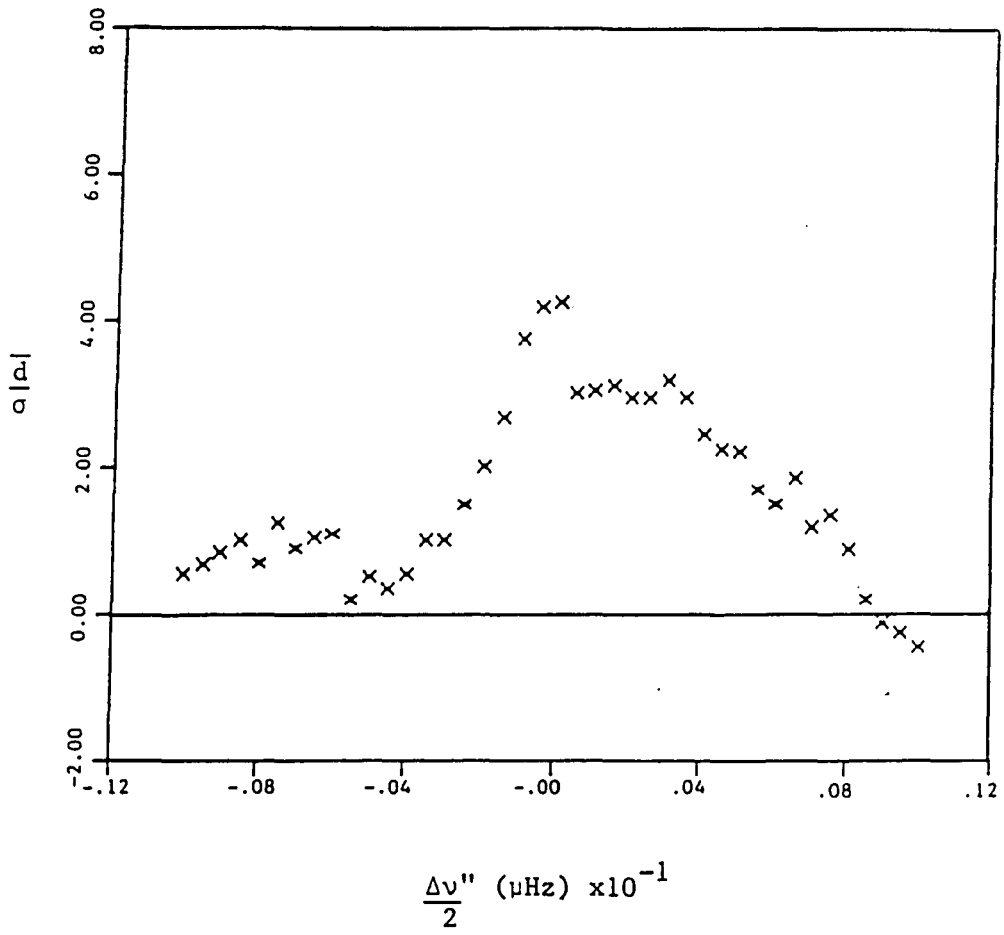

Figure 7.2. Coincidence rate between the 1985 power spectrum and the classified eigenfrequency spectrum for $7 \leq \ell \leq 12$ with $\Delta\nu$ and $\Delta\nu'$ held constant.

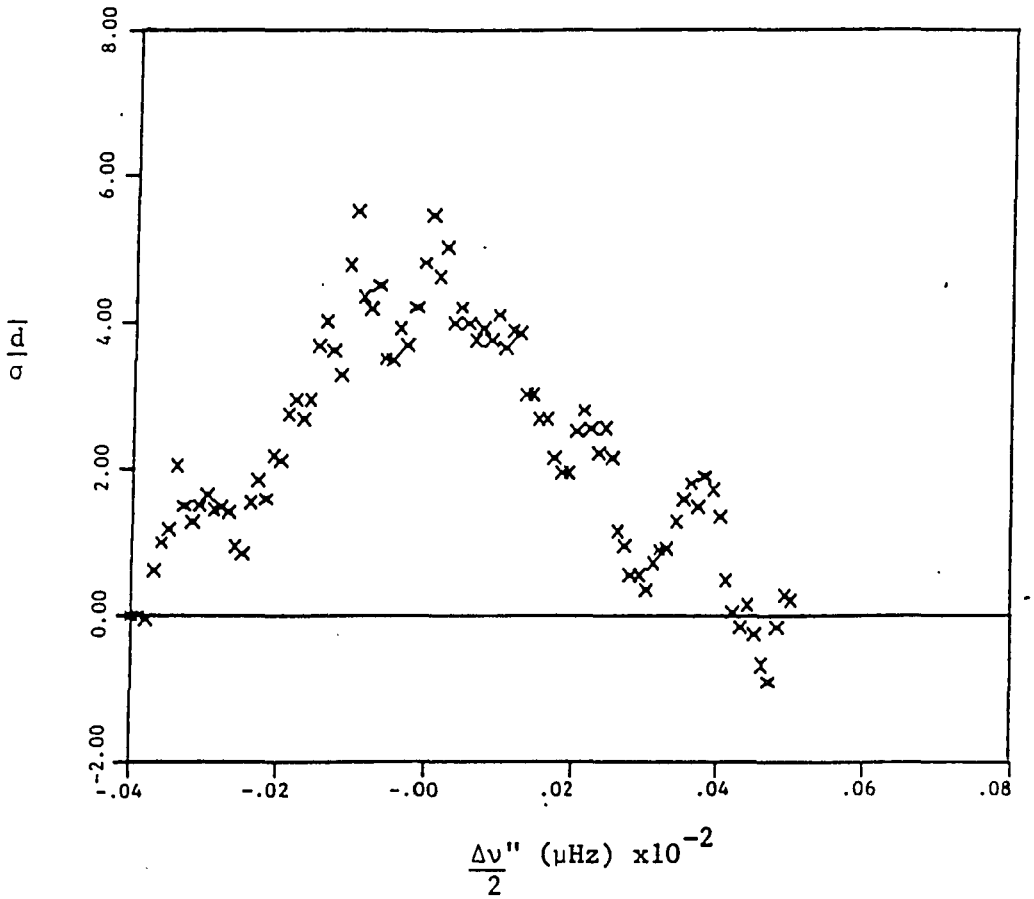

Figure 7.3. Coincidence rate between the 1985 power spectrum and the classified eigenfrequency spectrum for $13 \leq \ell \leq 17$ with $\Delta\nu$ and $\Delta\nu'$ held constant.

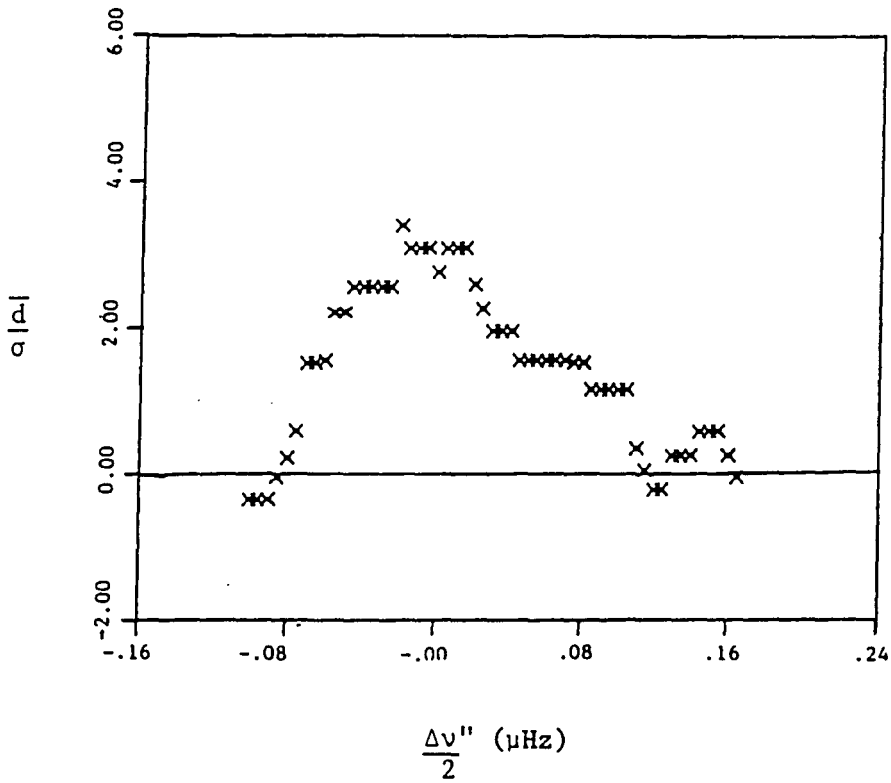

Figure 7.4. Coincidence rate between the 1985 power spectrum and the classified eigenfrequency spectrum for $18 \leq \ell \leq 22$ with $\Delta\nu$ and $\Delta\nu'$ held constant.

This shift is an order of magnitude smaller than the observed $\Delta\nu_{n\ell}$ given in Equation 6.6.2. Therefore, these results suggest that the contribution of the magnetic field to the observed changes in the normal modes of oscillation is approximately an order of magnitude less than the contribution due to changes in other properties of the convection zone.

CHAPTER 8

RESULTS FOR THE g-MODES OF OSCILLATION

One of the most important aspects of helioseismology is the availability of information which may be of value in the determination of how the Sun affects the climate. Due to the inability of current solar models to accurately predict the inner workings of the Sun (cf. Section 1.2), a prediction of the long-term solar variability is still out of reach. Even a slight change in solar output could have devastating effects on the Earth's climate (Parker, 1977).

Perhaps the most promising avenue to pursue for the purpose of predicting long-term solar variability is the study of the g-modes. The gravity modes are sensitive to the physical behavior of the Sun at its core. Of course, this is the region where nuclear burning occurs which is responsible for the energy production that is essential to all life on Earth. Certainly, understanding of what takes place in the core of the Sun is more than that of idle interest.

If evidence of gravity modes has been found in differential radius observations, as reported by Hill (1985), then evidence of these modes may be present in the 1985 power spectrum. Since these modes are expected to have long coherence times (>> 1 yr), there should ideally be a one-to-one mapping between the eigenfrequencies of the classified modes based on the 1979 observations and frequencies of peaks in the 1985 power spectrum. However, due to noise and possible incorrect mode classifications (cf. Section 8.4), a perfect mapping is not expected.

8.1 Evidence of Gravity Modes and Their Symmetry Properties in the 1985 Power Spectrum

To determine if evidence of gravity modes appears in the 1985 radiation intensity observations, the predicted values for the classified eigenfrequencies were checked for agreement with corresponding peaks in the 1985 power spectrum. If the separation in frequency between a classified eigenfrequency and a corresponding peak in the 1985 power spectrum was within a preselected window, $\pm \Delta\nu$, the latter was accepted as being in coincidence. Under the relative random distribution hypothesis, the probability of finding a peak in the 1985 power spectrum for $\Delta\nu = 0.07$ μHz is 0.542. This probability was determined by comparing 3×10^5 randomly generated frequencies with the peaks in the 1985 power spectrum in the region of interest. This value can be compared to the value obtained from the peak density (cf. Section 6.4) of

$$p = \bar{\rho}\Delta\nu = 0.539 \qquad 8.1.1$$

where $\bar{\rho}$ is the observed peak density in the relevant frequency range. The higher value of $p = 0.542$ will be used in this analysis.

Since the aperture was placed on the center of solar disk, symmetry properties of the eigenfunctions should be quite evident for the modes classified by Hill (1985), where the ℓ values are low, $\ell \leq 5$. The effect of having the aperture positioned near disk center, instead of the solar equator, will introduce complications in tests of symmetry properties only for higher ℓ values. Therefore, if the classification of the gravity modes by Hill (1985) is correct, the symmetry properties

discussed in Section 4.4 should be evident in the 1985 power spectrum for the low-degree gravity modes. For this reason the comparison of the classified eigenfrequencies will take a slightly different course than the comparisons involving the low-order, low-degree acoustic modes, and the f-modes in Chapter 6. Here, the classified eigenfrequency spectrum will be divided into two categories: 1) modes with even (ℓ+m); and 2) modes with odd (ℓ+m). It is apparent from the detector geometry used in the 1985 observations that signals associated with categories one and two will be of the symmetry allowed and symmetry forbidden types respectively.

Making the distinctions between the different symmetry properties expected to be observed for the low-degree gravity modes, the comparisons in this analysis will follow those of Chapter 6.

The ratio, N_ℓ/N_{max}, of the number of peaks in coincidence (within 0.07 μHz) with the classified eigenfrequencies to the number of maximum available classified states was determined. The result for even (ℓ+m) is

$$\frac{N_\ell}{N_{max}} = 0.692 \pm 0.045 \quad . \qquad 8.1.2$$

The comparison of this quantity to that expected for the null hypothesis is done by calculating $\bar{d}$ (cf. Section 6.1). The value of $\bar{d}$ for the above N_ℓ/N_{max} is

$$\bar{d} = 0.150 \pm 0.045 \quad . \qquad 8.1.3$$

This $\bar{d}$ is more than three standard deviations away from that expected under the null hypothesis. The probability of obtaining this if the null hypothesis is correct is

$$p = 5.0 \times 10^{-3} \quad . \quad . \quad 8.1.4$$

Therefore, for even (ℓ+m), the 1985 power spectrum shows evidence of the gravity modes at the 3.33σ level.

Next, a comparison similar to the one above for the symmetry allowed signals will be performed for the symmetry forbidden signals. Care must be taken in this comparison to avoid complications arising from the presence of 1/d sidebands in the power spectrum. It possible for the sidebands of an observed frequency, $\nu_{n\ell m}$, to be very close to the location of a another multiplet member with eigenfrequency $\nu_{n'\ell'm'}$. There are a total of ≈18 possible even (ℓ+m) 1/d sidebands for the classified frequencies, observed in 1979, that lie within $\Delta\nu = 0.07$ νHz of a classified odd (ℓ+m) eigenfrequency. Thus, it is obvious that the results for odd (ℓ+m) will be contaminated by these sidebands. If the frequency of an an odd (ℓ+m) mode of the classified spectrum was located within ±0.07 μHz of the 1/d sideband of the frequency of an even (ℓ+m) classified mode, the odd (ℓ+m) classified frequency was not included in this analysis. For example, there were a total of 69 classified eigenfrequencies with odd (ℓ+m) that were observed in the 1979 power spectra. There were 14 even (ℓ+m) classified eigenfrequencies that were also observed in the 1985 power spectrum with 1/d sidebands located

within ±0.07 μHz of the aforementioned 69 odd (ℓ+m) eigenfrequencies. Therefore, these 14 eigenfrequencies were not considered, and the value of N_{max}, given below in Equation 8.1.5, was reduced from 69 to 55.

The results for odd (ℓ+m) modes are

$$\frac{N_\ell}{N_{max}} = 0.472 \pm 0.067 \qquad 8.1.5$$

and

$$\bar{d} = -0.070 \pm 0.067 \quad . \qquad 8.1.6$$

This is 1.04σ below what is expected from a relative random distribution. The probability of this occurring under the null hypothesis is

$$p = 0.149 \quad . \qquad 8.1.7$$

Combining these results into a single symmetry test by comparing the results in Equations 8.1.2 and 8.1.5, the probability of obtaining a value in Equation 8.1.3 less than the value in Equation 8.1.6 under the assumption that the parity assignments for ℓ and m are incorrect is

$$p = 3.2 \times 10^{-2} \quad . \qquad 8.1.8$$

Again, to a statistically significant level, this indicates that the 1985 power spectrum is not random with respect to the classified g-modes. Furthermore, the symmetry properties tested above confirm that the classifications of the angular order and degree of the gravity modes are probably correct. The noise in the 1985 power spectrum and incorrect mode classification will be discussed in Section 8.4.

8.2 Search for Changes in the Classified g-mode Eigenfrequency Spectrum Over a Six-Year Period

Since the 1985 power spectrum does show evidence of gravity modes, it becomes possible to determine if the eigenfrequencies for these modes have changed over a period of six years. This is similar to the study of changes observed in the low-order, low-degree acoustic modes and f-modes in Chapter 7. Although the low-degree gravity modes are not expected to change over a period of several years, the availability of an independent power spectrum makes it possible to test this hypothesis.

For each multiplet, the location of a multiplet member for the g-modes is calculated by a polynomial for the eigenfrequency, $\nu_{n\ell m}$, given by Equation 6.5.1 using the values for $\nu_{n\ell}$, $\nu'_{n\ell}$, $\nu''_{n\ell}$, and $\nu'''_{n\ell}$ given in Hill (1985). Proceeding with the g-mode analysis in the same manner as the study of the p- and f-modes, the values of $\nu_{n\ell}$ and $\nu'_{n\ell}$ were simultaneously shifted over a restricted frequency range of ± 0.10 μHz and ± 0.04 μHz respectively. Again a window of $\Delta\nu = \pm 0.07$ μHz was used.

The results for these shifts are presented in Figures 8.1 and 8.2. We see from these figures that the results are consistent with the hypothesis that there has been very little, if any change of the classified low-degree gravity mode spectrum. An estimate of the values of these changes has been made directly from the figures yielding

$$\begin{aligned} \Delta\nu_{n\ell} &= -0.015 \pm 0.030 \ \mu\text{Hz} \quad , \\ \Delta\nu_{n\ell}' &= -0.002 \pm 0.012 \ \mu\text{Hz} \quad . \end{aligned} \tag{8.2.1}$$

These result are consistent with, and therefore, further support the hypothesis that evidence of the gravity modes classified by Hill (1985) exist in the 1985 observations. For example, if the peaks used to determine the $\bar{d}/\sigma$ in Figures 8.1 and 8.2 indicated statistically significant shifts in the eigenfrequencies, it would imply that drastic changes are occurring in the solar interior over a very short solar time scale, which is considered physically implausible. However, in the 1985 observations, no such shifts were observed.

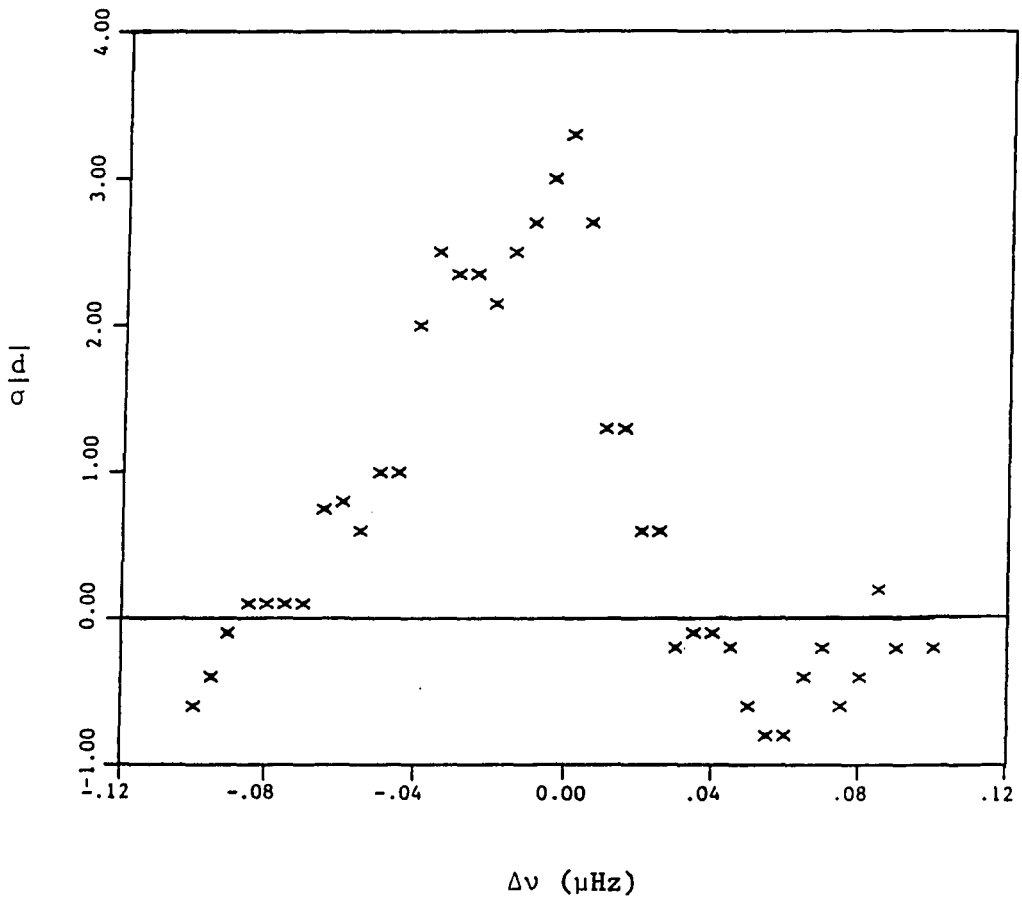

Figure 8.1. Coincidence rate between the 1985 power spectrum and the classified g-mode spectrum for $1 \leq \ell \leq 5$ with $\Delta\nu'$ held constant.

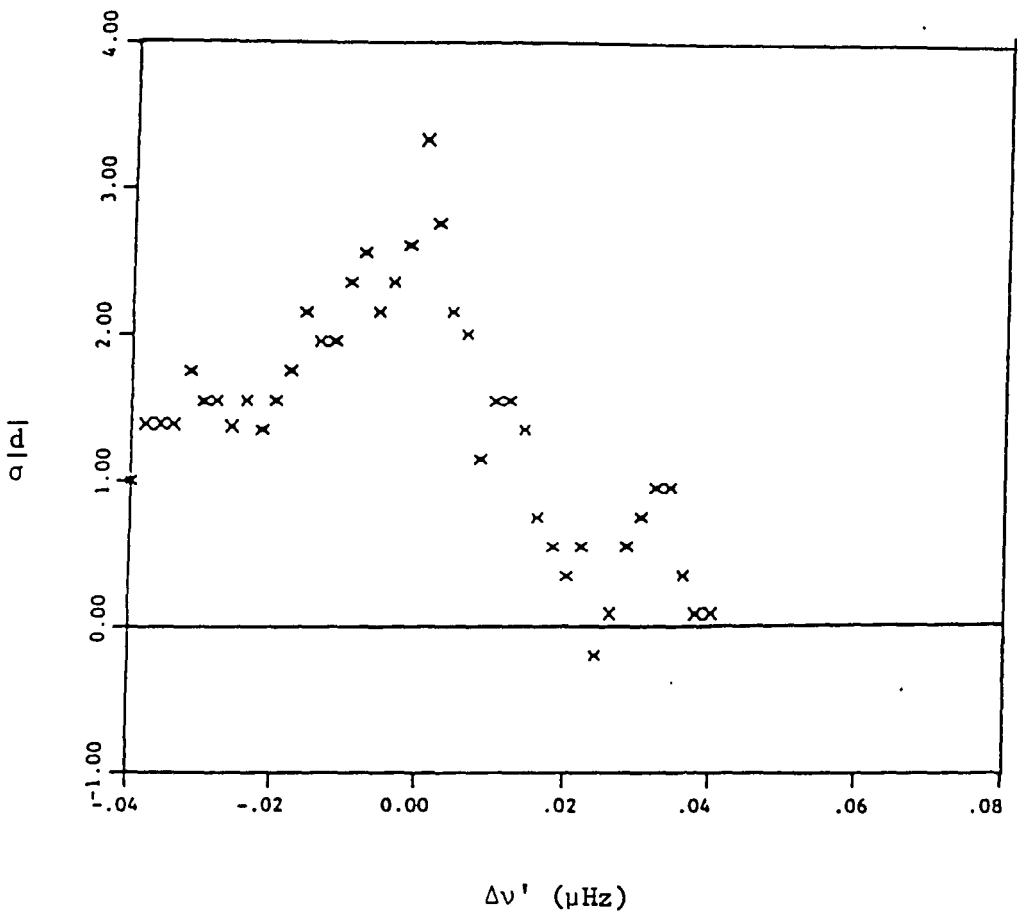

Figure 8.2. Coincidence rate between the 1985 power spectrum and the classified g-mode spectrum for $1 \leq \ell \leq 5$ with $\Delta\nu$ held constant.

8.3 The Observed m Dependence in the 1985 Power Spectrum

As mentioned in Section 4.4, the ratio of the 1979 to 1985 signal amplitudes, R(m), should be strongly dependent on m. Since the m dependence of R(m) is primarily through w(m), k w(m) is shown in Figure 8.3, where Equation 4.4.2 has been rewritten as

$$k\, w(m) = R(m)\,\mathrm{sinc}(m/10)\, \frac{\overline{Y_\ell^m}(\pi/2,0)\,|_{85}}{\overline{Y_\ell^m}(\pi/2,0)\,|_{79}} \quad . \qquad 8.3.1$$

The smooth curve drawn in Figure 8.3 is a weighted least-squares fit to the functional form of w(m). It is evident that the data points in Figure 8.3 behave in the manner expected for the correct m classifications.

The accuracy of the m classification of g-modes, based on the 1979 power spectra can easily be checked with the 1985 observations. From the detector geometry used in 1985, it is apparent that the sensitivity for detection of a classified gravity mode should be weakly dependant on m. However, the 1979 observations indicate a strong dependence on the solar signals in m. Therefore, the efficiency for mode detection in the 1985 observations should be strongly dependent on m. Extending the analysis presented above, the ratio of $N_{|m|}/N_{max}$ for even $(\ell+m)$ modes is presented as a function of $|m|$ in Figure 8.4. The results in this figure are consistent with what would be expected for

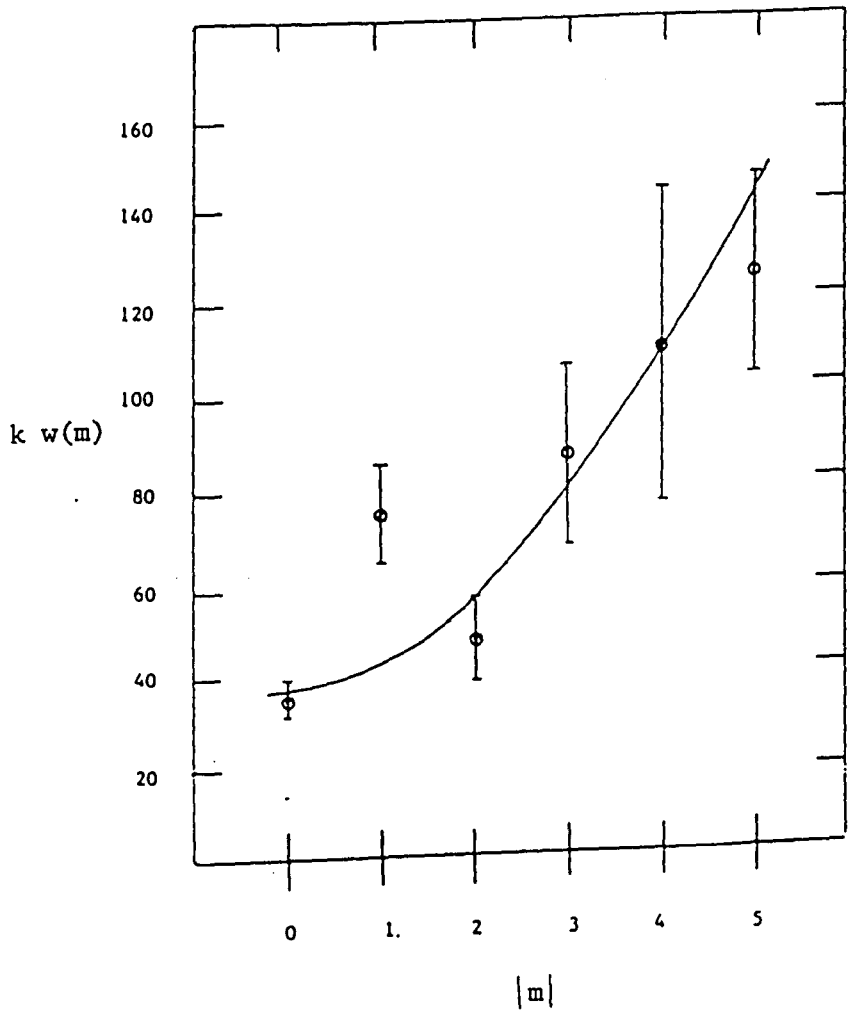

Figure 8.3. Evidence of the m dependence of the ratio of the 1979 to 1985 signal amplitudes exhibited through w(m).

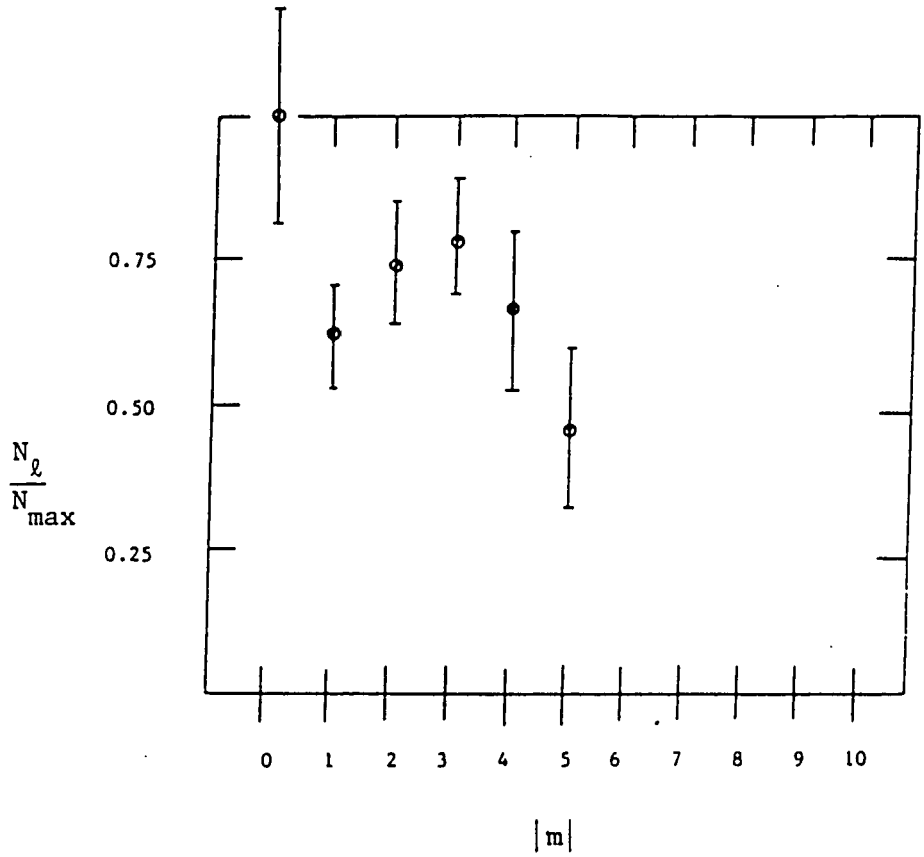

Figure 8.4. Observed coincidence rate, N_ℓ/N_{max}, as a function of m.

proper m classifications given the detector geometry used in the 1985 observations and the m dependence of the solar signal inferred from the 1979 observations.

8.4 Determination of the Signal-to-Noise Ratio as a Function of |m| in the 1985 Power Spectrum

Another test used to determine if there is evidence of gravity modes in a power spectrum is made by calculating the cross-correlation coefficient between the power densities (associated with the classified gravity modes) found in the 1979 power spectra and the one under study. In calculating the cross-correlation coefficients, the power densities at the location of the classified eigenfrequencies in the 1985 power spectrum were used. Therefore, the results can be represented using the work of Groth (1975). The standard deviations of the peak power densities, P_1 and P_2, of the 1985 and 1979 power spectra respectively, can be written as

$$\sigma^2_{P_i} = N_i + 2S_i \qquad 8.4.1$$

where N_i and S_i are the average noise and signal power densities in P_i assuming that N_i and S_i are randomly distributed. It has been determined for the 1979 observations that the average noise power density, N_2 is approximately 1.1% of the peak power density (Bos and Hill, 1983). Therefore,

$$\sigma_{P_2}^2 \approx 2S_2 \quad . \qquad 8.4.2$$

The cross-correlation coefficient, c_p, for a given value of $|m|$, is given by

$$c_p = \frac{\langle (P_1 - \bar{P}_1)(P_2 - \bar{P}_2) \rangle}{\sigma_{P_1} \sigma_{P_2}} \qquad 8.4.3$$

where the average is taken over the classified g-modes and σ_{P_1} and σ_{P_2} are the standard deviations of P_1 and P_2.

In order to obtain the signal-to-noise ratio in the 1985 power spectrum, Equation 8.4.1 and 8.4.2 can be used to rewrite Equation 8.4.3 as

$$c_p = c_p' \frac{S_1/N_1}{S_1/N_1 + 1/2} \qquad 8.4.4$$

where

$$c_p' = \frac{\langle (P_1 - \bar{P}_1)(P_2 - \bar{P}_2) \rangle}{\sigma_1' \sigma_2'} \quad , \qquad 8.4.5$$

$$\sigma_1' = (2P_1)^{1/2} \quad ,$$
$$\sigma_2' = (2P_2)^{1/2} \quad , \qquad 8.4.6$$

and it has been assumed that $S_2/N_2 >> 1$. Subscripts 1 and 2 refer to the 1985 and 1979 power spectra respectively.

The value c_p' in Equation 8.4.5 represents the cross-correlation coefficient between the signal power densities in the two data sets where the σ_1' and σ_2' for P_1 and P_2 respectively do not include the average noise power. Therefore c_p' should give an estimate of the incorrect mode classification. Hill (1985) has estimated the lower limit of the incorrect mode classification, r, of

$$1 - r = 0.77 \pm 0.04 \quad . \qquad 8.4.7$$

Since it is observed that the signal amplitudes in the 1985 observations decreases with increasing m, the signal to noise ratio in the 1985 power spectrum is expected to also decrease for higher $|m|$. The m dependence of the power of the 1985 data is expected to be of the form

$$\frac{S_1(m)}{S_1(m=0)} = \left[\frac{w(0)}{w(m)}\right]^2 \quad . \qquad 8.4.8$$

Therefore, Equation 8.4.4, can be written as

$$c_p = c_p' \left[\frac{S_1(0)/N_1}{S_1(0)/N_1 + \frac{1}{2}\left(\frac{w(m)}{w(0)}\right)^2}\right]^{1/2} . \qquad 8.4.9$$

The correlation coefficient between the 1985 and 1979 power densities associated with the classified gravity modes was fit to the functional form of Equation 8.4.9. A weighted least-squares curve fit was performed using different values of $S_1(0)/N_1$, and c_p' was determined directly from the fit. The value of $S_1(0)/N_1$ that minimized the weighted difference between the observed correlation coefficient and the theoretical curve (shown in Figure 8.5) is

$$\frac{S_1(0)}{N_1} = 1.68 \quad . \qquad 8.4.10$$

This value decreases to ≈0.5 for $|m| = 5$.

The determination of c_p' from the 1985 observations is an important result in that it provides an independent check of the estimate of the fraction of signals that have been incorrectly classified given by Hill (1985). The value of c_p' determined from the least-squares curve fit is

$$c_p' = .81 \pm .17 \quad . \qquad 8.4.11$$

which is consistent with the value of $(1 - r)$ in Equation 8.4.7.

8.5 Test for Correlation Between 1979-1985 Frequency Differences and 1979-1985 Relative Amplitueds

Thus far, the results presented in the previous sections indicate that evidence of gravity modes exists in the 1985 power

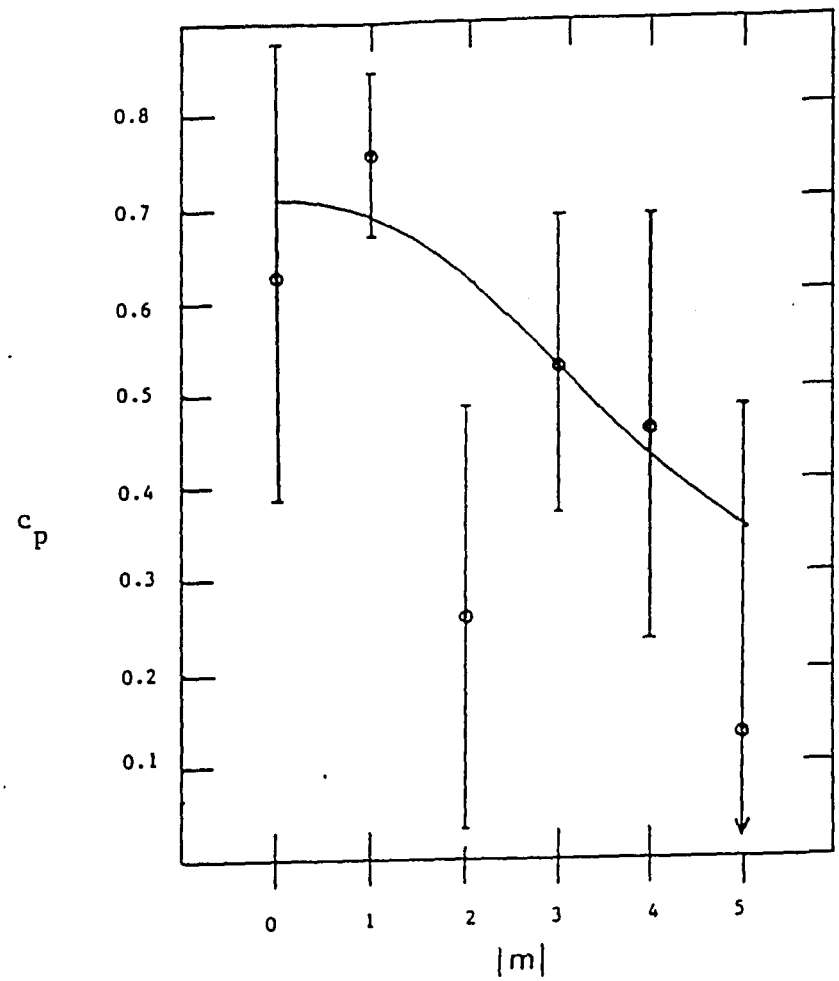

Figure 8.5. Observed correlation coefficient, c_p, between the 1985 and 1979 power densities associated with the gravity modes.

spectrum. Furthermore, from the agreement between the predicted m dependence of the 1985 detection sensitivity and the 1985 cross-correlation coefficients, the results strongly suggest that the m classifications made by Hill are probably correct.

Although the results presented in Equations 8.1.4, 8.1.7, 8.1.8, and 8.5.6 are statistically strong statements in support of the correct classification of the g-modes, a discrepancy still remains in the fact that the N_ℓ/N_{max} in Equation 8.1.2 is less than the predicted value of 1 - r. The predicted value of 1 - r is expected because the gravity modes are believed to be long-lived. However, this discrepancy can be understood by noting that the signal-to-noise ratio in the 1985 observations is ≈ 1.

It has already been demonstrated in the last section that the signal-to-noise ratio in the 1985 observations decreases with increasing $|m|$, and that this value for $|m| = 0$ is 1.68. However, as a further independent test of the hypothesis that the N_ℓ/N_{max} given in Equation 8.1.2 is less than 1 - r because of noise present in the 1985 power spectrum, we expect to find a positive correlation that is a function of the window, $2\Delta\nu$. The correlation coefficient, $\bar{c}_p$, between the 1985 and 1979 signal amplitudes is given as a function of $\Delta\nu$ in Figure 8.6, where $\bar{c}_p$ is the average of c_p over $|m|$.

Figure 8.6 clearly indicates that as $\Delta\nu$ decreases, the correlation coefficient increases. For the smaller values of $\Delta\nu$, $\bar{c}_p$ is 3.1 standard deviations away from zero. This result, along with the value

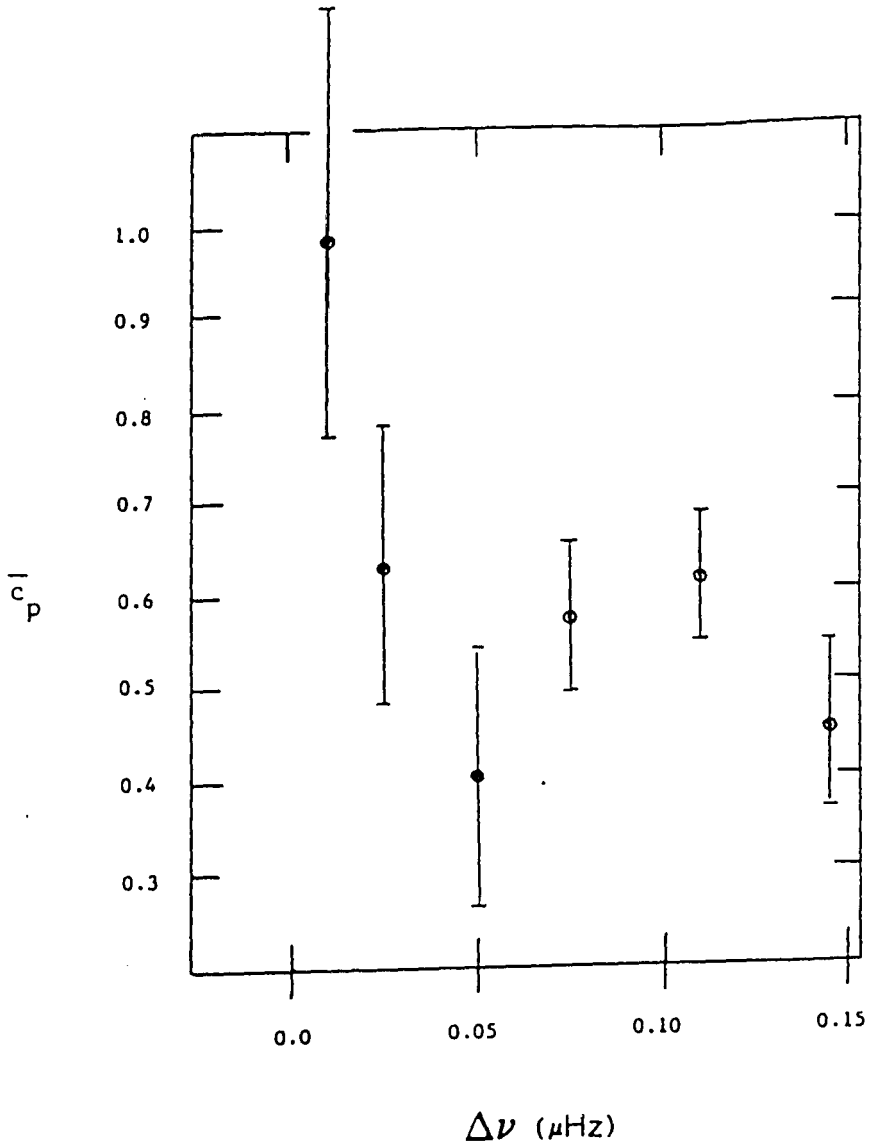

Figure 8.6. Correlation coefficient averaged over $|m|$, $\overline{c}_p$, as a function of $\Delta\nu$.

value calculated for the signal-to-noise ratio in Section 8.5 is in agreement with the hypothesis that the N_{ℓ}/N_{max} should be $\leq 1 - r$.

CHAPTER 9

SUMMARY

To a high degree of statistical significance, the classification by Hill (1984; 1985), Rabaey, Hill, and Barry (1986), Rabaey and Hill (1987), of the low-order, low-degree, acoustic modes; the intermediated degree f-modes; and the g-modes have been confirmed with the 1985 observations. Though these modes were not directly identified in the 1985 data, knowledge of a multiplet's existence a priori lends itself to a treatment that allows one to statistically accept or reject the presence of the multiplet in an independent data set.

The confirmation of the detection and classification of the low-order g-modes of oscillation was found to be at the 3.3 σ level. Additionally, the m dependence of the 1985 power spectrum was found to behave in the manner expected for the proper classifications in m for the g-modes.

For the low-order, low-degree, acoustic modes and the intermediate degree f-modes, a total of 40 multiplets were used in the analysis. The coincidence rates between the peaks in the power spectrum of the 1985 observations and the classified frequency spectrum for multiplets taken in subgroups of ≈ 5 (same n and contiguous in ℓ) are typically 4-5 σ above the accidental coincidence rate. The maximum coincidence rates for these same subgroups of multiplets were found to occur for frequency

shifts of the classified spectrum ranging from -0.27 μHz for modes that are sensitive to the internal properties near the bottom of the convection zone to 0.06 μHz for modes that are sensitive to internal properties near the top of the convection zone. These observed shifts in eigenfrequency may play an important role in inferring secular changes in the properties of the convection zone, which may bring us closer to more fully understanding the Sun.

LIST OF REFERENCES

Ando, H. and Osaki, Y., 1975, Publ. Astron. Soc. Japan, 27, 581.

Beckers, J. M., Ayers, T. R., 1977, Ap. J. Letters, 217, L69.

Bos, R. J. 1982, Ph.D. thesis, University of Arizona.

Bos, R. J., and Hill, H. A., 1983, Solar Physics, 82, 89.

Campbell, L., McDow, J. C., Moffat, J. W. and Vincent, D., 1983, Nature, 305, 508.

Caudell, T. P. 1980, Ph.D. thesis, University of Arizona.

Caudell, T. P., Knapp, J., Hill, H. A., and Logan, J. D., 1980, Lecture Notes in Physics, No. 125, Nonradial Stellar Pulsations, eds. H. A., Hill and W. A. Dziembowski (Springer-Verlag), 206.

Claverie, A., Isaak, G. R., McLeod, C. P., and van der Raay, H. B., 1979, Nature, 282, 591.

Conn, G. K. T., 1956, Am. Jour. Phys., 24, 451.

Duvall, T. L., Dziembowski, W. A., Goode, P. R., Gough, D. O., Harvey, J., Leibacher, J. W., 1984, Nature, 310, 22.

Dziembowski, W., and Goode, P. R., 1984, Proceedings of EPS Study Conference, Oscillations as a Probe of the Sun's Interior, (Catania, June 20-24, 1983).

Elder, T., and Strong, J., 1953, J. Franklin Inst., 255, 189.

Elsworth, Y. P., 1986, Helioseismology, IAU Colloq., 123, (Aarhus, Denmark, July 1986).

Gengerich, O., Noyes, R. W., and Kalkofen, W., 1971, Solar Physics, 18, 347.

Goldberg, L., 1954, The Solar System, Vol. 2, ed. G. P. Kuiper, Univ. of Chicago Press, Chicago, 434.

Groth, E. J., 1975, Ap. J. Suppl., 29, 286.

Hill, H. A., 1984, SCLERA Monograph Series in Astrophysics, no. 1.

Hill, H. A., 1985, SCLERA Monograph Series in Astrophysics, no. 3.

Hill, H. A., Bos, R. J., and Goode, P. R., 1982, Phys. Rev. Let., **49**, 1794.

Hill, H. A., Alexander, N., and Caudell, T. P., 1985, SCLERA Monograph Series in Astrophysics, no. 2.

Hill, H. A., and Caudell, T. P., 1985, Ap. J., **299**, 517.

Hill, H. A., and Stebbins, R. T., 1975, Ann. of N. Y. Aca. of Sci., **262**, 472.

Hill, H. A., Stebbins, R. T., and Brown, T. M., 1976, "Recent Solar Oblateness Observations: Data Interpretation and Significance for Earlier Work," Atomic Masses and Fundamental Constants 5, eds. J. H. Sanders and A. H. Wapstra, **622** (Plenum, New York, 1976).

Hill, H. A., Stebbins, R. T., and Oleson, J. R., 1975, Ap. J., **200**, 484.

Hill, H. A., Tash, J., and Padin, C., 1986, Ap. J., **304**, 560.

Hill, H. A., Rabaey, G. R., Yakowitz, D., and Rosenwald, R. D., 1986, Ap. J., **310**, 444.

Hill, H. A., and Rosenwald, R. D., 1986, Proceedings of the NATO Advanced Workshop, Mathmatical Aspects of Gravity and Supergravity, (Logan, UT, July 21-24).

Leighton, R. B., Noyes, R. W. and Simon, G. W., 1962, Ap. J., **135**, 474.

Logan, J. D., 1984, Ph.D. thesis, University of Arizona.

Mihalas, D., 1978, Stellar Atmospheres, ed. W. H. Freeman, San Francisco.

Musman, S., and Nye, A. H., 1976, Ap. J. Letters, **212**, L95.

Oglesby, P. H., 1986, Proceedings of Conference-Stellar Pulsation: A Memorial to John P. Cox, (Los Alamos, Aug 11-15, 1986).

Oglesby, P. H., 1987, 169th AAS Meeting, Pasadena, CA, Jan 4-8, Bulletin American Astronomical Society, **18**, No. 4, 988.

Parker, E., N., 1978, Solar Physics in a Broad Perspective, ed. J. A. Eddy.

Rabaey, G. R., Hill, H. A., and Barry, C. T., 1986, Proceedings of Conference-Stellar Pulsation: A Memorial to John P. Cox, (Los Alamos, Aug 11-15, 1986).

Rabaey, G. R., and Hill, H. A., 1987, 169th AAS Meeting, Pasadena, CA, Jan 4-8, Bulletin American Astronomical Society, 18, No. 4, 988.

Roberts, B., and Campbell, W. R., 1986, Nature, 323, 603.

Rowley, J. K., Cleveland, B. T., and Davis, R. Jr., 1985, AIP Conference Proceedings, Solar Neutrinos and Neutrino Astronomy, ed. M. L. Cherry, W. A. Fowler, and K. Lande.

Severny, A. B., Kotov, V. A., and Tsap, T. T., 1976, Nature, **259**, 87.

Vernazza, J. E., Avrett, E. H., and Loeser, R., 1976, Ap. J., **30**, 1.

Willson, R. C., and Hudson, H. S, 1981, Ap. J. Letters, **244**, L185.

Woodard, M. F., and Noyes, R. W., 1985, Nature, **318**, 449.